ISBN 978-82-471-2440-6 (printed ver.)
ISBN 978-82-471-2441-3 (electronic ver.)
ISSN 1503-8181

Fabrice Caline
Doctoral Thesis

Doctoral theses at NTNU, 2010:226

Fabrice Caline

Coastal-sea-ice action on a breakwater in a microtidal inlet in Svalbard

NTNU
Norwegian University of
Science and Technology

Doctoral theses at NTNU, 2010:226

NTNU
Norwegian University of
Science and Technology
Thesis for the degree of
doctor philosophiae
Fakultet for ingeniørvitenskap og teknologi
Institutt for bygg, anlegg og transport

NTNU
Norwegian University of
Science and Technology

Fabrice Caline

Coastal-sea-ice action on a breakwater in a microtidal inlet in Svalbard

Thesis for the degree of doctor philosophiae

Trondheim, October 2010

Norwegian University of
Science and Technology
Faculty of Engineering Science and Technology
Department of Civil and Transport Engineering

NTNU
Norwegian University of
Science and Technology

NTNU
Norwegian University of Science and Technology

Thesis for the degree of doctor philosophiae
Faculty of Engineering Science and Technology
Department of Civil and Transport Engineering

ISBN 978-82-471-2440-6 (printed ver.)
ISBN 978-82-471-2441-3 (electronic ver.)
ISSN 1503-8181

Doctoral Theses at NTNU, 2010:226

Printed by Tapir Uttrykk

"If I were a medical man, I should prescribe a holiday to any patient who considered his work important."

Bertrand Russel, Autobiography

Abstract

In order to open a coal mine in *Ispallen*, a prospect of the company *Store Norske*, it will necessary to transport the coal across a tidal inlet, *Sveasundet*, in Svea, Svalbard. In anticipation of this challenge, Store Norske partly funded a PhD position at UNIS to study the action of the ice on a possible causeway across the inlet and, more generally, to better understand the action of sea ice on coastal structures.

I designed and supervised the construction of a 50-m-long, 8-m-high and 25-m-wide breakwater in this microtidal environment—2.0 m maximum tidal range—where the sea-ice period lasts between 4 and 6 months.

At the tip of the breakwater I installed a cabin with a weather and ground temperature station and time-lapse cameras. On the seabed I installed a tide and wave gauge. I went on the site on a weekly basis during a full ice season and documented the ice conditions both visually and quantitatively. I used a differential GPS to monitor tidal ice movements, measured ice stresses and took cores to analyse the properties of the coastal ice. To my knowledge, nowhere in the world have ice conditions ever before been documented so thoroughly throughout a whole season.

Most engineering literature on sea ice is related to offshore structures. There is so little literature on coastal sea ice that several terms lack a precise definition. In this thesis *coastal ice* is defined as the ice in the zone that is affected by the boundary conditions at the shore.

I identified and documented a variety of coastal-ice processes, most notably the formation, growth and decay of the *ice foot*, the tidal movement, and the break-up.

The observations of the *ice foot* lead me to revise its definition. At the site of study, the term is essentially relevant during the formation of the sea ice cover and during the break-up. In between, it is more relevant to consider the *hinge zone*, which is the area where the *tide cracks* occur.

The ice pile-ups that occurred during the break-up perpertrated little damage because that late in the season, the ice was rotten and soft. Since these were the most destructive events,

the ice conditions may be characterised as mild.

Measurements of the ice strength, elasticity and creep across the coastal zone revealed that the coastal ice was weaker, less stiff and crept less than the free-floating ice. From the shore to the free-floating ice, the measured value of strength ranged monotonously from about 3 to 4 MPa and the measured value of elasticity ranged monotonously from about 1 to 1.5 GPa.

Measuring the stresses in metre-thick ice was challenging but the peak stresses of about 150 kPa is in the range of those found in similar studies (Frederking et al., 1986; Sayed et al., 1988; Moslet, 2001; Nikitin et al., 1992). Surprisingly, the highest stresses were measured in the direction not perpendicular but parallel to the tide cracks. More work is needed to understand the process of stress-build up.

Copyright

The thesis is available online at the following persistent address:
http://purl.org/com/fabice/caline-2010.pdf

The three papers in appendix, some of the data, and videos of the tidal movement of the coastal ice are available at http://fabice.com

Requests for pictures in full resolution and additional data may be sent to fc@fabice.com

Preface

I found great writing help in Van Leunen's *A Handbook for Scholars*, Strunk and White's *The Elements of Style* and Fowler's *A Dictionary of Modern English Usage*.

Contrary to what has become the custom, I have written the thesis as a monograph, mainly for the following reasons:

- The work consists of too many small parts to be suited for the paper format. In addition, the pictures in Appendix B are key to understanding the context, and they would not fit in an article.
- When I started writing the thesis, I had already almost run out of time. Writing a monograph seemed quicker than writing papers, and, therefore, the best choice. In addition, had I written papers, I would not have received the peer reviews until after delivery. For someone who plans a scientific career, it's part of the game to continue working on the papers in overtime. For someone who has other plans, however, it just feels like a hell of a lot of painful, unpaid work.
- I resent the simplistic way scientific research is evaluated through the number of papers published and journals ranking. Writing a monograph is a way of taking a stand.
- Last, but not least, I want to keep control over my work instead of letting stockholders of a publicly listed publishing corporation make money on it and deny me the right to use it as I please.

In the beginning, I experimented writing the thesis as a wiki. Although it worked well for organising notes, it soon became unpractical: saving took too much time, attaching documents was complicated and backing up was a real pain. One of the reasons I tried it out, was to possibly obtain some kind of peer review by active visitors, but all I got instead was spam.

The observation work at Barryneset felt like true research, not knowing where it would lead me and requiring qualitative observations and getting a feeling of what was going on

before I could do any quantitative work. I may have been lucky that my observations were relevant enough to be published, and not knowing until the end if they would be, felt like taking a serious risk and made for some stressful moments. I wish the PhD would have left more room for taking risks and for serendipity. To paraphrase Carlo Petrini, I wish the PhD would allow for *slow research*. Unfortunately, I feel that the pressure on producing papers and on finishing in time gets in the way and, instead, leads to safe, but less exciting work.

When I applied for the position, I had great admiration for Store Norske and did not have the slightest afterthought about working with a coal mining company. After all, I was working in the oil industry. Since then, I have become a bit of an environmental fundamentalist. So how does one deal with working on the development of a coal mine the opening of which one is opposed to? I have no good answer. Personally, at some point, I made the decision that I would get out of the hydrocarbon-business but that I would complete the work I had started. On the positive side, as opposed to most environmentalists, I have been *on the inside* and met people who, even if I disagree with them on environmental issues, I have all the respect in the world for. That has lead me to hope that they too, some day, will realise what a dead end we are pushing our species into.

Finally, I would like to raise a taboo, namely the mental health of PhD candidates. I have probably been all the more aware of it as I am struggling with a mental illness (bipolar disorder). Although outsiders may just have the impression that a PhD is incredibly difficult, few understand the mental loads of the deadline and of the loneliness. I can see that not anyone should be able to obtain a PhD, but there has to be a better way of selecting than destroying the lives of PhD candidates. Of the dozen PhD candidates at UNIS during my time there, I know of at least three, including me, who have or will quit academia after their PhD. When I talk with my peers, *hell* is the word most often used to characterise the PhD. Is that really how we want higher education to be? I suspect researchers are too busy with their own work to take part in fighting this psychopathic system. Raising the issue here is hardly a fight, but it is better than nothing.

Acknowledgements

Although I wrote the acknowledgements in a mildly sarcastic tone, I am *sincerely* thankful to all the people named below.

I particularly want to thank two close friends: Lene Kristensen, whose charm is, I suspect, what got me such goodwill in the male-dominated community of Svea, and Marta Slubowska, my faithful and lovely swimming partner.

I would also like to thank my academic colleagues: Jomar Finseth, the best fieldwork partner ever; Sébastien Barrault, the master of doubtfull, Swiss humour; my supervisor Lars Grande, always keen to engage in discussions about sailing; Knut Høyland, who read my thesis so thoroughly that he understands it better than I do; Aleksey Marchenko, with his distracting ideas; Ingrid Eggenfellner, who has understood that a personnel manager's role is to defend the staff against the management and not the other way round; Berit Jacobsen, for playing *Deep Purple* in her library; Arnstein Watn, "because he deserves it..."; John Inge Karlsen, the arctic cowboy; Jørgen Haagensli, for his kindness; Per Olav Moslet, with his irritating serenity; Marit Skjåk-Bræk and Heine Larsen Nersund, the administrative staff of my dreams come true; Arnfinn Emdal, thanks to whom I got *some* money in overtime; Thomas Benz, who tried his best motivating me when the thesis was refused; finally, cameraman Fred Sigernes—sorry about the camera that the bear smashed to pieces, mate!

At Store Norske and LNS Spitsbergen, the following people were particularly nice to me: Jan Sandvold was almost like a father to me; Atle Brekken was a fantastic problem solver; Rune Hesthammer allowed me fly to Svea for leisure; Arne Langeland let me ravage with impunity; Rolf Andersen and Bengt Olav Moholt, who still believe in Santa, managed to lift my mood even from its lowest levels; Stein Erik Myre's and Gudmund Løvli's spread their buoying enthusiasm.

I tried my best to be nice to my field assistants but did probably not always succeed. Therefore, I am thankful to them for bearing with me. With Dag Theodor "Theo" Røsvik Andreassen we would play *Dirty Deeds Done Dirt Cheap* on the cabin-"stereo" and all our problems disappeared; Hilde Landrø was wise enough to get back on land right before

the ice broke up; Tore Hattermann will probably never again fall asleep in an elevator bucket; Gro Vestues beared with *both* me and Theo; Magne Wold, the arctic macho and Bjørn Pedersen, the arctic pirate. Edwin Zengerink accepted to work as an improvised field assistant although he was supposed to be the boss. Finally, I valued Bror Johansen's down-to-earth attitude.

It was a pleasure to stay at the Helsinki University of Technology during the spring of 2008 under the supervision of Jukka Tuhkuri, with whom I also had several discussions about sailing. Janne Ranta's generous help with numerical modelling was much appreciated.

I had many invaluable email communications with people at the Norwegian Mapping Authorities (Statkart), who helped me with the tide calculations: Birgit Kjos-Lynge, Daniel Hareide, Tor Tørresen and Einar Kvale.

I am also grateful to all the students who stood behind the morning swimming sessions.

Finally I would like to thank the management at Lufttransport in Longyearbyen, for neither reporting nor black-listing me after I—stupidly, though unintentionally—transported dangerous goods on the plane to Svea.

Contents

List of Figures

List of Tables

Abbreviations

AFDD: Accumulated Freezing Degree-Days

ATDD: Accumulated Thawing Degree-Days

CAD: Computer-Aided Design

DGPS: Differential GPS

EUREF89: A global datum using a version of the WGS84 ellipsoid. Geocentric and geographical coordinates are based on the ellipsoid. The difference with the original WGS84 ellipsoid are only of theoretical interest (of the order of the 5th–6th decimal). In practice the two ellipsoids are the same and often referred to as *WGS84(Euref89)*.

FDD: Freezing Degree-Days

GIS: Geographical Information System

GPS: Global Positioning System

HOW: Highest Observed Water level

LAT: Lowest Astronomical Tide

LNSS: LNS Spitsbergen AS (a contractor based in Longyearbyen, Svalbard)

LGO: Leica Geo-Office (a computer program for processing DGPS data)

LOW: Lowest Observed Water level

MHW: Mean High Water level

MLW: Mean Low Water level

MSL: Mean Sea Level

NP: the Norwegian Polar Institute

SI: International System of Units (Système International d'Unités)

Store Norske: Store Norske Spitsbergen Grubekompani (a coal mining company based in Longyearbyen, Svalbard)

WGS84: World Geodetic System from 1984. WGS84 is a satellite-based ellipsoid. It is also used when referring to this ellipsoid's datum.

UTC: Coordinated Universal Time

UTM: Universal Transverse Mercator coordinate system consisting of 60 zones, each of which is based on a specifically defined secant transverse Mercator projection.

UTM33X: UTM zone covering Svalbard

Conventions

Geographical coordinates: The projection is UTM zone 33X and the geoid is WGS84.

Altitude: The altitude—also referred to as *elevation*—is the official orthometric height in accordance with the Norwegian Polar Institute's (NP) reference point in Svea, NP150. It is approximately 0.32 m less than the altitude above MSL (the MSL is, in other words, 0.32 m below map datum).

NP150 is located 400 m to the north west of the breakwater. Its position (Table A.5) has been triangulated with use of static GPS measurements from NP's network of main reference points. Its orthometric height (9.081 m) is based on the official altitude network, which is used in the NP maps (NP is the mapping authority for Svalbard). The orthometric heights of the main reference points of this network are based on GPS-measured vectors, older triangulation measurements (angles and distances), gravity measurements and sea level observations performed in the end of the 1980s and the beginning of the 1990s.

In Svea the orthometric height is in good accordance with a geoid model from the Norwegian Mapping Authority's (Statens Kartverk) called ARCGP-SK-2006, which is based on gravity measurements performed from the air, a digital terrain model of Svalbard and sea level observations. The height of NP150 relative to this geoid model is 9.278 m, which is 0.197 m higher than the official orthometric height.

NP is currently having discussions with the Norwegian Mapping Authority about the possibility to revise the ARCGP geoid so that it is better fitted to the network of reference points (Melland, 2009).

Sea height: The height of the sea relative to the datum.

Sea level: Used in a more general way than *sea height* as in *high sea level* or *low sea level*.

Directions: Angles are clockwise and 0° is North.

Wind direction: The wind direction is the direction *from which* the wind is blowing.

Time: The time is in UTC+1 and 24-hour format.

Temperature: The temperature is given in degree Celsius [°C], angles in degrees, the salinity in practical salinity units (psu) and all other data in SI units.

Pictures: Unless specified otherwise, I am the author of the pictures.

Tide cracks numbering: The tide cracks are numbered from 0 to 5: crack 0, 1, . . . (Section 5.8)

Slope angles: Slope angles are given as the tangent of the angle between the slope and the horizontal plane and expressed as a ratio of a vertical length to a horizontal length, for example 1V:3.5H, where 1 is the vertical length and 3.5 the horizontal length.

Breakwater: The different zones of the breakwater are named according to Figure 1.

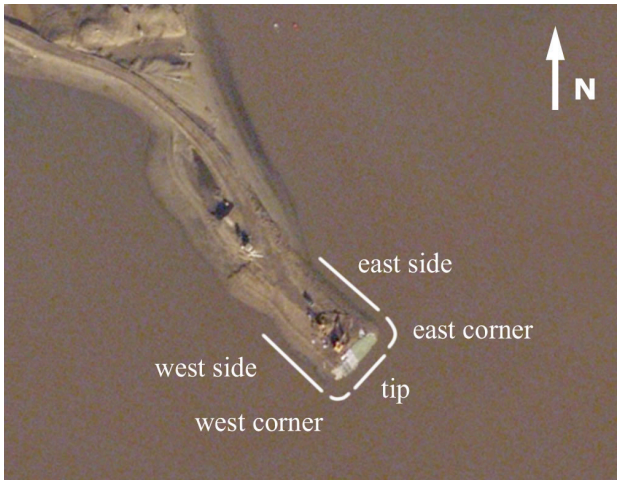

Figure 1: Orthophotography of Barryneset with the nomenclature of the different zones of the breakwater – Summer 2006

To those who dare swim against the tide

Chapter 1

Introduction

1.1 Context

Most coastal communities are dependent on one form or another of coastal infrastructure like breakwaters or quays. In polar regions coastal structures are subjected to the destructive action of sea ice.

Today, the world's addiction to hydrocarbons is pushing production into the fragile wilderness and remoteness of the Arctic. In the Barents Sea, the Snøhvit field entered production in 2006, the Goliat field is due to start production by 2013 and the gigantic Shtokman project is in the planning phase. Although those projects are offshore, they require coastal infrastructure for supply and rescue ships.

At the other end of the pipe, it is widely accepted that the climate is warming up from the burning of fossil fuels, accelerating the thawing of the permafrost. While frozen ground withstands sea erosion forces, thawed permafrost, on the contrary, is easily eroded away. Numerous communities in Siberia, Canada and Alaska therefore experience an increase in the erosion of their shore.

Surprisingly little literature is found on the action of sea ice on coastal structures. Some studies are related to the issue of ice encroachment on riprap—pile-up and ride-up—(Wuebben, 1995; Sodhi et al., 1996). In the Arctic, however, if local rocks are available, their quality is usually too poor to be used as riprap. There is, hence, a need for non-traditional shore protection methods, for example using geosynthetic bags. Private-funded studies were done in the 70s and 80s, but nothing of interest is found in the public domain. This research field is wide open and this thesis will hopefully help lay its foundation.

One limitation with a fieldwork-based study is that some results are site-specific. In this

case the site was Barryneset and Sveasundet, Svalbard, where Store Norske is considering to build a causeway and possibly a bridge.

There are a number of similarities between Barryneset and arctic river sites, although ice jam and flooding—one of the major river ice concerns—do not occur at Barryneset.

1.2 Objectives

The objective of this thesis is to document and analyse coastal-ice conditions at Barryneset and try to generalise the results to arctic coasts. It is written from the point of view of an engineer eager to better understand sea ice loads on coastal structures.

The following topics were specifically investigated:

- the physico-mechanical properties of the ice in the coastal zone and in the free-floating ice
- the intensity and direction of the stresses along tide cracks
- the ice foot and its role with respect to shore erosion
- the influence of the tide and current
- the dynamic action of drift ice during the break-up

1.3 Scope

I analysed coastal-ice processes relevant for the design of coastal structures and classified them in 15 themes. The most achieved analyses concern the ice properties and the effect of the tide on ice movement in the hinge zone.

The data are also mostly related to the upper 50 cm of the ice, which can reach 300 cm in thickness.

1.4 Organisation

Chapter 2 is a review of the literature on coastal ice and a proposed nomenclature for coastal-ice processes.

Chapter 3 is a summary of environmental conditions at the fieldwork site.

Chapter 4 describes the construction of the breakwater and the installation of the monitoring equipment.

The data from the fieldwork are given in Chapters 5 and discussed in Chapter 6.

1.5 Readership

This thesis is intended at persons studying or working with coastal sea ice—geographers as well as engineers. Engineers may, however, find it to be too theoretical.

It is also of relevance for river-ice engineers who value the importance of season-long observations (Morse et al., 1999).

Chapter 2

Literature review

2.1 Nomenclature

2.1.1 Coastal zone

As noted by Morang and Parson (2002), the nomenclature for coastal zone features is not standardised. The nomenclature used in this thesis is based on a variety of sources, including USACE (2002a), which is illustrated in Figure 2.1. It should be noted that even within USACE (2002a) there are inconsistencies in the definitions.

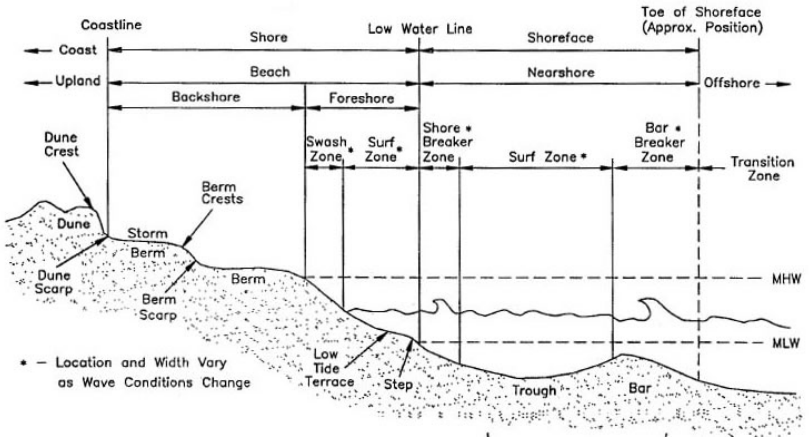

Figure 2.1: Typical beach profile (USACE, 2002a)

Some of the features drawn in Figure 2.1 are defined below.

Backshore: The zone of the shore or beach lying between the foreshore and the upland and acted upon by waves only during severe storms, especially when combined with exceptionally high water (USACE, 2002a).

Coastline: See *shoreline*.

Foreshore: The part of shore that lies between high- and low-water marks at ordinary tide (IHB, 2009).

Low-water line: The intersection of the plane of low water with the shore. The line along a coast, or beach, to which the sea recedes at low water (IHB, 2009).

High-water line: A line or mark left upon tide flats, beaches, or alongshore objects indicating the elevation of the intrusion of high water. The mark may be a line of oil or scum along shore objects, or a more or less continuous deposit of fine shell or debris on the foreshore or berm. This mark is physical evidence of the general height reached by wave run-up at recent high waters. It should not be confused with the mean high water line, which is a calculated value (NOAA, 1999).

Nearshore: Extending seaward or lakeward an indefinite, but generally short distance from the shoreline; specifically said of the indefinite zone extending from the low-water line well beyond the breaker zone, defining the area of nearshore currents, and including the inshore zone and part of the offshore zone. Depths are generally less than 10 m (Jackson and Bates, 1990).

Shore: The shore extends from the low-water line to the normal landward limit of storm wave effects. Where beaches occur, the shore can be divided into two zones: the backshore (or berm) and the foreshore (or beach face) (USACE, 2002a).

Shoreface: The narrow zone seaward from the low-water line, covered by water, over which the beach sands and gravels actively oscillate with changing wave conditions (USACE, 2002a).

Shoreline: Shoreline and coastline refer to the boundary line, in the mathematical sense, between water and land. While *coastline* is generally used to describe the approximate boundaries at large spatial scales, *shoreline* is used to describe its precise location (Schwartz, 2005).

Tidal inlet: An opening in the shore through which water penetrates the land, thereby proving a connection between the ocean and bays, lagoons, and marsh and tidal creek systems. Tidal currents maintain the main channel of a tidal inlet (Schwartz, 2005).

2.1.2 Tide

Datum: For marine applications, a base elevation used as a reference from which to reckon heights or depths (Glickman, 1999).

Ebb: The portion of the tide cycle between high water and the following low water (Glickman, 1999).

Ebb current: The movement of a tidal current away from the shore or down a tidal river or estuary (Glickman, 1999).

Flood (also called rising tide): The portion of the tide cycle between low water and the following high water (Glickman, 1999).

Flood current: The movement of a tidal current toward the shore or up a tidal river or estuary (Glickman, 1999).

High water (popularly called high tide): The maximum water level reached in a tidal cycle (Glickman, 1999).

Lowest astronomical tide (LAT): The lowest level of tide that can be predicted to occur under average meteorological conditions and under any combination of astronomical conditions; often used to define chart datum in places where the tides are semidiurnal (Glickman, 1999).

Low water (popularly called low tide): The minimum water level reached in a tidal cycle (Glickman, 1999).

Mean high water (MHW): The mean height of all the high waters recorded at a given place over a 19-year period or a computed equivalent period (Jackson and Bates, 1990).

Mean sea level (MSL) (popularly called sea level): The arithmetic mean of hourly heights observed over some specified period (Glickman, 1999).

Microtidal: Characteristic of places where the amplitude of the tide is less than two metres (Davis Jr., 16 March 2009; Schwartz, 2005).

Neap tide: A tide of decreased amplitude, occurring semi-monthly one or two days after quadrature (Glickman, 1999).

Quadrature (in astronomy): The arrangement of the Earth, Sun and another planet or the Moon, in which the angle subtended at the Earth between the Sun and the third body, in the plane of the ecliptic, is 90°. The first and third quarters of the Moon are positions of quadrature (Glickman, 1999).

Semidiurnal tide: A tide having two high waters and two low waters each lunar day, with little or no diurnal inequality (Glickman, 1999).

Spring tide: Tide near the time of syzygy, when the height difference between high water and low water is greatest (Glickman, 1999).

Swash: The intermittent landward flow of water up a beach face driven by the action of breaking waves (Glickman, 1999).

Syzygy: The astronomical condition of alignment of the Earth, Moon, and Sun at new and full Moon. At these times the range of tide is greater than average (Glickman, 1999).

Tidal prism: The amount of water that flows into and out of an estuary or bay with the flood and ebb of the tide, excluding any contribution from freshwater inflows (Schwartz, 2005).

Tidal range (or tide range): The difference in height between consecutive low and high water tidal levels, equal to twice the tidal amplitude (Glickman, 1999).

Tidal amplitude: Half of the tidal range (Glickman, 1999).

2.1.3 Ice

As pointed out by Morse et al. (2001) there is no good estuary ice nomenclature. The following nomenclature is based both on river and lake ice terminology and on sea ice terminology.

Active zone: Same as *hinge zone* (Section 2.2.5)

Coastal ice (proposed definition): The zone of the sea ice that is affected by the boundary conditions at the shore.

Degree-day: Also termed freezing degree-day (FDD). A measure of the departure of the mean daily temperature below a given standard, usually 0 °C. For example, one day with an average temperature of –5 °C represents 5 freezing degree-days (USACE, 2002b).

Drifting ice: Pieces of floating ice moving under the action of wind, waves and currents (USACE, 2002b).

Dry crack: Crack visible at the surface but not extending through the ice cover and, therefore, dry (USACE, 2002b).

Fast ice (also called landfast ice): Consolidated solid ice attached to the shore, to an ice wall or to an ice front. It forms when the ice cover in the coastal zone freezes to the shore or when drifting ice. Vertical tidal movement may be occur. It can be preserved without fracturing for two or more years transforming from first-year ice to multiyear ice and even shelf ice. The fast ice width can reach several hundreds of kilometers (WMO, 2007).

Floe: Any fairly flat piece of ice 20 m or more across. Floes are subdivided according to their horizontal extent as follows: giant (over 10 km across), vast (2–10 km across), big (500–2000 m across), medium (100–500 m across) and small (20–100 m across) (WMO, 2007).

Free-floating ice: Sea ice that moves freely with the tide, as opposed to the ice foot or the hinge zone, which tidal movement is restricted due to their proximity to the shore. The term is used in Frederking and Nakawo (1984), though not defined.

Grease ice: A later stage of freezing than frazil ice, when the crystals have coagulated to form a soupy layer on the surface. Grease ice reflects little light, giving the sea a matt appearance (WMO, 2007).

Grey ice: Young ice, 10–15 cm thick. Less elastic than nilas and breaks in swell. Usually rafts under pressure (WMO, 2007).

Grounded ice: Ice that has run aground or is in contact with ground beneath it (USACE, 2002b).

Hinge zone: Zone of the coastal ice where tide cracks occur (Section 2.2.5)

Ice cake: Any fairly flat piece of sea ice less than 20 m across. If it is less than 2 m across, it is called a small ice cake (WMO, 2007).

Ice cover period: Period of the year where the sea is covered with continuous ice. The term *stationary ice cover period* is also found in the literature. For rivers the term *cover* is usually used when the whole width of the river has frozen over.

Ice floe: See *floe*.

Ice foot: A fringe of ice of varied width at the edge of the shores in cold regions (Dionne, 1994). Discussed in Sections 2.2.3, 5.10 and 6.7.

Ice ledge: Narrow fringe of ice that remains along the shores of a river after break-up (IAHR, 1980).

Ice raft: A discrete block of slow-moving land ice that has been incorporated into either an ice stream or an ice shelf (Glickman, 1999).

Ice rind: A brittle shiny crust of ice formed on a calm surface by direct freezing, or from grease ice, usually in water of low salinity. It may be up to about 5 cm thick. Easily broken by wind or swell, commonly breaking in rectangular pieces (WMO, 2007).

In situ break-up: Melting in place (USACE, 2002b).

Hummock: A hillocky conglomeration of broken ice formed by pressure at the place of contact of one ice floe with anther ice floe (WMO, 2007).

Landfast ice: See *fast ice*.

Nilas: A thin elastic crust of ice, easily bending on waves and swell and under pressure, thrusting in a pattern of interlocking 'fingers'—a process called finger rafting. It has a matt surface and is up to 10 cm thick (WMO, 2007).

Pack ice: Any ice at the sea surface, except for fast ice and stamukhas, regardless of its age, form, origin and other characteristics, that has a possibility of movement (drift) under the action of winds, currents and tides. As a result of the dynamic processes (drift, divergence, convergence), the total and partial concentrations of drifting ice constantly change (WMO, 2007).

Pancake ice: Predominantly circular plates of ice from 30 cm to 3 m in diameter, and up to 10 cm in thickness, with raised rims due to their striking against one another. It may be formed on a slight swell from grease ice, shuga or slush or as a result of the breaking of ice rind, nilas or, under heavy swell, of grey ice (WMO, 2007).

Puddle: An accumulation of meltwater on the ice surface, mainly due to melting snow, but in the more advanced stages, also to the melting of ice. The initial stage consists of patches of melted snow (WMO, 2007; USACE, 2002b).

Rafted ice: Type of deformed ice formed by one piece of ice overriding another. When young ice under pressure is forced alternately over and under like thrusting fingers, the ice is termed finger rafted ice (WMO, 2007).

Rotten ice: Ice in an advanced stage of disintegration (WMO, 2007; USACE, 2002b).

Sheet ice: A smooth, continuous ice cover formed by in situ freezing (lake ice) or by the arrest and juxtaposition of ice floes in a single layer (USACE, 2002b).

Shuga: An accumulation of spongy white ice lumps, a few centimetres across. They are formed from grease ice or slush (WMO, 2007).

Slush (also called *snow slush*): Snow that is saturated with water on ice surfaces, or as a viscous mass floating in water after a heavy snowfall (USACE, 2002b).

Snow ice: Ice that has been formed when snow slush has frozen. When it contains air bubbles, it has a whitish appearance (Jackson and Bates, 1990).

Stamukha (grounded hummock): A thick, hummocked grounded ice formation (WMO, 2007).

Stranded ice: Ice that has been floating and has been deposited on the shore by a lowering of the water level (USACE, 2002b).

Thaw holes: Vertical holes in the ice formed when surface puddles melt through to the underlying water (USACE, 2002b).

Tide crack (also called *tidal cracks*): Cracks appearing in the sea ice under the effect of the tidal movement. Defined in Section 2.2.4.

Unconsolidated ice cover: Loose mass of floating ice (USACE, 2002b).

2.2 Literature review: coastal ice

Most engineering literature on sea ice is related to offshore structures. Little work has been done on coastal sea ice. Except for the study of ice forces on the Nanisivik wharf on Baffin Island (Frederking and Nakawo, 1984), most of it relates to ice pile-up and ride-up. The ice conditions observed in Svea turned, however, out to have a number of similarities with river and lake ice. Several studies of static forces on dams and quays are, therefore, of interest (Stander, 2006; Carter et al., 1998, 2001). The literature reviews of river and lake ice research written by Brian Morse and his colleagues also contain valuable information (Morse et al., 1999, 2001; Morse and Hicks, 2005).

2.2.1 Coast vs. shore

Shore and *coast* are often used interchangeably but from a scientific point of view there is a difference of scale. Both describe a strip of land adjacent to a water body but *coast* is used in a theoretical way, for large spatial scales—typically on maps and satellite images—, while *shore* is used in an exact sense: the actual area between the upland and the low-water elevation line (Schwartz, 2005, p. 323). In this thesis, the adjective *coastal* is, therefore, used for processes that are affected by their proximity to the shore, while the adjective *shore* is used for processes taking place in the shore zone. Hence, *coastal ice* refers to the ice foot and the hinge zone, while *shore ice* refers to the ice in the shore zone. Following this nomenclature, *shoreface ice* refers to the ice in the shoreface zone.

In the literature the definition of *shore ice* is generally less exact. The definition of *shore ice* given in Glickman (1999) is unprecise, and of the three definitions given in Jackson and Bates (1990), the one that is closest to that sense is unprecise as well. When used for

river ice, however, a precise definition is found in Michel (1971): “the first type of ice to appear in a river in areas of laminar flow along the banks.”

2.2.2 Coastal-ice conditions

Along open coasts or beyond barrier islands the coastal ice usually consists of a strip of landfast ice held in place by grounded ridges at some distance from the shore, as along the Alaskan Beaufort Sea (Kovacs and Sodhi, 1980; Reed and Sater, 1974). Pack ice is generally found seaward of the rigdes. In embayments, fjords, lakes and shoreward of barrier islands the body of water may be anything from ice-free to covered with drift ice to frozen over, and parts of the shore are covered with an ice foot.

2.2.3 Ice foot

The term *ice foot* was introduced by (Kane, 1856) and comes from the word *isfod*, used by the Danish explorers.

Dionne, a geographer, did a thorough review of definitions of the ice foot found in dictionaries and in the literature (Dionne, 1994). The term *ice foot* has two main meanings. Dionne referred to the Glossary of Geology of the American Geological Institute (Gary et al., 1972) for the first meaning: “the bottom of a glacier front or a bank of snow, hardened or partially transformed into ice, located at the foot of a steep hill”. For the second meaning, which is used in this study, Dionne proposes the following definition: “a fringe of ice of varied width at the edge of the shores in cold regions, entirely or partially attached to the shore (at the bottom or by the side) and affected or unaffected by the vertical movements of the water surface.”

References to the ice foot are found essentially in geographical literature. The engineering literature on the topic is limited. Geographers study the ice foot and, more generally, the coastal ice mainly for its role in shore erosion and sediment transport (Allard et al., 1998; Dionne, 1981; Owens, 1976). From the engineering point of view, the ice foot and the active zone need to be taken into consideration for the calculation of forces on coastal structures (Frederking and Nakawo, 1984).

Different types of ice feet are shown in Figures 2.2, 2.4 and 2.3. Depending to a great extent on shore topography, the size of the ice foot may vary from a small strip of ice like (Figure 2.4) to estuary ice sheets several kilometres wide (Dionne, 1994). Kovacs et al. (1982) and Kovacs and Sodhi (1981) described a 15-m-high, up-to-over-100-m-wide ice foot at Fairway Rock in the Bering Strait, although it would be preferable to call it *pressure ridge* or—a more general term—*shorefast ice*. Both terms are used by George

et al. (2004) to describe the coastal ice along the northern Chukchi Sea from Point Hope to Barrow. For vertical walls or piles, although Frederking and Nakawo (1984) used the term ice foot, the term *ice bustle*, used both by Løset and Marchenko (2008) and by Frederking (1983), is probably more precise.

Figure 2.2: Winter ice foot on a gentle slope in the winter. Between the new and the old harbour of Longyearbyen – 2 March 2005

Figure 2.3: Ice foot on a gentle slope in the spring. Between Carolinedalen and Deltaneset, Isfjorden, Svalbard – 15 April 2006

As Dionne pointed out, three spellings are being used: *ice foot*, *icefoot* and *ice-foot*. He recommended *icefoot* in one word in order to differentiate from the glaciological sense

Figure 2.4: Ice foot on a steep slope in the winter. Port of Longyearbyen – 27 April 2005

written *ice foot* in two words. In this thesis, however, I have chosen to use the two-word spelling *ice foot*, mainly because it is used in WMO (2007), which is a widely adopted reference for terms related to sea and sea ice. Unaware of any grammatical exception that would apply to *ice foot*, I have chosen, as did Morse et al. (2006), to decline its plural as *ice feet*, although Dionne wrote *icefoots*, not *icefeet*.

The very definition of the ice foot is ambiguous. Several authors have proposed to distinguish between different types of ice feet depending on how they were formed: storm ice foot, drift ice foot, stranded-floe ice foot (Wright and Priestly, 1922). Dionne preferred to classify ice feet into "the upper and lower strand ice feet for tidal coasts, or high and low beach ice feet for other water surfaces".

The general absence of consensus is an indication that further work is required to fully comprehend the notion of ice foot and, more generally the coastal-ice processes in the Arctic, from freeze-up to break-up. Short and Wiseman Jr. (1974) made valuable observations throughout a whole season at two sites along the northern Alaskan coast. In this thesis, a similar approach was adopted to describe the coastal ice at Barryneset. Observations from the 2006–07 season at Barryneset are used to further discuss the concept of ice foot in Sections 5.10 and 6.7.

2.2.4 Tide cracks

Tide cracks, often called *tidal cracks*, are cracks appearing in the sea ice under the effect of the tidal movement. Dionne (1994) also used the term *tide crevasse*. To simplify matters,

the coastal ice may be considered as a plate fixed to land along one side and freely moving with the tide along the opposite side. As the ice grows, bending stresses increase, and the plate eventually yields.

Tide cracks are mostly parallel to the shore, although meanders in the shoreline, such as the corners of the breakwater at Barryneset, may cause shore-perpendicular cracks as well (Figures B.46, B.47 and B.48).

WMO (2007) defined a tide crack as "a crack between fast ice subject to sea level tidal rise and fall and the fast ice foot or ice wall, or shore". Unfortunately this definition does not take into account the fact that there are often more than just one tide crack.

References to tide cracks are found both in sea ice literature (Charlesworth, 1957; Owens, 1976) and in the literature on water reservoirs (Stander, 2006; Carter et al., 1998).

Carter et al. (2001) proposed a method to calculate the distance between the tide cracks (Section 6.6).

2.2.5 Hinge zone

Tide cracks are acting like hinges, therefore, Owens (1976) and Forbes and Taylor (1994) called *hinge zone* the zone of the coastal ice where they occur. In the polar literature, the term *hinge zone* is also used to describe the zone between a grounded glacier ice sheet and a floating ice shelf (Vaughan, 1995).

The term *active zone* is sometimes used in the engineering literature. Frederking and Nakawo (1984) used it to refer to the hinge zone in their study of the ice surrounding the Nanisivik wharf. Croasdale (1980), on the other hand, used it to refer to the zone of ice failure seaward of the grounded ice belt surrounding an artifical island.

In this thesis, the zone of the coastal ice where tide cracks occur is called *hinge zone* rather than *active zone* because *hinge zone* is more illustrative.

The tidal movement of the hinge zone generates stresses in the ice. Frederking and Nakawo (1984) studied the hinge zone surrounding the piles of the Nanisivik wharf and, although they did not measure the ice pressure directly, estimated it to be of the order of 70 kPa. Nikitin et al. (1992) measured stresses perpendicular to the tide cracks in a hinge zone along the coast of the Okhotsk Sea. The tidal range was 1.25 m and they reported that the stresses were varying between 100 and 300 kPa depending on the tide. Carter et al. (2001) also observed that water level fluctuations were creating static stresses in five dams of northern Québec. Stander (2006) measured them in the La Gabelle reservoir in Quebec and found that they were increasing by 50 kPa per millimetre of water level rise.

Horizontal movements in and around the hinge zone were also observed during several studies. Carstens et al. (1979) and Instanes (1979) recorded movements around Kapp Amsterdam in Svea, Svalbard. Frederking and Nakawo (1984) measured the horizontal movement at Nanisivik wharf, where the growth of the active zone was more than 5 m during a winter season. Based on measurements from Adams Island and Pond Inlet, both at the northern extremity of Baffin Island, it seems that Stander et al. (1988) proved that the horizontal movement of the ice close to the shore was partly caused by *tidal jacking*, which "occurs by the adfreezing of sea water along the vertical surfaces of dilatating shore parallel cracks during the falling tide, and subsequent closing of these fractures during the rising tide". They thus verified the hypothesis made by Frederking et al. (1986), which is the oldest reference to *tidal jacking* that I was able to find. According to Stander (2006), the stresses measured in the La Gabelle reservoir were also caused by tidal jacking.

2.2.6 Superimposed ice

In their widely used classification of ice, Michel and Ramseier (1971) defined *superimposed ice* as being "caused by flooding of the ice cover from any imaginable water source" and added that "if there is snow on the ice surface, snow ice may form." Thus, *snow ice* appears to be a type of superimposed ice. It is sometimes called *white ice* (Ledley, 1985). Frederking and Nakawo (1984) used the term *flooded ice* for superimposed ice formed in the absence of snow.

Granskog et al. (2004) restricted the term *superimposed ice* to ice that "forms solely of snowmelt water [...] or from liquid precipitation."

Superimposed ice is also used in glaciology to describe "ice exposed at the surface of a glacier that was formed by the freezing of melted snow after deposition" (Glickman, 1999).

Given the wide use of the classification found in (Michel and Ramseier, 1971), their definition is used throughout the thesis.

Chapter 3

Studied area

3.1 Place names

The following definitions are based on NPI (2003)

Braganzavågen: The northernmost inner part of Van Mijenfjorden. Braganzavågen is a tidal bay almost separated from the fjord by Credenermorenen but connected to Sveabukta through Sveasundet.

After Aldegonda, née Princess of Braganza, 1858–1946, married 1876 to Prince Henry of Bourbon, leader of expeditions to Spitsbergen and Novaya Zemlya in 1891 and 1892. The Princess accompanied the expedition in 1892.

The Norwegian word *våg* means *bay*.

Barryneset: Point between Bragazavågen and Sveasundet.

After Richard Ritter von Barry, born 1861. Austrian naval officer, admiral, then lieutenant, master of the ship of Prince Henry of Bourbon's expeditions to Spitsbergen and Novaya Zemlya 1891 and 1892.

Svea residents used to call it *Høvdingodden*—the Chief's Point.

The Norwegian word *nes* means *headland*.

Crednermorenen: Large, ice-cored moraine, about 4 km long, east of Van Mijenfjorden and Sveabukta, deposited by the Paulabreen glacier, which calves into Rindersbukta, the southernmost inner part of Van Mijenfjorden.

After professor Herman Credner, 1841–1913, German geologist.

The Norwegian word *morene* means *moraine*.

Ispallen: 805-m-high, partly-snow-covered, coal-rich mountain on the eastern side of Braganzavågen.

Kapp Amsterdam: Point on the north-western side of Sveasundet from where coal is shipped today.

A/B Svea's steamer *Amsterdam* arrived and anchored 300 m from the point on 11 August 1917, and the point was later named Kapp Amsterdam.

Kjellströmelva: River through Kjellströmdalen.

The Norwegian word *elv* means *river*.

Kjellströmdalen: About-27-km-long, ice-free valley debouching into Braganzavågen.

After Carl Johan Otto Kjellström, 1855–1913, Swedish topographer, member of Swedish geologist and arctic explorer A. E. Nordenskiöld's expedition to Greenland 1833, and of Nathorst's expedition to Bjørnøya and Spitsbergen 1898.

The Norwegian word *dal* means *valley*.

Liljevalchfjellet: About-10.5-km-long mountain ridge west of Svea, with the highest peak at 941 m, and the northernmost peaks called Deinbolltoppane.

After Carl Fredrik Liljevalch, 1837–1909, Swedish business man, patron of science, who gave donations to Stockholms Högskola.

The Norwegian word *fjell* means *mountain*.

Sveagruva (or just *Svea*): Coal-mine settlement innermost in Van Mijenfjorden on the lowland between Liljevalchfjellet, Braganzavågen and Sveabukta.

Formerly owned by Svenska Stenkolsaktiebolaget Spetsbergen (1917–25). The property was purchased in 1934 by Store Norske Spitsbergen Kulkompani Aktieselskap, Oslo.

Swedish magnetic and aerological station at Sveagruva during the Second International Polar Year 1932-33.

After *Svea*, the old name of *Sweden*.

The Norwegian word *gruve* means *mine*.

Svea Nord: Coal mine next to Svea. Opened in 2001. The production in 2009 was 2.6 million tons.

Sveasundet: About-2-km-long sound between Sveabukta and Braganzavågen.

The Norwegian word *sund* means *sound*.

Van Mijenfjorden: 83-km-long fjord on the western coast of Spitsbergen.

After Willem Van Muyden, chief of the Dutch whaling fleet 1612–13. Nordenskiöld mistakenly wrote his name Van Mijen, and that spelling has been used since.

Figure 3.1: Map over the Svea area – Courtesy of Store Norske Spitsbergen Grubekompani

3.2 Svea and Ispallen

3.2.1 Svalbard

Svalbard is an archipelago between Northern Norway and the North Pole under Norwegian sovereignty as stipulated in the Spitsbergen Treaty of 9 February 1920. The main island is called Spitsbergen. Svalbard was supposedly discovered by the Norse in the 12th century and rediscovered in 1596 by the Dutchman Willem Barents. During the 17th and 18th centuries, whaling was the main activity. During that period, Pomor trappers also came to the area. The 20th century saw the start of coal mining, which is still going on today. Tourism and research developed from the end of the 20th century. The administrative *capital* is Longyearbyen, a Norwegian settlement with 1500–2000 inhabitants. There

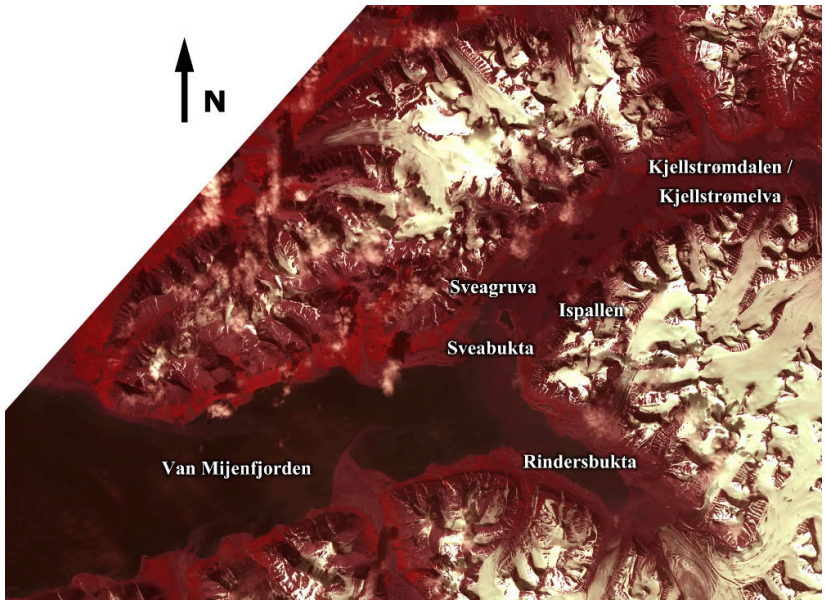

Figure 3.2: Satellite picture over the Svea area – 23 July 2005 (ASTER Data Purchased by UNIS from LP DAAC)

is a smaller Russian settlement called Barentsburg, an international research station in Ny Ålesund, a mining camp in Sveagruva and a Polish research station in the southern part of Spitsbergen (Figure 3.4).

3.2.2 Svea

The first mine in Svea, *Sveagruvan*, was started in 1917 by a Swedish company. It was bought by Store Norske in 1934. By the turn of the 21st century, Store Norske opened a new mine, Svea Nord, which it has been operating since. Annual production in 2009 was about 2.6 million tons. Plans for opening a new mine in Lunckefjellet, between Svea and Longyearbyen, are well under way. Further ahead, Ispallen, 4 km south of Svea, is a prospect with an estimated gross production potential of 11 million tons of coal.

3.2.3 Research in Svea

Since 1979 the quay infrastructure at Kapp Amsterdam has been the object of several studies (Carstens et al., 1979; Instanes, 1979; Moslet, 2001).

Figure 3.3: Arctic Ocean (Schwartz, 2005)

Figure 3.4: Svalbard (source: U.S. Central Intelligence Agency)

In the past years Svea has been a site of choice for ice mechanics research at UNIS thanks, to a great extent, to the goodwill of Store Norske. The site is ideal for several reasons. Contrary to Longyearbyen, in Svea there is sea ice every winter. Board and lodging is arranged in agreement with Store Norske. Last, but not least, there are several workshops and heavy machinery is available.

A few years ago, Moslet and Liferov performed experiments on ice-structure interactions and ridges, respectively (Moslet, 2007a), (Liferov, 2005). Sébastien Barrault continued the research on the thermal expansion of the ice initiated by Teigen, Høyland and Moslet (Teigen et al., 2005). In 2008 Aleksey Shestov started to study the tidal flow in Sveasundet with his supervisor Aleksey Marchenko. Every year the courses in arctic technology at UNIS perform fieldwork in Svea. Høyland (2009) summarised the measurements of the ice conditions in Van Mijenfjorden and Sveabukta from 1998 to 2006.

In recent years geologists and biologists have also performed fieldwork in Svea. Lene Kristensen studied the surge-type glacier Paulabreen and its associated late Holocene terrestrial and submarine moraines (Kristensen, 2009).

3.3 Barryneset: physical environment

This section is a summary of meteorological and geographical conditions at Barryneset and its surroundings. The instruments and methods used are described in Section 4.2.

3.3.1 Geography

Barryneset is a headland between Braganzavågen and Sveabukta, on the north side of Sveasundet. Braganzavågen is a tidal flat at the mouth of Kjellströmelva near Svea, and Sveabukta is the northern inner arm of Van Mijenfjorden. Sveasundet is 690 m wide at its narrowest, between Barryneset to the north and Littrowneset, a headland on Credner-morenen, to the south.

3.3.2 Climate

The characteristics of the high-arctic climate of Svea (77°54'N) are given in Table 3.1 and Figure 3.7. The snow cover is seldom more than a few decimetres thick due to a combination of little precipitation and frequent wind. The wind is seldom stronger than 15 m s^{-1}, and about 40 % of the time, it is blowing from the 15–45° sector (Figure 3.5).

The polar night lasts for 4 months (26 October to 16 February). During this period, northern lights (Figure 3.6) occur regularly.

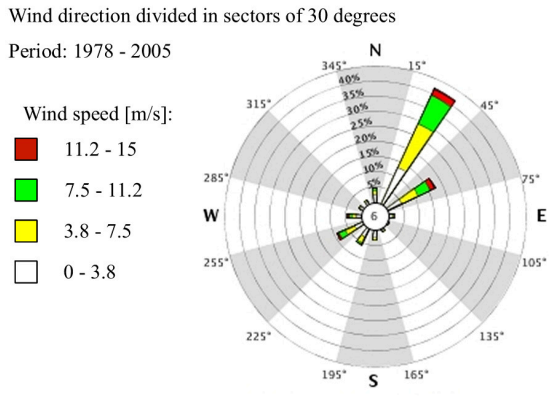

Figure 3.5: Wind rose for Svea (1978–2005)

Figure 3.6: Northern light at Barryneset – 16 January 2009

Annual precipitation	266 mm
Winter precipitation	175 mm
Summer precipitation	91 mm
Maximum snowdepth	106 cm
Mean air temperature	–5.9 °C
Maximum air temperature	+15.2 °C
Minimum air temperature	–43.5 °C
Maximum hourly mean wind speed	21.1 m s^{-1}

Table 3.1: Key figures of the climate in Svea (1 May 1978 to 31 October 2002) (Rike, 2003)

3.3.3 Ice conditions

The maximum yearly ice thickness in Sveasundet between 1998 and 2006 varied between 0.72 and 1.28 m. The sea usually freezes over between November and January, reaches its maximum thickness in mid-May and breaks up between the middle of June and the middle of July (Høyland, 2009).

During freeze-up, a sizeable amount of ice is generated in the shallow waters of Bragan-zavågen and transported into the fjord with the tidal current. From what I understand—based on a discussion with a person who used to work in Svea in the 1980s—anchor ice may occur in Sveasundet.

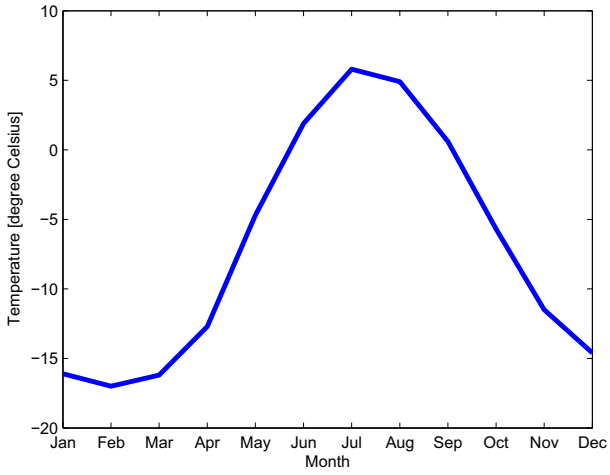

Figure 3.7: Monthly mean air temperature in Svea (1975–1990 mean)

3.3.4 Waves

Because Sveabukta is approximately perpendicular to the rest of Van Mijenfjorden, the waves are essentially wind-generated. The fetch from the Braganzavågen direction is about 1 km. The fetch from the opposite direction is found in Table 3.2.

Wind direction range [°]	Fetch [km]
187–207	10–13
207–223	3

Table 3.2: Longest fetch, from the Van Mijenfjorden direction

The fetch in the 187–207° direction range is by far the longest. The wind statistics in that range are plotted in Figure 3.8. The significant daily maximum hourly mean wind speeds for 10 and 50 years are 10.0 and 11.0 m s^{-1}, respectively (Section A.2.5). The corresponding significant wave heights and peak periods are calulated with the method found in (Vegvesen, 1981) (Table 3.3).

3.3.5 Tide

The tide is semidiurnal and its range is microtidal—less than 2 m (WMO, 2007)). Key figures for the tide in Svea are summed up in Table 3.4. They were obtained from the

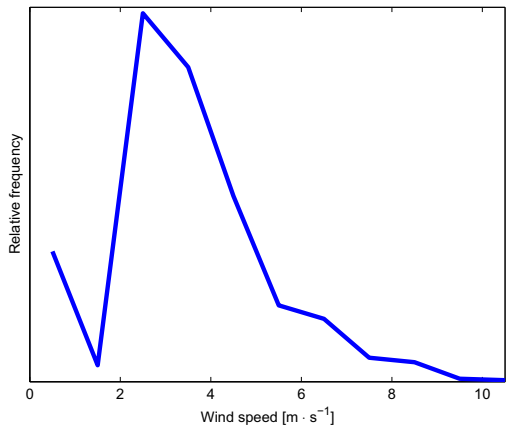

Figure 3.8: Frequency of the daily maximum hourly mean wind speed in the direction range of longest fetch (187–207°) – 1996–2005

Return period [yr]	Significant wave height [m]	Peak period [s]
10	0.70	3.4
50	0.79	3.5

Table 3.3: Significant wave heights and peak periods for 10 and 50 years return period

analysis of the tide data collected at Barryneset (Section 4.2.2).

3.3.6 Tidal current

The tidal prism may be estimated by modelling Braganzavågen as a quadratic area of $4 \cdot 4$ km with a constant slope, the north-east end being at MHW and the middle of the bay at MLW. The vertical cross-section along the north-east direction is then a trapezium with a height equal to the tidal range (1.1 m), the long base equal to the length of the bay (4 km) and the short base equal to its half. The tidal prism is the product of the surface of the trapezium with the width of the bay (4 km):

$$V = 1.1 \cdot \frac{(4+2) \cdot 10^3}{2} \cdot 4 \cdot 10^3 = 1.3 \cdot 10^7 \,\mathrm{m}^3 \tag{3.1}$$

Parameter name	Value [m]
Mean sea level	–0.28
Minimum tidal range	0.30
Maximum tidal range	1.96
Mean tidal range	1.13
Mean high water level (MHW)	0.29
Mean low water level (MLW)	–0.84
Highest observed water level (HOW)	1.13
Lowest observed water level (LOW)	–1.55
95 %-interval	–1.04 to 0.48
90 %-interval	–0.95 to 0.39
80 %-interval	–0.83 to 0.27

Table 3.4: Key figures for the tide in Svea based on data from 22 October 2006 to 27 October 2008 – The choice of datum is explained in the Conventions section.

The mean flow rate is:

$$q = \frac{V}{T} = \frac{1.3 \cdot 10^7}{(6.5 \cdot 3600)} = 560\,\mathrm{m^3\,s^{-1}} \tag{3.2}$$

Considering that Sveasundet is 690 m wide and 1.8 m deep in average, the cross section is:

$$A = 690 \cdot 1.8 = 1240\,\mathrm{m^2}, \tag{3.3}$$

and the mean flow velocity is

$$v = \frac{q}{A} = 0.5\,\mathrm{m\,s^{-2}} \tag{3.4}$$

This figure is comparable with the maximum values Marchenko and Shestov (2007) measured with an acoustic Doppler current profiler (ADCP).

3.3.7 River discharge

Lund (2005) made a first estimate of the river discharge using a numerical model calibrated with snow measurements from a single season. He found that the maximal yearly

discharge for the period from 1989 to 2004 varied between 120 and 270 m^3 s^{-1}. For 2004, the flow started in the first half of June and reached 100 m^3 s^{-1} by 1 July. In 2003, the river practically stopped flowing (less than 5 m^3 s^{-1}) by the middle of September.

Figure 3.9 shows Kjellströmelva on 22 June 2005, 4 days before the start of the break-up.

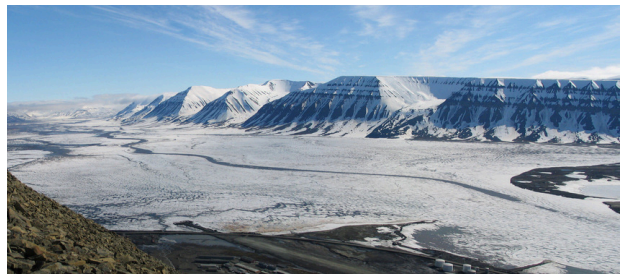

Figure 3.9: Braganzavågen, in the middle, and Kjellströmdalen and Kjellströmelva, to the left . The mountain on the right side is Ispallen – 22 June 2005

3.3.8 Permafrost

Gregersen and Eidsmoen (1988) measured negative temperatures down to at least 100 m in a borehole near the shoreline at Kapp Amsterdam, characterised the permafrost near the shore as *warm* and created a model that rejected the possibility of offshore permafrost. Based on seabed soundings, Finseth et al. (2002) were of the same opinion: they assumed there is a tongue of permafrost extending to the nearshore zone but not to the entire bay. Kristensen et al. (2008) (Paper 3), however, proposed a model, based on a series of water temperature measurements in addition to ground temperature data from boreholes in Crednermorenen, which suggests that there is a thin layer of subsea permafrost.

3.3.9 Seabed profile

Sveasundet consists of two 4.5-m-deep canals separated by a 1-m-deep ridge. Close to Barryneset the water depth is 3 m +/- 20 % (Figures 3.10 and 3.11).

3.3.10 Seabed properties

The seabed, from Barryneset and toward the eastern side of Crednermorenen (160° direction), consists of a 1.5-to-3.5-m-thick soft layer on top of a hard layer (Finseth, 2002b;

Figure 3.10: Seabed elevation map of Sveasundet – 25 July 2006 – Courtesy of Norges Geologiske Undersøkelser (NGU)

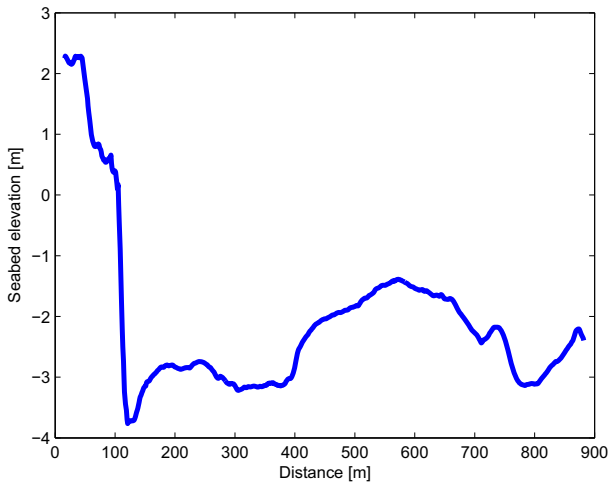

Figure 3.11: Seabed elevation profile across Sveasundet (breakwater to the left, Credner-morenen to the right) – 25 July 2006 – Courtesy of Norges Geologiske Undersøkelser (NGU)

Finseth et al., 2002; Finseth, 2002a). Figure 3.12 shows the seabed composition and profile up to 120 m seaward of Barryneset.

The water content of the soft layer is about 40 %. The layer consists of up-to-10-cm-thick layers of clayey silt—85–90 % silt, 5–10 % clay and 5 % sand—of varying softness. It does not extend beyond about 60 m seaward of Barryneset, probably because the tidal flow velocities in the rest of Sveasundet are too high to allow sedimentation.

The hard layer contains coarser materials and its penetration resistance is increasing with depth.

300–500 m to the west of Barryneset, the seabed is at 10 to 15 m below water level (Finseth, 2002b).

Bæverfjord and Thakur (2006) analysed the stability of the seabed.

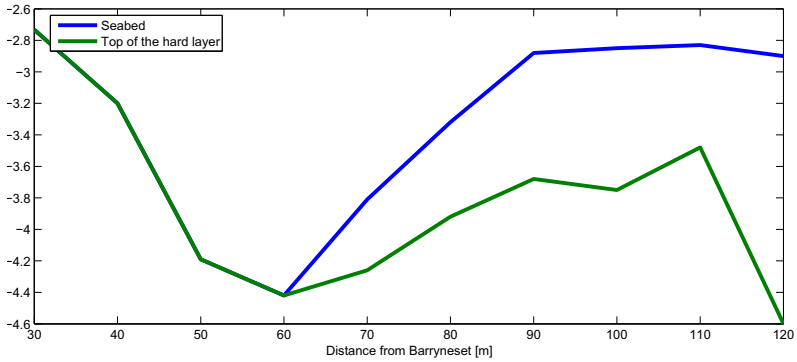

Figure 3.12: Elevation and composition of the seabed up to 120 m seaward of Barryneset (profile oriented along the 160° direction) – the underlying data are given in Table A.3.

3.3.11 Sedimentation

As seen in Figure 3.13, Kjellströmelva carries a high amount of sediments into Braganzavågen and Sveabukta.

There are pictures from the beginning of the 20th century of large sailboats inside Braganzavågen in a place that is so shallow today that it is not possible to get there with a small rowing boat. In addition, while inner Braganzavågen was drawn as shallow sea on the 1983 map of the Svea area—drawn from orthophotos from 1936 and 1938—, it was drawn as land on the 2008 map—drawn from orthophotos from 1990 and 1995.

The marine map of Sveasundet is based on measurements from 1948. According to a note on the map, control soundings performed in 1975 showed appreciable sedimentation compared to 1948. To my knowledge Sveasundet was not sounded during the recent mapping campaign.

At the harbour of Kapp Amsterdam dredging is required every few years.

Figure 3.13: Orthophotography of the Svea area – Summer 2006

3.3.12 Fauna

The presence of polar bears and reindeers must be taken into consideration when installing equipment in the field. In December 2008 a polar bear caused substantial damage at the measurement site. He severed most of the exterior cables and broke the solid steel arm that was holding one of the video cameras. I never found back the camera. In the course of the PhD, reindeers or bears also severed two thermistor cables on Crednermorenen.

Chapter 4

Fieldwork

4.1 Construction

A breakwater was built at Barryneset in order to reproduce ice conditions similar to those that would occur along a causeway going from Barryneset to Crednermorenen. The construction started in 2005 but was interrupted after a fire broke out in the Svea Nord mine. It was resumed and finished in 2006. The structure was 50 m long and oriented along the 132° direction. Its top was 5 m wide and 3.2 m above datum except for the last 15 m, which 1.6 m above datum. The slopes were 1V:3.5H (Figure 4.1). Since the part built in 2005 was oriented along the 160° direction, its tip stuck out at the west corner (Figure 4.3). The total volume of dumped masses was of the order of 7000 m^3. The masses were carried by trucks and laid out with an excavator.

4.1.1 2005-fill

The fill was built between 1 and 3 April 2005. It was 50 m long, 12 m wide at the top for the first 25 m and 5 m wide for the last 25 m. The altitude of the top was 0.0 m and it was oriented along the 160° direction, which is the direction of one of the route alternatives proposed in (Larsen, 2004). The masses used—about 1000 m^3—were from the tunnel built between Svea and Svea Nord. The slope was approximately 1V:1H.

4.1.2 2006-breakwater

In 2006 the masses were taken from the mountainsides surrounding Svea. They were placed with an excavator that had a too short reach (7 m) to make it possible to shape the slope the bottom of the breakwater. The angle was, therefore, the (underwater) friction angle.

Following investigations of the soil conditions on Crednermorenen (Kristensen et al., 2008) (Paper 3), the route alternative along the 132° direction—from Barryneset to the north-west end of Crednermorenen—stood out as the best one from a geotechnical perspective. Therefore, the breakwater was built in that direction.

The breakwater was built in two phases in order to prevent pore pressure buildup.

Phase 1: 26–29 June 2006 The breakwater was built up to a height of 0.45 m—16 cm above MHW. It was 50 m long and 25 m wide at the top. It was compacted with a wheeled loader equipped with a compacting roll. Due to the inhomogeneity of the masses, compaction was difficult.

Phase 2: 10–13 August 2006 The breakwater was built to full height—3.2 m—except for the last 15 m, which were kept at 0.45 m to facilitate the placement of the lower geosynthetic bags (Section C.3).

A slope failure occurred along the west side of the breakwater on 15 August 2006 (Figure 4.4). Due to a lack of seabed topography data elsewhere than along the 160°-line, it was difficult to model the failure with good precision. Andreassen's proposed model showed that the breakwater load caused a seabed failure, which, in turn, propagated to the breakwater (Røsvik Andreassen, 2006). It is reasonable to assume that the seabed was softer below the failed slope than elsewhere below the breakwater. This, combined with a gradual accumulation of masses at the toe, may have prevented the failure to spread to the whole embankment.

Phase 3: 25 August 2006 A survey of the slope at the tip of the breakwater showed that it was steeper than planned. Since the 7-m excavator reach was too short to reach the bottom of the slope it was decided to remove a 2-m-wide strip from the upper tip of the breakwater, creating a step-like slope.

Phase 4: 30 August 2006 After placement of the lower rows of geosynthetic bags (Section C.3), the tip of the breakwater was elevated to 1.6 m. Following the failure along the west side of the breakwater, I decided, for safety reasons, to limit the risks and not build the toe to full elevation (3.2 m).

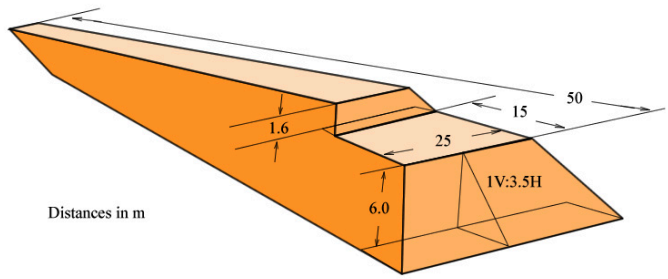

Figure 4.1: Sketch of the breakwater

Figure 4.2: “Barge” used for marine operations in preparation of the construction of the breakwater

4.2 Instrumentation and site investigations

The present section sums up the instruments and methods used to collect some of the data presented in Section 3.3.

4.2.1 Cabin

A small cabin was installed at the tip of the breakwater and served as a shelter for data-logging equipment. It was connected to the power grid and equipped with a wireless

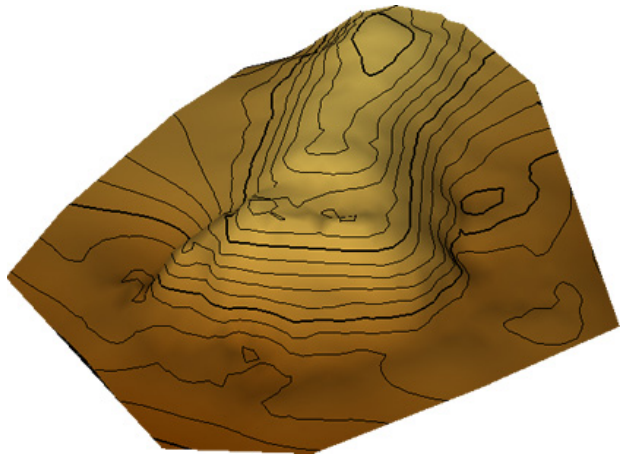

Figure 4.3: 3D view of the breakwater (height scale factor: 3) – Courtesy of Tine Larsen

Figure 4.4: Aerial view of the breakwater – 30 August 2006

internet connection. During my weekly visits to Svea in the winter of 2006–07, I also used it as an office. Having a warm cabin proved to be an invaluable asset: it made it possible to stay at Barryneset for longer periods of time, which was necessary for observing ice processes over a full tidal cycle.

4.2.2 Tide and waves

Tide is monitored several places in Svalbard but not in Van Mijenfjorden. As a rule of thumb, the tide in Longyearbyen is one hour ahead of the tide in Svea and both have the same range. In order to better quantify the difference between the two tidal regimes,

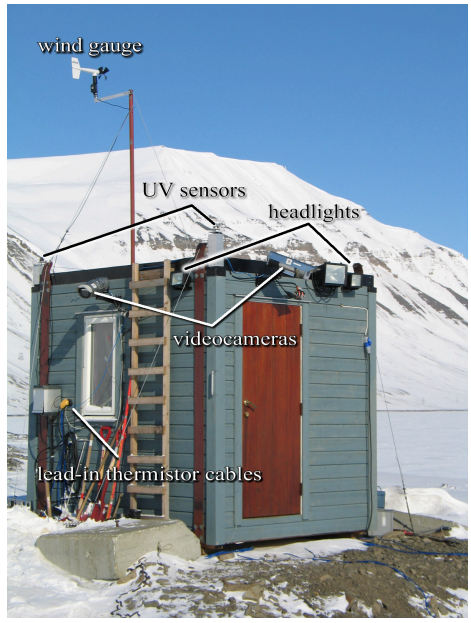

Figure 4.5: Measurement cabin – 5 May 2007 (week 18)

we mounted a tide and wave gauge (SBE 26 Plus from Seabird Electronics, Inc.) on a steel frame and installed the frame in a fixed position by pressing its 25-mm-in-diameter vertical legs into the soft seabed. It was necessary to install the gauge on the seabed since there was no pontoon close by. The instrument depth was –2.71 m and its position 8647026N – 541044E (measured with 20 m precision with a handheld GPS).

Tide data were recorded continuously and the average stored every 20 minute. The recording period was from 21 October 2006 to 29 October 2008 with one interruption to upload the data on 10 September 2007. The data upload required a diver to unscrew the gauge and bring it to land, then dive again to put it back in place. Since the sight in the sediment-rich waters outside Barryneset is usually close to zero, a steel chain was put on the seabed between Barryneset and the frame of the tide gauge. By following the chain, the diver could easily find the frame. Due to the strong tidal currents, the diving had to be done around slack water.

4.2.3 Thermistor cables

The ground temperature was recorded hourly with 5 thermistor cables (C1–C5) from EBA Engineering Consultants Ltd. as shown in Figures 4.7, C.9 and C.10.

Figure 4.6: Tide gauge mounted on the steel frame

I installed cables C1, C2 and C3 each inside a different geosynthetic bag; they entered the respective bag from beneath, in the middle and were perpendicular to the slope.

Cable C4 was placed along the slope, underneath the filter layer and the nineteenth bag column (bags 76 to 80). It was attached to the filter layer with plastic strips. A fifth bag row was installed at the bottom of the three columns of bags surrounding C4 to prevent the end of the cable from floating freely. The lowest thermistor, C4T16, was, however, lower than the lowest bag and its position may, therefore, have been affected by waves, current, ice and the tide.

Cable C5 was placed in a vertical hole, approximately 6.5 m inwards from the crest of the slope at the tip of the breakwater.

The approximate altitudes of the thermistors are given in Table 4.1.

C1, C2, C3 and C4 were connected to a Campbell Scientific CR10X datalogger while C5 was connected to a Lakewood Inc. datalogger. Both loggers were located inside the cabin.

The thermistors on each cable are named *CnTmm* where *n* is the cable number and *mm* is the thermistor number.

4.2.4 Weather observations

The Norwegian Meteorological Institute (DNMI) has a weather station at the Svea Airfield, 700 m to the north-west of Barryneset, which records air temperature and pressure,

Thermistor name	Altitude [m]
C1T03	0.4
C1T04	0.6
C1T05	0.7
C1T06	0.8
C2T03	–0.3
C2T04	–0.1
C2T05	0.0
C2T06	0.1
C3T03	–0.1
C3T04	0.1
C3T05	0.2
C3T06	0.3
C4T08	0.4
C4T09	0.0
C4T10	–0.2
C4T11	–0.7
C4T12	–0.9
C4T13	–1.4
C4T14	–1.8
C4T15	–2.1
C4T16	–2.3
C5T12	1.88
C5T13	0.88
C5T14	–0.12
C5T15	–1.12
C5T16	–2.12

Table 4.1: Altitude of the thermistors

among others. The data is retrievable from eKlima, an open-access climate database (eKlima, 2009).

The quality of pressure data series retrieved from eKlima was unsatisfactory so I installed a Setra Barometric Pressure Sensor model 278 (sold by Campbell Scientific under the name CS100) in the cabin and connected it to a Campbell Scientific CR10X data logger. The pressure data was needed to process the tide gauge data.

I also installed a wind gauge because the wind conditions can vary appreciably between

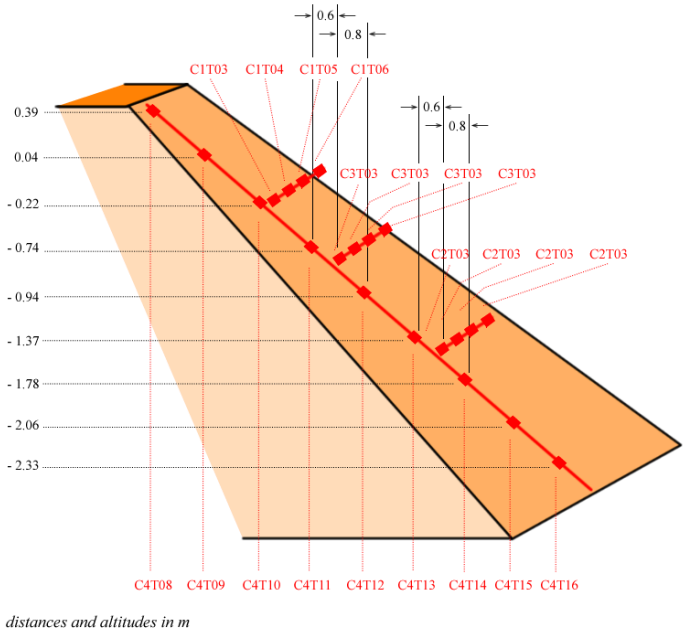

Figure 4.7: Set-up of thermistor cables C1, C2, C3 and C4

Barryneset and the DNMI station. Figure 4.5 shows the mast with the wind gauge.

4.2.5 Video cameras

I installed two Axis 211 surveillance cameras in heated boxes and mounted them to the walls of the cabin, one pointing toward the west side, the other toward the tip. The cameras took VGA-quality pictures every minute during the whole season. I also mounted a 500-W halogen headlight next to each of them in order to light up the areas covered by the cameras.

Although the cameras were placed in heated housings, there where periods when the housing window was covered with snow. In some periods, stalactites also formed along the brim surrounding the window. Still, most of the time the sight was good. The lack of autofocus was a major drawback. Apart from the fact that setting the focus was tedious, it kept going wrong after a few days and required regular adjustments.

4.2.6 Time-lapse cameras

I installed a Harbortronics time-lapse camera on top of Liljevalchfjellet. It took a picture of Sveasundet every hour during the pre-break-up and the break-up. I processed the pictures into time-lapse videos. Figure 4.8 shows the camera box and the view from Liljevalchfjellet.

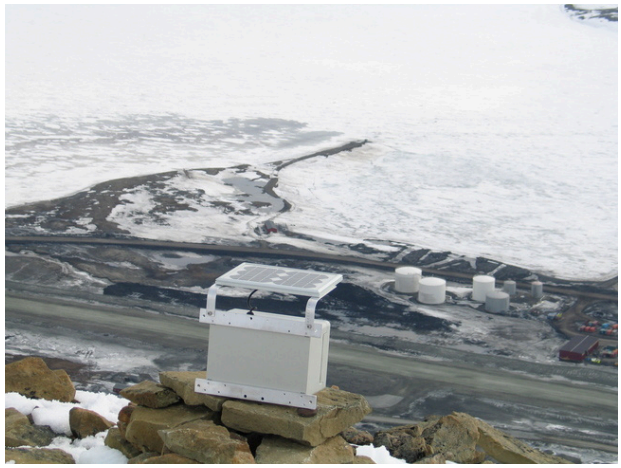

Figure 4.8: Time-lapse camera on Liljevalchfjellet, above Svea, taking pictures of the sea ice in Sveasundet – 22 May 2007 (week 21)

4.2.7 Stress sensors

Sébastien Barrault and I installed BP stress sensors (Moslet and Høyland, 2003) in the hinge zone along the tip of the breakwater in order to measure stresses in the ice on both sides of a tide crack. The full set-up is described in detail in Caline and Barrault (2008) (Paper 1).

4.2.8 Differential GPS

Although a total station was used in the start of the project, most surveys were done with differential GPS (DGPS) equipment from Leica (DGPS 1200 model). The accuracy was of the order of 1 cm.

4.2.9 Seabed properties

Along the planned location of the breakwater, I probed the seabed by hand from the sea ice using a steel rod. The measured soft layer thickness is found in Figure 3.12.

Lars Grande, Philippe Delmas and I performed a vane test of the soft layer from the ice 140 m seaward of Barryneset on 2 May 2006. We used a Geonor vane with 110 x 55 mm blades. The point position, measured with 20 m precision with a handheld GPS, is given in Figure 4.9. The seabed elevation was –3.0 m and the thickness of the soft layer 2.85 m. The results from the vane tests are given in Figure 4.9.

WGS84, UTM zone 33X	
Northing [m]	8647087
Easting [m]	541089

Table 4.2: Location of the vane test

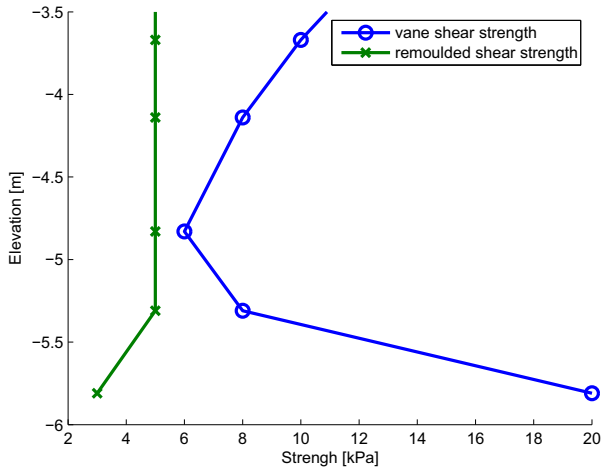

Figure 4.9: Results from a vane test 140 m seaward of Barryneset – the underlying data are found in Table A.4

4.2.10 Seabed profile

The seabed profile was measured with a shallow-water swath bathymetry system (GeoSwath) on 25 July 2006 during a seabed measurement campaign in Van Mijenfjorden organised

by the Norwegian Geological Survey (NGU) (Ottesen et al., 2008). Louise Hansen (NGU) kindly processed the data.

My field assistants and I did additional soundings by hand, close to the breakwater, where it was too shallow to measure with the GeoSwath. Depending on the season, we measured either with a steel rod, either from the ice or from a small boat. When measuring from a boat, the precision was probably around 2 m, while it was of the order of 10 cm when measuring from the ice.

4.2.11 Ice properties

Magnus Gabrielsen (UNIS), Sébastien Barrault (UNIS) and I investigated the properties of coastal and free-floating ice in Svea during the winter of 2007. Such data help understand how the ice forms and are invaluable for the creation of numerical models.

We took a total of 33 cores, of which we measured both physical and mechanical properties. The work was presented at the 19th IAHR International Symposium on Ice in 2008 (Gabrielsen et al., 2008) (Paper 2).

Fieldwork

On 13 and 14 February 2007, we measured the temperature in two vertical ice cores on each side of crack 1: C3, 0.3 m shorewards of the crack, and C5, 2.1 m seawards. The ice at the location of C3 was 0.8 m thick, and the core went all the way from the top to the bottom; at the location of C5, the ice was 1.3 m thick, and only the upper 90 cm were cored. We measured the salinity in two cores on each side of crack 1: C3 and C4, which was located 1.0 m seawards of the crack.

On 14 and 21 March 2007, we took 6 horizontal ice cores of the free-floating ice, at a site situated in Sveabukta (Pt5), approximately 2.5 km to the south-west of Barryneset. On 19 April, we took 24 horizontal cores at 4 different locations in the hinge zone (Pt1, Pt2, Pt3 and Pt4), along a line perpendicular to the tip of the breakwater (Figures 4.10 and 4.11). The points were respectively 3, 6, 10 and 15 m seaward of crack 1. At all locations we took cores at the following depths from the ice top: 10 cm (H1), 30 cm (H2) and 50 cm (H3). All samples had a diameter of 70 mm and a length of 170 mm. We transported them in sealed plastic bags to a –20 °C storage room at UNIS. The time from sampling to storing was between 3 and 5 hours and the temperature was kept below the freezing point all the time. The samples were stored up to three weeks before testing. All samples were tested at –10 °C.

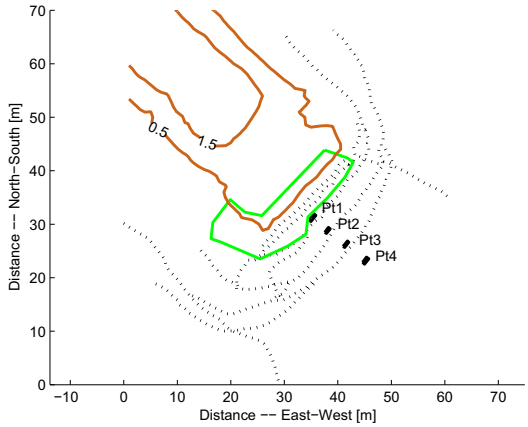

Figure 4.10: Map of the location of the ice cores taken on 19 April 2007 (week 16). Tide cracks in dashed black lines. The zone covered with geosynthetic bags is delimited by a green, solid line. The brown, thin contour lines show the topography of the breakwater.

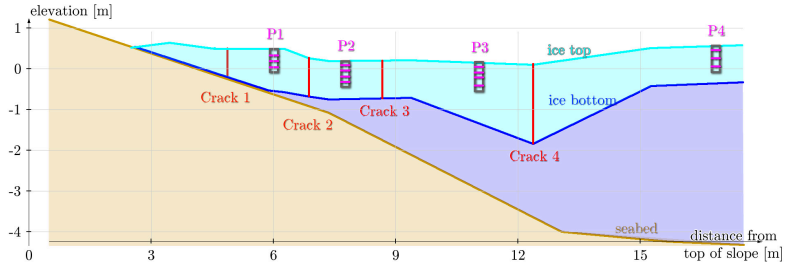

Figure 4.11: Cross-section of the hinge zone with the location of the horizontal cores

Laboratory work

In 1996, a NTNU-team developed a stationary uniaxial compression device, named *Knekkis*, which is installed in a cold-laboratory at UNIS. The device can perform maximal strength, creep and relaxation tests. A piston moves upwards, and a load cell placed in the upper part of the device records pressure. Data are recorded at a frequency of 0.5 Hz.

We performed relaxation tests by applying a start-stress of 500 kPa and keeping the piston immobile for one hour. This was the first ice-relaxation study ever made at UNIS.

For the compression tests we ran *Knekkis* at a constant strain rate of 10^{-3} s^{-1}. For the Pt5 cores, we reused the cores from the relaxation tests after having checked that relaxation

testing did not affect their Young's modulus. For these cores, the data is the average of two samples while for the coastal ice, we only performed one test. We considered the Young's modulus to be the steepest slope of the stress-strain plot.

After the tests, we melted the samples to measure salinity. Air and brine fractions and porosity were calculated as functions of salinity, density and temperature from equations developed by Cox and Weeks (1982).

We made thin-sections of four hinge-zone samples in order to analyse the ice texture. The sections were 70 mm in width, and the orientation of the vertical sections was, unfortunately, unknown.

4.2.12 Ice stresses in the hinge zone

Sébastien Barrault and I measured the horizontal stresses on both sides of crack 2 and in the free-floating ice from 6 to 11 May 2007. The goal was to get an order of magnitude of the stresses in the hinge zone and to study to which extent they were influenced by the tide.

The work was presented at the 19th IAHR International Symposium on Ice in 2008 (Caline and Barrault, 2008) (Paper 1).

We installed the sensors in rosettes of three sensors each. The centre of the rosettes placed on each side of crack 2 were 30 cm from the crack and 18 cm below the ice top. In both rosettes, one sensor measured stresses perpendicular to the crack, and the angle between each sensor was 120° (Figures 4.12, 4.13, 4.14, 4.15). We froze another rosette in the free-floating ice, 2.6 km away from the breakwater, in the middle of Sveabukta (Barrault and Høyland, 2007).

The instruments used for the rosettes at crack 2 were Amplified Solid State Pressure Sensors 242PC100G. They consist of a disc of 10.5 cm in diameter filled with hydraulic oil and a transducer head measuring the voltage difference. Compressive stresses are measured with $\pm$ 0.1 kPa resolution. Tensile stresses are not measured. They were connected to a CR10X Campbell Scientific datalogger.

On the free-floating ice we used BP stress sensors (Barrault and Høyland, 2007).

4.2.13 Ground resistivity

Lene Kristensen (UNIS) helped me measure the ground resistivity using two dimensional (2D) resistivity profiling with equipment from ABEM Instrument AB. The goal was to

Figure 4.12: Set-up of the stress sensors. Datalogger in orange box – 26 April 2007 (week 17)

Figure 4.13: Slots in the ice for a stress-sensors rosette – 26 April 2007 (week 17)

map the ground conditions and detect the presence of permafrost, using the fact that the electrical resistivity of ice is considerably higher than that of water (Hoekstra and McNeill, 1973).

We drove electrodes in the ground along a line, with 2 m spacing (Figure 4.16). The system measured the ground resistivity by automatically switching current and potential electrodes in a wide range of possible combinations in a Wenner array. The data

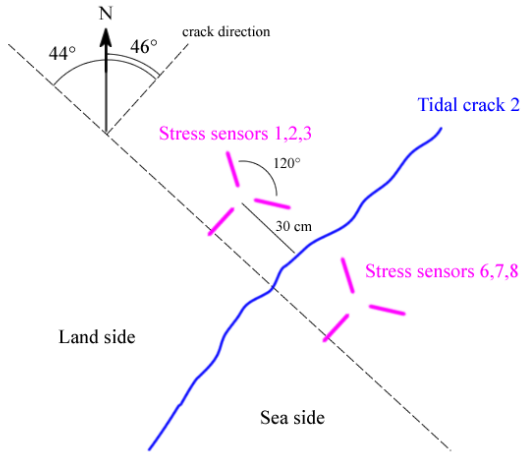

Figure 4.14: Set-up of the rosettes placed on each side of crack 2

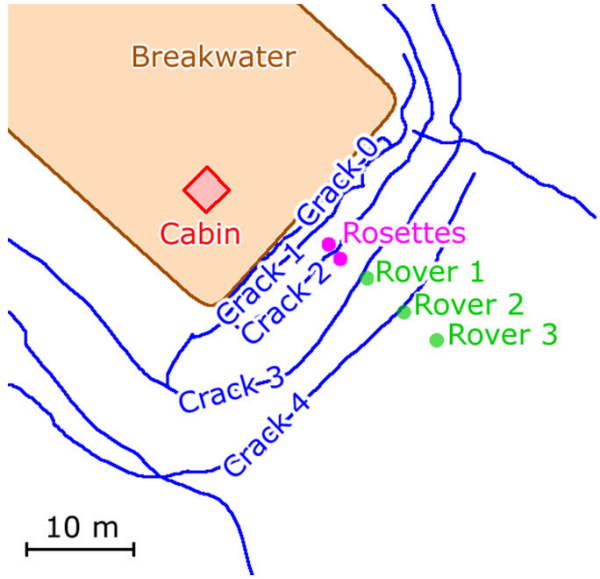

Figure 4.15: Location of the rosettes placed at on each side of crack 2

were inverted using a quasi-Newton optimisation method using the software RES2DINV (Geotomo Software Sdn. Bhd) (Loke and Barker, 1996). A full description of the method is found in Kristensen et al. (2009).

Figure 4.16: Measurement of ground resistivity – 2 September 2006

Chapter 5

Results

5.1 Temperature and ice cover

The water temperature measured by the tide gauge is plotted in Figure 5.1. On 15 November it fell to –1.8 °C, which is close to –1.9 °C, the freezing temperature of the sea water in Sveasundet, the salt content being around 30 psu. This corresponds to the period where the sea ice froze over for the first time (week-46 section, page 141). A few days later the air temperature rose to around 0 °C and the ice cover broke up (week-47 section, page 144). In the same period the sea water rose to –1 °C.

The pictures from the video cameras show that there was a short period, from 8 to 9 December, where an ice cover formed, corresponding with a fall of the sea temperature to –1.9 °C. The cover broke rapidly up again as the sea temperature rose to –1.2 °C.

On 19 December the sea water temperature was down to –1.9 °C and an ice cover had formed again (week-51 section, page 151). From that moment on the ice cover did not break up until the spring.

The sea water stayed close to –1.9 °C for the whole winter season until it increased suddenly on 23 May. This corresponded to the onset of the spring thaw (week-20 section, page 186). The snow on top of the ice was starting to melt and the fresh meltwater, which had a temperature of 0 °C or more, was warming up the sea water. It is also possible that Kjellströmelva had started to flow.

From 23 May to 16 June 2007 the sea-water temperature increased with an almost constant rate from –1.9 to 0.0 °C (Figure 5.2). It was followed by a more rapid increase to 1.3 °C on 21 June, at the end of the break-up. Since 16 June marks the transition from a high to a low concentration of drift ice in Sveasundet, two processes may explain why the sea water

temperature did not increase until after that date. First, the ice cover works as a mirror for the solar radiations, thus isolating the sea water. Second, ice melting is tapping heat from the sea water.

Accumulated freezing or thawing degree-days (AFDD and ATDD, respectively) are often used when analysing the processes of freeze-up and break-up. Key values for these parameters are summed up in Table 5.1 and the AFDD is plotted in Figure 5.37.

A sudden change of 1.4 °C in the temperature of C4T14 occurred on 24 March 2007 between 10:00 and 11:00 (Figure 5.18). It is likely that it was related to the sudden weather change that occurred on 23 March at 18:00, when the temperature surged from –4.5 to +5.3 °C within 6 hours and the wind increased from 0 to 12.4 m s^{-1} within 3 hours. Yet, the temperature change is surprisingly big.

Event	Date	AFDD	ATDD
1st freeze-up	15 November	388	
2nd freeze-up	8 December	454	
3rd freeze-up	19 December	528	
start of break-up	12 June		24
end of break-up	22 June		53

Table 5.1: AFDD and ATDD for freeze-up and break-up dates

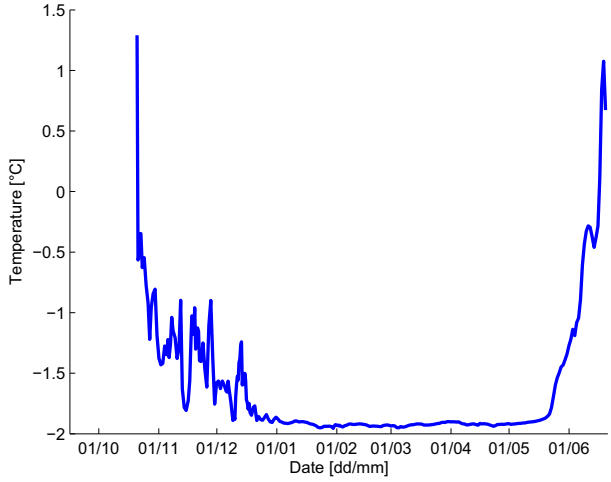

Figure 5.1: Water temperature at the tide gauge – daily means, 2006–07 season

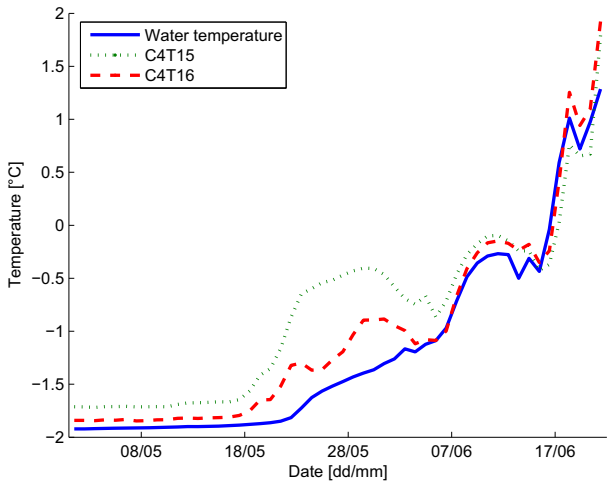

Figure 5.2: Water temperature at the tide gauge (–2.7 m), C4T15 (–2.4 m) and C4T16 (–2.8 m) (defined in Section 4.2.3) – daily means, 1 May to 22 June 2007

5.2 Ice thickness

Ice thickness measurements are summed up in Figure 5.3. The thickness of the free-floating ice, measured at a site further west in Sveabukta, was 0.52 m in week 7, 0.66 m in week 11 and 0.58 m in week 15. During the first part of the winter—until at least week 8—the ice growth was highest in the first 5 m seaward of crack 1. In week 4 it was up to twice as thick in this zone as 20 m seawards. While the ice gradually became grounded close to crack 1, it continued to grow further seawards. The maximum measured thickness was 3.1 m, in week 16, 12.3 m seaward of crack 1.

During break-up I surveyed the ice thickness at a point 50 m seaward of the breakwater (Figure 5.4). After 12 June the ice was broken up in front of the breakwater so it was not possible to access that location anymore.

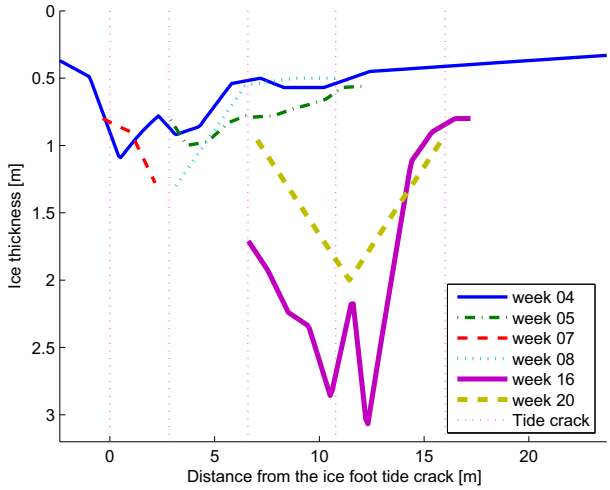

Figure 5.3: Ice thickness throughout the season. The tide cracks locations are indicated with vertical, dotted lines.

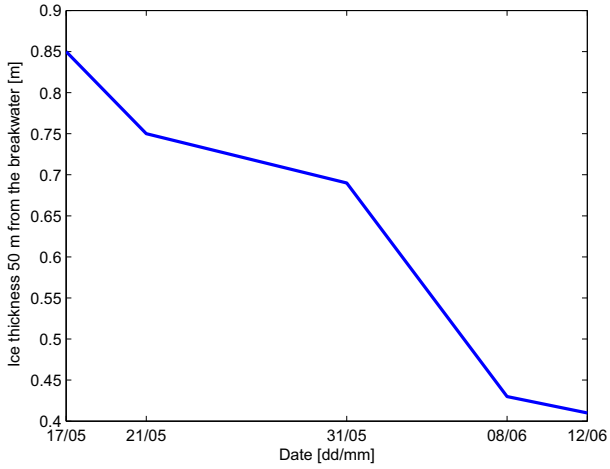

Figure 5.4: Evolution of the ice thickness 50 m seaward of the breakwater in the period leading to break-up

5.3 Snow thickness

I measured the snow thickness in weeks 5, 8 and 16 (Figure 5.5). Most places, it was between 15 and 25 cm, but along crack 3, it was almost 40 cm. In week 10, I did not take into account the slush in the flooded area, therefore, the value of the snow thickness was close to 0.

In week 16, the snow density was between 340 and 420 kg m^{-3}, with an average of 380.

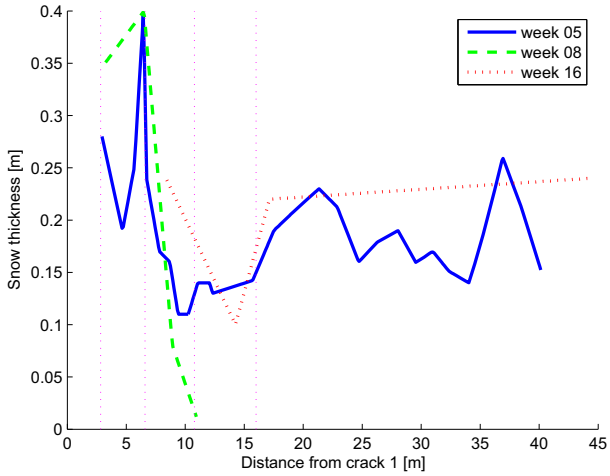

Figure 5.5: Snow thickness in weeks 5, 8 and 16. The tide cracks locations are indicated with vertical, dotted lines.

5.4 Break-up

In this section, *break-up* is defined as the period starting when the ice broke up in front of Barryneset and ending when Braganzavågen was ice-free. After the break-up, smaller cakes still occurred, but apart from them, the sea was ice-free.

I determined the dates of break-up for three consecutive years (2005–07) thanks to time-lapse pictures taken from Liljevalchfjellet. Table 5.2 sums up the key break-up data. The winter season of 2005–06 was particularly mild and, consequently, the break-up occurred early. Although seasons 2004–05 and 2006–07 were comparable in AFDD, the break-up occurred two weeks earlier in 2007 than in 2005.

According to Høyland (2009), break-up occurred in the first half of July in the eighties and nineties.

The break-up mechanism was similar all three years: after the ice had been melting for several weeks, it started to break into individual cakes that drifted back and forth with the tide. After a few days, large chunks of the Braganzavågen ice cover broke loose. These floes, which were several hundred metres in diameter got stuck in Sveasundet due to their size and generated shore pile-ups (Section 5.5). Figure 5.6 shows a sequence of a floe getting stuck, rotating into Sveasundet and eventually cracking up.

Season	Break-up period	Total seasonal FDD [°C day]	Spring tide date and range	Tide at break-up onset
2004–05	26–30 June	2187	26 June, 1.6 m	1.6 m
2005–06	8–19 June	1715	13 June, 1.4 m	1.0 m
2006–07	13–21 June	2170	17 June, 1.5 m	1.3 m

Table 5.2: Dates of break-up, seasonal FDD and tide data

5.5 Ice jams and encroachment

Contrary to Canadian rivers like the Saint Lawrence, Svalbard rivers flow little during freeze-up. Consequently, the ice cover mostly melts in place at break-up, and ice jams seldom occur.

Until break-up, Kjellströmelva seemed to be flowing on top of the ice cover in Braganzavågen (Figure B.93). It is also possible that what looked, at a distance, like a surface flow, was actually a melted-through channel. Unfortunately I did not find a safe method to investigate this.

Ice encroachment is a major concern in ice engineering (Kovacs and Sodhi, 1980; Gawne, 1999). Figure 5.7 shows an event that happened in Longyearbyen in December 2004.

At Barryneset, however, the only damage caused by pile-up was a geosynthetic bag being teared open.

As mentioned above, pile-up commonly occur during break-up. I do not know whether it occurred in 2005, but it occurred both in 2006 and 2007. Figure 5.8 shows the biggest pile-up I witnessed at Barryneset. It was caused by the event shown in Figure 5.6. Piled-up ice was about 30 cm thick and mostly rotten.

Although some horizontal movement was measured during the winter (Section 5.7.1), it was too small to cause any ride-up.

During break-up two pile-up episodes occurred, on 18 and on 19 June. As explained in Section B.3 pile-ups occurred when ice floes wider than Sveasundet broke loose from the Braganzavågen ice cover and hit Barryneset.

A few kilometres west of Kapp Amsterdam, in the bay north of Linderotneset a more sizeable pile-up occurred in 2006, following a 9-hour-long period of strong westerly winds (12 m s^{-1}). The pile-up was about 4 m high and went up to 30 m shoreward (Figures 5.9 and 5.10).

(a) time: 19:42

(b) time: 20:42

(c) time: 21:42

Figure 5.6: Big ice floe from Braganzavågen getting stuck in Sveasundet – 14 June 2006

Figure 5.7: Ice pile-up on the east side of the harbour of Longyearbyen – December 2004 – Picture: Per Olav Moslet

Figure 5.8: Pile-up at Barryneset – 14 June 2006

Figure 5.9: Pile-up on the shore of Damesbukta west of Kapp Amsterdam – 15 June 2006

Figure 5.10: Pile-up on the shore of Damesbukta west of Kapp Amsterdam – 15 June 2006

5.6 Vertical tidal ice movement

5.6.1 Movement in the course of a tidal cycle

I surveyed the amplitude of the vertical tidal movement of the ice several times throughout the winter (Figure 5.11). In the hinge zone, the ratio of the amplitude of the ice movement to the amplitude of the tide was a linear function of the distance from the shore. The vertical tidal movement of free-floating ice, on the other hand, had the same amplitude as the tide.

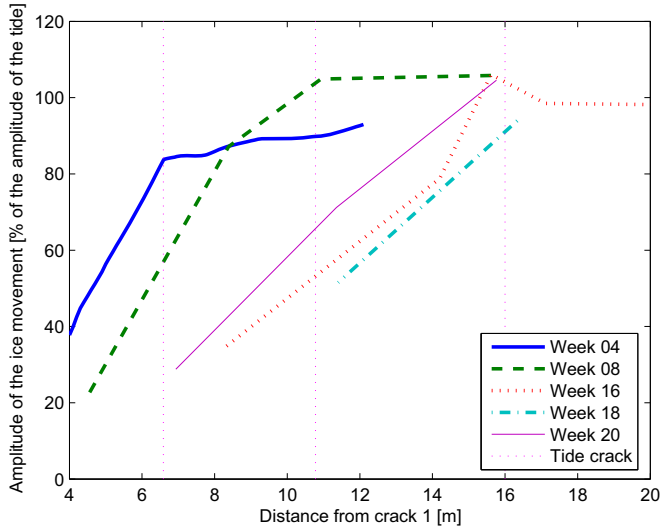

Figure 5.11: Influence of the tide on the vertical movement of the ice in the hinge zone in weeks 4, 8, 16, 18 and 20 – the data series correspond to 0.66 m sea level displacement (from –1.02 to –0.36 m).

5.6.2 Hysteresis

Since the ice in the hinge zone is not floating freely, I examined whether there was a hysteresis in the relation between sea level and ice elevation. I recorded the elevation of a given point in the hinge zone with a DGPS over several tidal cycles and, for a given value of the sea level, compared the ice elevation for two consecutive flows and for flow and ebb (Figure 5.12). For two consecutive flows, the elevation difference was less than

4 cm, which is small considering that the DGPS has a 2 cm precision. For flow and ebb, however, the variation was up to 7 cm. Around low tide, the ice was resting some 3–4 cm higher during ebb than during flow. Around high tide, although the trend was less pronounced, the data suggest that the ice was also resting a few centimetres higher during ebb than during flow.

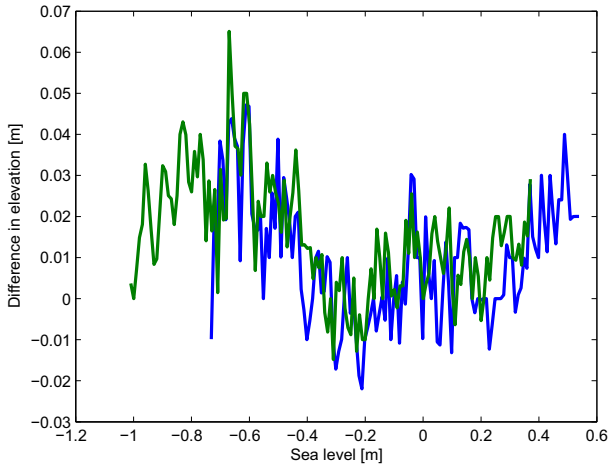

Figure 5.12: Difference in ice top elevation between ebb and flow (2 data series). A positive difference means the ice is higher during ebb than during flow

5.6.3 Spatial variability of the vertical tidal ice movement

On 22 February 2007 (week 8), I studied the 3-dimensional tidal movement of the ice along the tip of the breakwater by surveying a 30-m-long and 4-m-wide zone delimited by cracks 3 and 4 ten times between 17:20 (sea height = 0.4 m) and 23:17 (sea height = –1.17 m).

The long side of the zone was parallel with the shore. The measurement points were located in 5 shore-parallel lines: one line along each side of cracks 3 and 4, and one line along the seaward side of crack 2 (Figure 5.13).

A line's elevation is defined as the mean elevation of the points along it.

The shore-perpendicular tilting between two lines is defined as the elevation difference between those lines and is directly related to the slope of the ice between those lines, in the direction perpendicular to the shore. Values are positive when the shoreward line is higher than the seaward line.

The shore-parallel tilting is defined as the difference in elevation between the short sides of the zone and is directly related to the slope of the ice in the direction parallel with the shore. Values are positive when the east side of the zone is higher than its west side.

The shore-perpendicular tilting between two sides of a crack was small: the highest tilting was 6 cm, between each side of crack 3. Between crack 2 and crack 3, the tilting was a linear function of the sea level and changed from 0.47 m, when the sea height was –0.98 m, to –0.06 m, when the sea height was –0.17 m. The shore-perpendicular tilting between crack 3 and crack 4 was an almost linearly decreasing function of the sea level. It was about 0.33 when the sea level was –1.17 m and 0.05 m when the sea level was 0.36 m (Figure 5.14).

Shore-parallel tilting also decreased almost linearly from 0, when the sea height was –1.17 m, to –0.17 m, when it was 0.36 m (Figure 5.15).

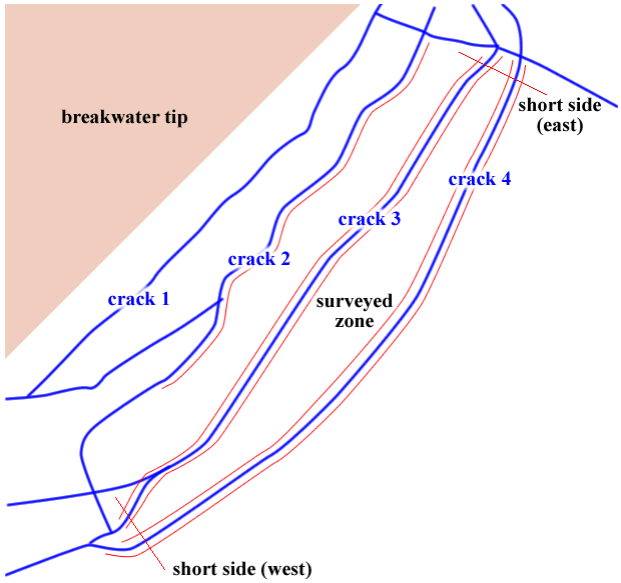

Figure 5.13: Cracks, in blue, and the 5 shore-parallel lines along which the elevation was measured, in red

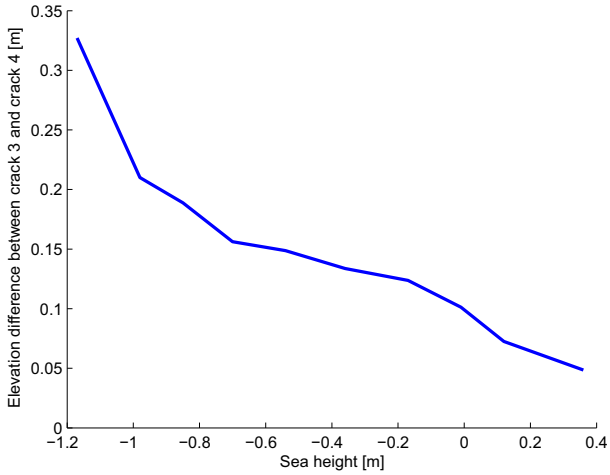

Figure 5.14: Shore-perpendicular tilting of the ice zone between crack 3 and crack 4 as a function of the sea height – 22 February 2007 (week 8)

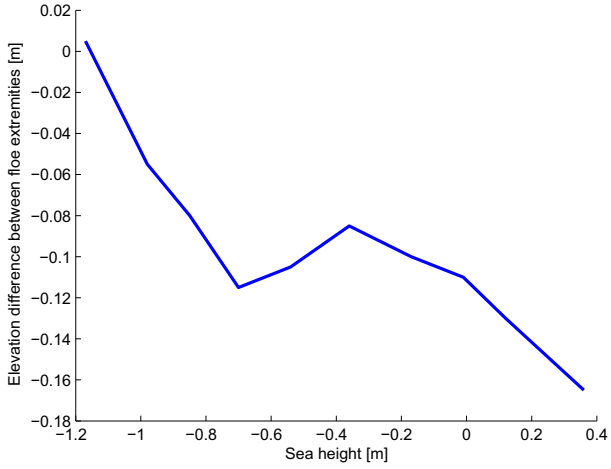

Figure 5.15: Shore-parallel tilting of the ice zone as a function of the sea height – 22 February 2007 (week 8)

5.7 Horizontal ice movement

5.7.1 Throughout the tidal cycle

In weeks 8 and 16, I monitored the horizontal tidal movement and observed that, perpendicularly to the shore, the ice was moving horizontally. Up to crack 4, the amplitude of the movement was decreasing with the distance from the shore (Figure 5.16). Between cracks 4 and 5, it was V-shaped, going from about 0.03 to 0.01 then 0.02 m. The largest measured horizontal displacement was 0.09 m. The corresponding sea level variation was 0.90 m.

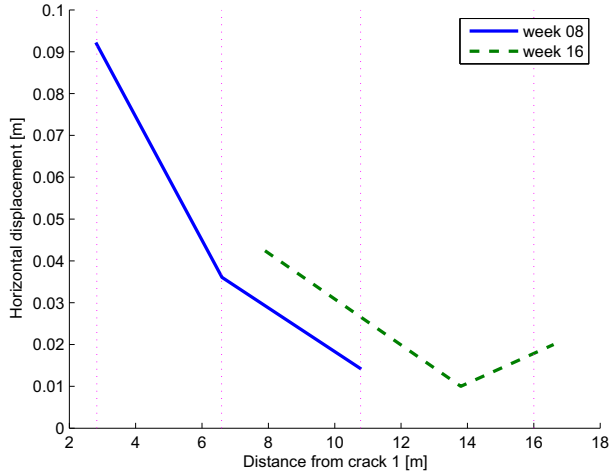

Figure 5.16: Horizontal tidal movement of the ice in the direction perpendicular to the breakwater – sea level variation: 0.9 m. The tide cracks locations are indicated with vertical, dotted lines.

5.7.2 Throughout the season

I also monitored the horizontal movement of the ice over a period of several weeks. In week 5, I set two wood sticks in the ice, one in front of the tip of the breakwater, 12 m from crack 1, (stick 1), the other on the west side of the breakwater, about 30 m from land. I surveyed their posision in weeks 7 and 8. The sea level was different for each survey: –0.21 m in week 5, –0.5 m in week 7 and –1.15 m in week 8. Based on the data from the horizontal tidal movement of the ice (Section 5.7.1), it is possible to rectify the data, at least for the point in front of the tip of the breakwater: a –1 cm correction was applied

for week 5 and a –2 cm correction for week 8. As to the point on the west side, it was assumed that the effect of the tide was less than 1 cm. The rectified displacements are shown in Figure 5.17. There was around 0.1 m drift within two weeks. The ice in front of the breakwater drifted in the direction perpendicular to the shore while the ice on the west side drifted toward south. Unfortunately, I was not able to continue the measurements because the ice was flooded and the wood sticks disappeared into snow ice. The few measurements available suggest that the long-term horizontal movement of the ice was not negligible. Apparently, it was highest in the beginning of the ice cover period.

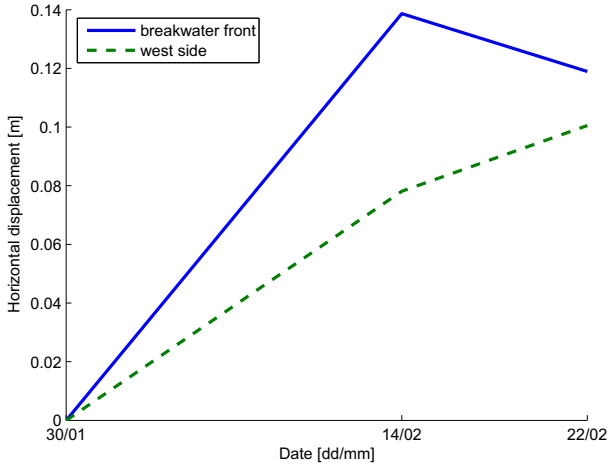

Figure 5.17: Movement of the ice surrounding the breakwater, rectified for horizontal tidal movement

5.8 Tide cracks

The date and location of the formation of the tide cracks is summed up in Table 5.3, and Figure 4.10 is a map of the cracks. The indexed cracks were running parallel with the tip of the breakwater. Their index is increasing with the distance from shore. Crack 1 was located approximately above the top of the fourth row of geosynthetic bags (Figure C.10. In addition, there was one shore-perpendicular crack starting at each of the corners of the breakwater. Finally, based on the video camera pictures, it looks like one crack—crack 0—appeared shoreward of crack 1 in week 12.

Crack name	Distance from crack 1 [m]	Date of formation
Crack 0	–2.5	week 12
Crack 1	0.0	between week 47 and week 51
Crack 2	2.5	between week 52 and week 1
Crack 3	6.0	between week 1 and week 4
Crack 4	9.5	between week 5 and week 8
Crack 5	16.0	between week 15 and week 16

Table 5.3: Position and date of formation of the tide cracks (0.5 m precision)

5.9 Surface water

As mentioned in Sections 6.1 and 6.8, the presence of surface water leads to the formation of superimposed ice and, therefore, has an effect on the properties and the thickness of the sea ice.

During several periods throughout the season the ice was flooded with surface water (Table 5.4). The flooding occurred from the moment that the ice cover started to stick to the shore. Along the tip, it did in week 52, and in along the west side, in week 1. Until week 12, flooding occurred from time to time and was to some extent connected to spring tides. From week 12 to week 18, no flooding was observed. From week 19, the snow was starting to melt and flooding occurred again until break-up.

In week 10, flooding started precisely at the time when the temperature rose—on 6 March at 06:00—indicating that the temperature probably has an influence on flooding.

Although the pictures from the video cameras may give an indication of the extent of the flooding, they do not reveal whether there was surface water below the snow top. In week 13, for example, there was at least 20 cm of water on top of the ice but since the snow cover was thicker, it was impossible to see it on the video camera pictures.

The only way to reliably record the flooding is, therefore, to dig away the snow and measure the freeboard. Since the freeboard varies with the tide, this should be done both at high tide and at low tide. Such measurements would allow to study the influence of temperature and ice thickness on flooding thoroughly.

Week	breakwater-tip observation	west-side observation
52	flooding	free-floating ice
01	no observations	flooding
02	cameras out of order	
03	cameras out of order	
04	unknown: thick snow cover	no flooding
05	flooding	flooding at the end of the week
06	no flooding	no flooding
07	limited flooding	no flooding
08	limited flooding	limited flooding
09	no flooding	flooding at end of week
10	flooding	flooding
11	pond freezes over	flooding at end of week
12	no flooding	no flooding
13	no flooding	no flooding
14	no flooding	almost no flooding
15	no flooding	no flooding
16	no flooding	no flooding
17	no flooding	no flooding
18	no flooding	no flooding
19	some spots of rotten snow and meltwater	flooding at high sea levels
20	flooding at high sea levels	size of flooded area is increasing
21	same as week 20	same as week 20
22	same as week 20	same as week 20
23	same as week 20 and crack 1 is widening	same as week 20
24	break-up	break-up

Table 5.4: Observations of the surface water close to the breakwater

5.10 Ice foot and coastal ice

Thanks to the spatial variation in ice conditions along the breakwater, it was possible to observe different mechanisms of ice foot formation, growth and decay.

5.10.1 Ice foot formation – freeze-up

Spray, swash and tide Before the sea ice froze over, an ice cap formed from a combination of sea water spray, swash and moisture (Figure B.5). The lower limit of the ice cap almost coincided with the MHW (week-43 section, page 131). An analysis of the temperature along the top of the slope shows that the temperature below MHW was close to the sea water temperature, while above MHW it was strongly affected by the air temperature (Section A.2.6).

Pancakes As the sea water was cooling down, pancakes were gradually covering the water surface. They were deposited on the backshore along both the west and the east side of the breakwater and formed a soft berm that consolidated within a few days into a solid ice foot under the cementing action of spray, swash and moisture (Figures B.27 and B.3).

Ice cakes Due to the shallowness of Braganzavågen, the ice formed there first. Under the influence of wind and tide, ice cakes could break loose, drift away and be washed up, like the ice cake observed in week 43 on the west side of the breakwater (Figure B.4). The bottom of that cake had an elevation of approximately –0.10 m, which was 40 cm lower than MHW. Two weeks later the ice foot had grown downwards to MHW along both the east side and the tip of the breakwater but not around the ice cake, which was cemented to the bags and had been integrated into the ice foot. The stranded ice cake had, hence, contributed to extend the area covered by the ice foot.

5.10.2 Ice foot growth – ice-cover period

Sea ice When the sea froze over, the ice cover was reaching to the bottom of the ice foot and moving vertically with the tide (Figure B.34). As the sea ice grew (Figures B.19 and B.33), the ice cover became grounded during an increasing part of the tidal cycle. In addition, the area of contact with the ice foot increased, and the resulting friction forces kept it from moving freely with the tide at the ice-foot boundary. As a result, the ice cover was bending under the influence of the tide. Eventually, the ice cover failed and cracks appeared (Figure B.46). Topographic measurements

in week 4 show that the ice top was unaffected by the tide shorewards of crack 1. Crack 1 was easily identifiable as a cracked ridge with almost the same height as the top of the ice foot.

It seems reasonable to assume that the ice was frozen fast to the ground whenever the temperature at the ice–ground interface was below the freezing temperature of the water in Sveasundet, which is –1.9 °C. During the winter of 2006–07 the temperature at C2T06 (altitude: 0.1 m) was lower than –1.9 °C in periods, while it was constantly around –1.8 °C at C4T14 (altitude: –1.8 m) (Figure 5.18)—except for the surge in March (Section 5.1)—Figure 4.7 shows the position of the thermistors. Therefore, it is likely that the ice was frozen fast down to somewhere between C2T06 and C4T14, which corresponds approximately to the bottom of the fourth row of geosynthetic bags, at –1.0 m (Figure C.9), and down to C4T14, 2 m shorewards of crack 2, in the beginning of May. Figure B.95 confirms that the ice was frozen fast at least up to crack 1 at the end of the season. It was not frozen fast between crack 1 and crack 2 at that time, but it is possible that it had been so earlier and had melted off. Figure 5.11 confirms that the ice was not frozen fast seawards of crack 2.

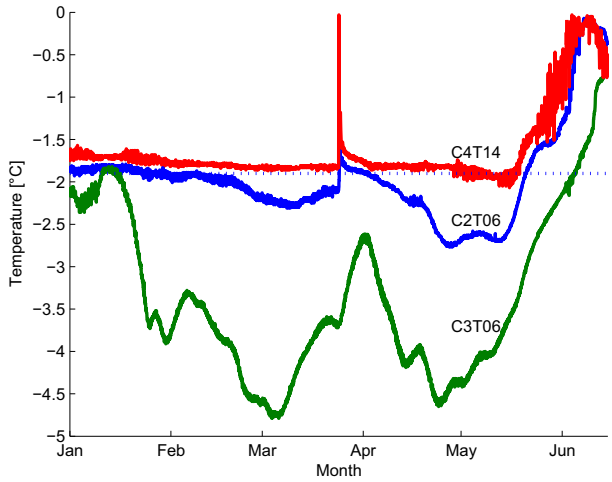

Figure 5.18: Temperatures recorded by thermistors C2T06 (altitude: 0.1 m), C3T06 (altitude: 0.3 m) and C4T14 (altitude: –1.8 m) between 1 January and 15 June 2007. The dashed line corresponds to –1.9 °C (sea water freezing temperature).

Snow ice The repeated flooding of the ice surface (Figure B.62) lead to the formation of a top layer of snow ice. The presence of snow ice was confirmed by the ice cores analyses (Section 5.11). It also appeared clearly when digging down the top of the

ice—the snow ice has a characteristic whiteness and high porosity.

Ice cakes As described in the week-1 Section, page 160, after the sea had frozen over, the ice cover broke up close to the shore and generated ice cakes that were stranded on top of the existing ice foot and became a part of it (Figure B.43).

5.10.3 Ice foot decay – break-up

I documented the mechanisms leading to the disappearance of the ice foot only along the tip of the breakwater. The upper shore ice started melting around the middle of May (Figure B.79). At the start of the break-up, on 13 June, the remaining ice was covering a zone extending from MLW to somewhere between MSL and MHW. The ice shorewards of crack 2 remained attached to the shore (Figure B.92). While the ice shorewards of crack 1 was frozen fast to the ground, the ice between crack 1 and crack 2 was held in place by adhesive forces along crack 1 (Figure B.95). The combination of the mechanical loads from the tide and the heat of the sea water cleared all the remaining shore ice within 19 June.

5.11 Ice properties

The results presented in this section were obtained from the ice cores taken during the winter of 2007 (Section 4.2.11).

5.11.1 Temperature profiles

Apart from a few centimetres at the top, where the temperature variation was about 3 °C, the temperature of the C3 core was almost constant and around –10 °C in C3. The temperature of the C5 core increased linearly from –9.6 to –2.1 °C from the top to the bottom (Figure 5.19). The temperature gradient of C3 was –1.27 °C m^{-1} and that of C5 –8.82 °C m^{-1}.

At the location of C3, the sea level was 1.2 m below the ice top when the core was taken, therefore, its temperature was unaffected by the sea water temperature. At the location of C5, the sea level was 0.5 m below the ice top, which means that the temperature of the bottom half of the core was affected by the sea water temperature.

5.11.2 Salinity profiles

In C3, the salinity was low—between 0.4 and 1.3 psu—except for the top-0.1-m section, where it was around 3.0 psu. In the lower section, the salinity seemed to decrease with depth. The difference in salinity might be caused by the presence of a stranded ice cake on the top of the ice at the location of C3. Indeed, pictures from the video cameras show that several cakes were stranded along the location of crack 1 in week 52, right before the formation of the ice cover. The presence of surface water, which also results in high salinity, is ruled out since even when the sea level was low (–0.5 m), the elevation of the ice top was 0.7 m, which is higher than the highest sea level observed for over two weeks.

The salinity of C4 was low—between 0.4 and 1.7 psu—down to 0.8 m below the ice top, then decreased almost linearly down to the lowest measurement point, 1.2 m below the ice top. The sea level was 1.0 m below the ice top when the core was taken. The low salinity zone was probably a result of rapid brine drainage due to high ice porosity. The salinity of the lower part of the core (below 0.8 m from the ice top) was in accordance with values measured on the free-floating ice in Sveabukta (Høyland, 2009)—around 6 psu in week 7.

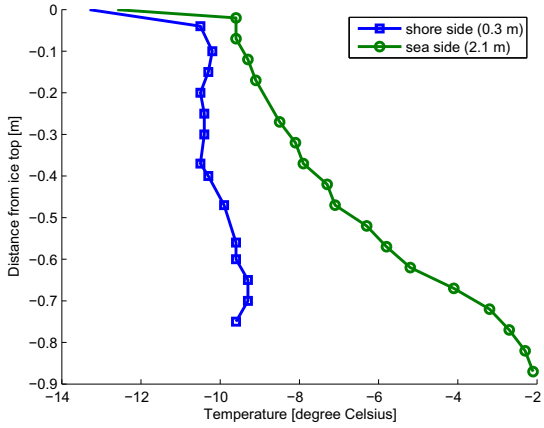

Figure 5.19: Temperature profiles of two cores taken on each side of crack 1. The temperature at the ice top is the air temperature – 13 and 14 February 2007 (week 7)

5.11.3 Physical and mechanical properties

Table 5.5 summarises the physical and mechanical properties of the ice cores. The data are also plotted in Figures 5.21 to 5.29. All parameters varied monotonously with the

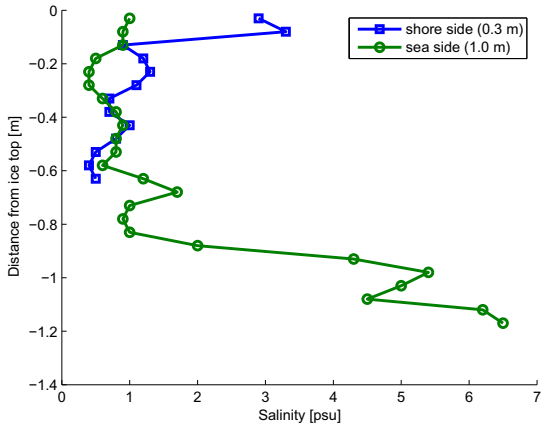

Figure 5.20: Salinity profiles of two cores on each side of crack 1 – 13 and 14 February 2007 (week 7)

distance from the shore:

- The porosity of the coastal ice decreased from Pt1 to Pt4, and the free-floating ice (Pt5) was 6 times less porous than the ice at Pt1.
- The air fraction decreased from Pt1 to Pt4 as well. The highest air fraction—99.4 %—was found at Pt1. In the free-floating ice, it was 37 %.
- The salinity increased with the distance from the shore.
- The brine fraction and the density were highest in the free-floating ice.
- The Young's modulus was up to 50 % higher in the free-floating ice than in the coastal ice.
- All failures were ductile except for Pt3-H1 and Pt5-H3
- The residual stress was up to three times higher in the coastal ice than in the free-floating ice.

We chose not to study the relaxation function for two reasons. First, it takes up to 30 minutes for its slope to stabilise after the initial loading. Secondly, ice is a non-linear visco-elasto-plastic material, therefore, it does not have a unique relaxation function.

		Coastal Ice				Free-floating ice
	Depth	Pt1	Pt2	Pt3	Pt4	Pt5
Residual stress [kPa]	H1	170	162	156	156	103
	H2	128	150	149	127	76
	H3	132	151	–	104	57
Strength [MPa]	H1	2.7	3.7	2.6	5.1	4.3
	H2	3.2	3.0	4.2	4.3	4.1
	H3	3.0	4.3	5.2	6.0	3.3
Young's modulus [GPa]	H1	1.1	1.2	1.1	1.2	1.5
	H2	1.1	1.0	1.2	1.2	1.5
	H3	1.0	1.3	1.4	1.6	1.5
Salinity [psu]	H1	0.3	1.0	0.9	2.5	4.6
	H2	0.4	0.9	2.6	6.1	4.6
	H3	0.3	0.7	3.3	4.4	3.7
Density [kg m^{-3}]	H1	724	789	806	842	916
	H2	720	731	818	861	915
	H3	703	777	–	894	900
Brine fraction [%]	H1	0.13	0.47	0.44	1.26	2.53
	H2	0.17	0.40	1.28	3.15	2.53
	H3	0.13	0.33	–	2.36	2.00
Air fraction [%]	H1	21.2	14.2	12.3	8.6	0.8
	H2	21.6	20.5	11.2	7.0	0.9
	H3	23.5	15.5	–	3.2	2.5
Porosity [%]	H1	21.3	14.7	12.8	9.9	3.4
	H2	21.8	20.9	12.5	10.1	3.5
	H3	23.6	15.8	–	5.5	4.5

Table 5.5: Comparison of physical and mechanical properties of the free-floating ice and the coastal ice. All tests performed at –10 °C.

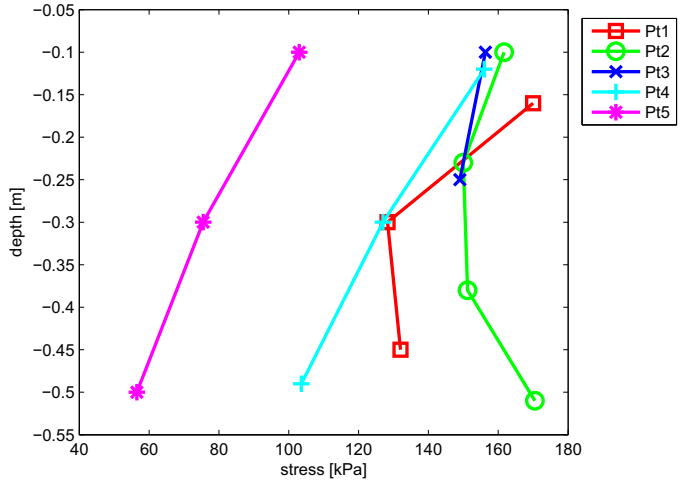

Figure 5.21: Residual stress of the ices cores (stress stabilisation level after one hour relaxation) – initial stress = 500 kPa

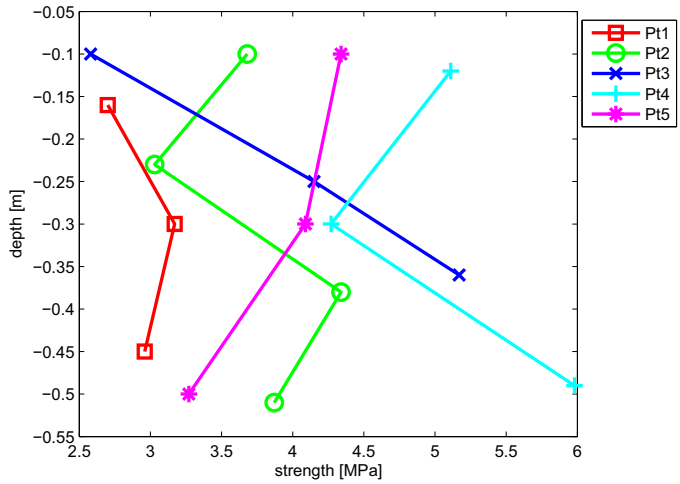

Figure 5.22: Strength of the ice cores – strain rate = 10^{-3} s^{-1}

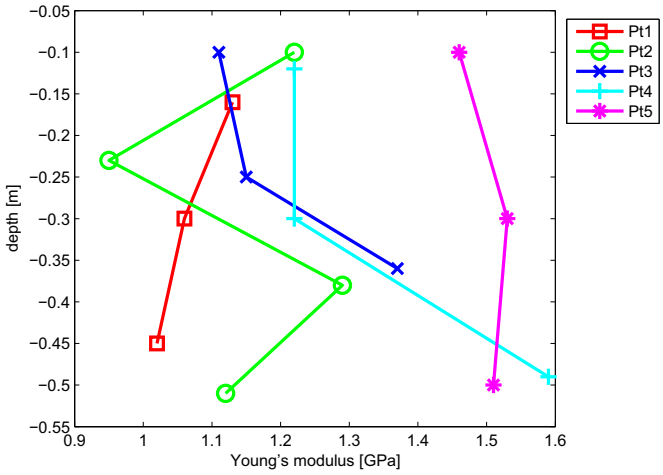

Figure 5.23: Young's modulus of the ices cores

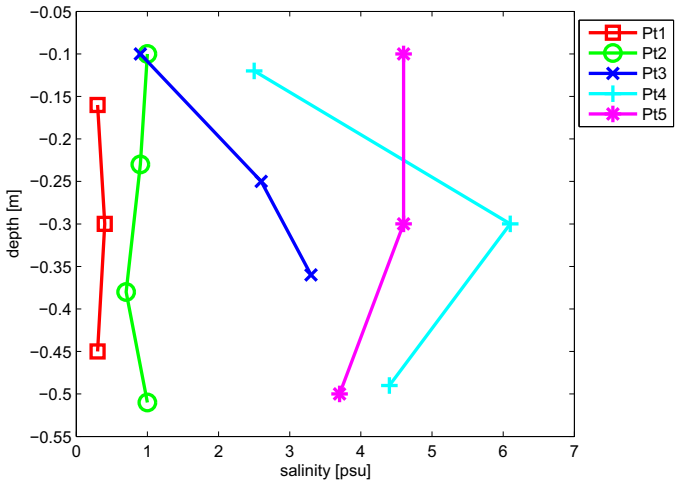

Figure 5.24: Salinity of the ice cores

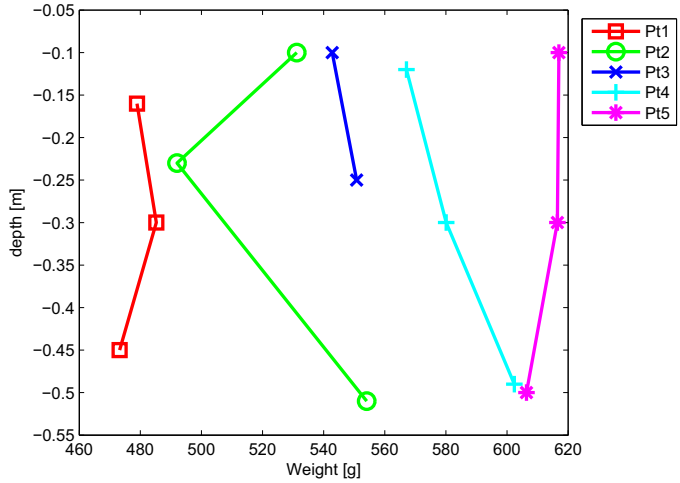

Figure 5.25: Weight of the ice cores (70 mm in diameter and 170 mm in length)

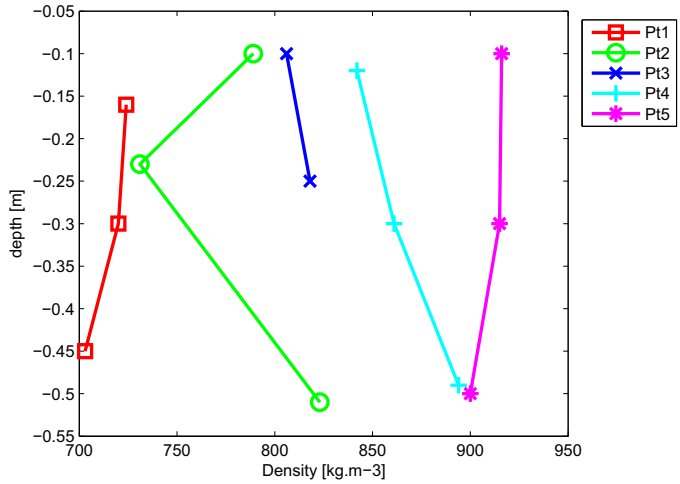

Figure 5.26: Density of the ice cores

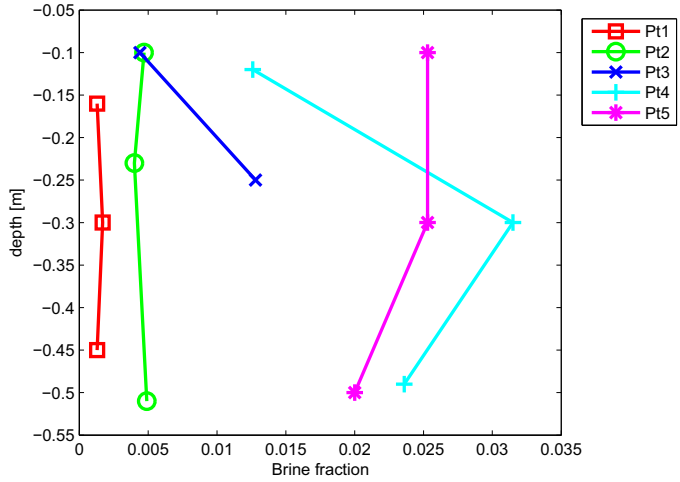

Figure 5.27: Brine fraction of the ice cores

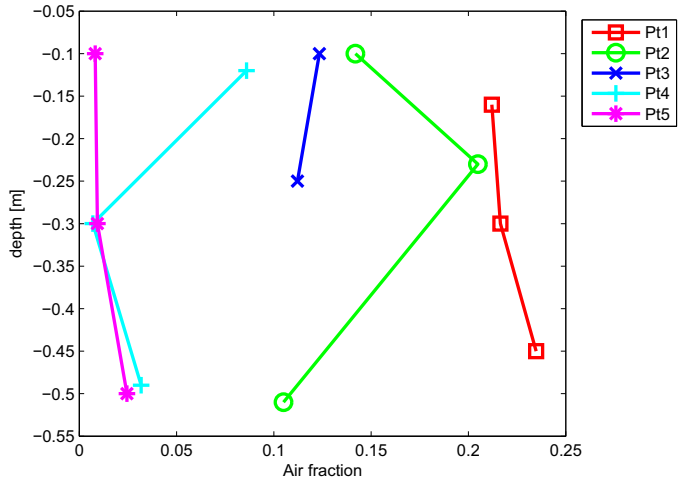

Figure 5.28: Air fraction of the ice cores

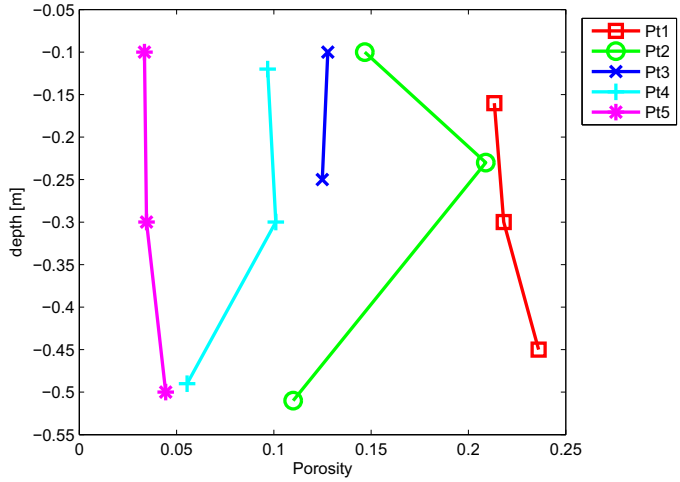

Figure 5.29: Porosity of the ice cores

The ice structure is classified in Figures 5.30, 5.31, 5.32 and 5.33 according to the classifications found in Michel and Ramseier (1971) and Weeks and Ackley (1982).

There was snow ice at the top of the ice cover in all hinge-zone cores. At Pt2 it extended to at least 50 cm below the top. Pt3, 10 m from crack 1, was located within the boundaries of the water pond observed in week 10 (week-10 section, page 174), and although we did not make any thin-section of the Pt3 cores, the snow ice at was at least 40 cm thick since it covered the wood sticks used to delimit the water pond (Section 5.7.1).

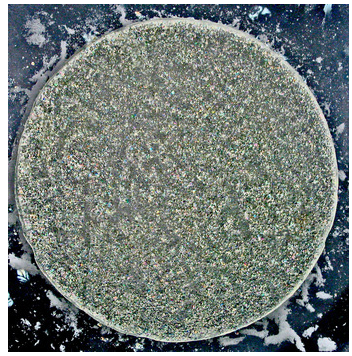

Figure 5.30: Pt1: vertical section — Depth: 0.16 m — Density: 724 kg m^{-3} — Structure: granular, very fine grains — Ice type: T2 (drained snow ice)

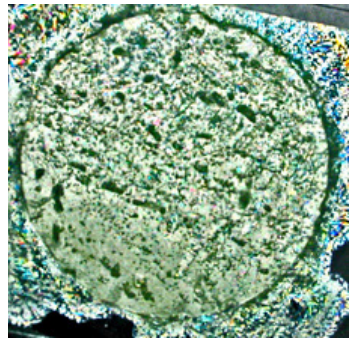

Figure 5.31: Pt2: vertical section — Depth: 0.51 m — Density: 823 kg m^{-3} — Structure: granular, grain size bigger than at Pt1, air bubbles, some brine pockets — Ice type: T2 (drained snow ice)

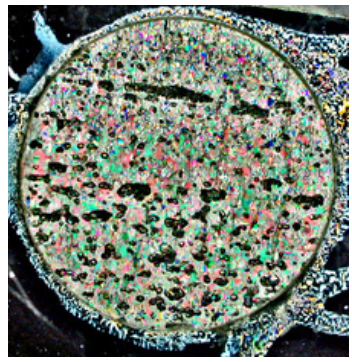

Figure 5.32: Pt4: vertical section — Depth: 0.12 m — Density: 842 kg m^{-3} — Structure: grains of different sizes ranging from fine to medium, bigger than at Pt1, a few air bubbles, several brine pockets — Ice type: T2 (drained snow ice)

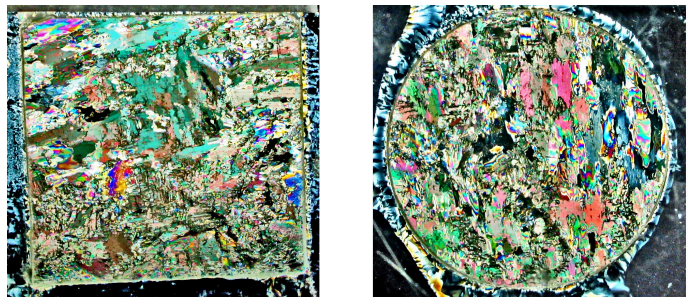

Figure 5.33: Pt4: horizontal (left) and vertical (right) — Depth: 0.49 m — Density: 894 kg m^{-3} — Structure: grain sizes fine to medium, tabular shape, random orientation — Ice type: R (agglomerated)

5.12 Ice stresses in the hinge zone

Figure 6.4 shows the data from the sensors installed along crack 2 for the whole measurement period. The land-side sensor oriented along the 46° direction did not record data when stresses were lower than 24 kPa. During the 6 days of measurements, the temperature increased almost linearly from –15 to 0 °C. The wind was around 11 m s^{-1} until 9 May then fell to 5 m s^{-1} and was blowing towards north-east (same direction as the tide crack). The tidal range decreased from 1.26 m on 6 May to 0.56 m on 11 May. There was a clear correlation between the tide and the stress intensities and directions. The highest intensities were 245 kPa on the land side and 139 kPa on the sea side.

Figure 6.5 shows data for the crack-2 sensors during one and a half tidal cycle between 10

and 11 May. Only the principal stresses are plotted. The direction is relative to 46°, which is the direction of the shore-parallel tide cracks. Thus, 0° corresponds to the direction of the cracks. The stresses on both sides of the crack were similar in amplitude, frequency and phase. The highest stresses, about 150 kPa, were reached at low tide, lasted for about 3 hours and were parallel with the crack. At high tide, the major principal stress was about 70 kPa and perpendicular to the crack. Finally, there was a short 100–150-kPa stress-peak parallel with the crack when the tide was around mean sea level. This peak was more evident on the sea side.

The sensors located on the free-floating ice did not record tidal variations. Neither did they record thermal variations, probably because a 40-cm-thick snow layer was covering the ice.

5.13 Thermal regime and frost heave

The comparison of the data recorded by C5T16 (altitude: –2.12 m) between seasons 2006–07 and 2007–08 (Figure 5.34) shows that:

- the temperature was colder in 2007–08—more than 0.5 °C, between May and August;
- from October to the end of March, it was similar and above –1.9 °C, which is the freezing temperature of the sea water at Barryneset;
- the ground thawed one and a half month later in 2007–08

The average temperature profiles in July and September also show that the breakwater was cooler in 2008 than in 2007 (Figures 5.35 and 5.36).

Freeze-thaw cycles of the ground are expected to generate vertical displacements—*frost heave*—. The altitude of the top of the breakwater, measured at regular intervals at a given point, *FC3*, on the roof of the cabin (Figure 5.38), seems, indeed, to vary seasonally. There is, in addition, a long-term settling trend.

More measurements are required to analyse the frost heave, though. In 2008, for example, no measurement was done between April and October. In 2007–08 the seasonal variation was of the order of 50 cm. It looks as if no seasonal variations occurred in the 2008–09 season.

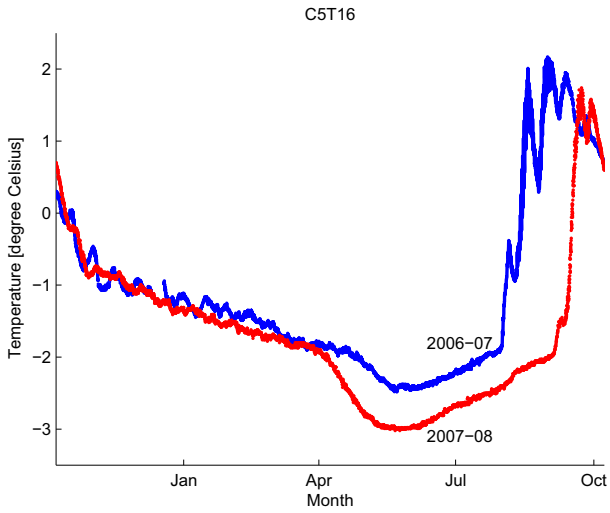

Figure 5.34: Thermistor-C5T16 data (altitude: –2.12 m): comparison between season 2006–07 and season 2007–08

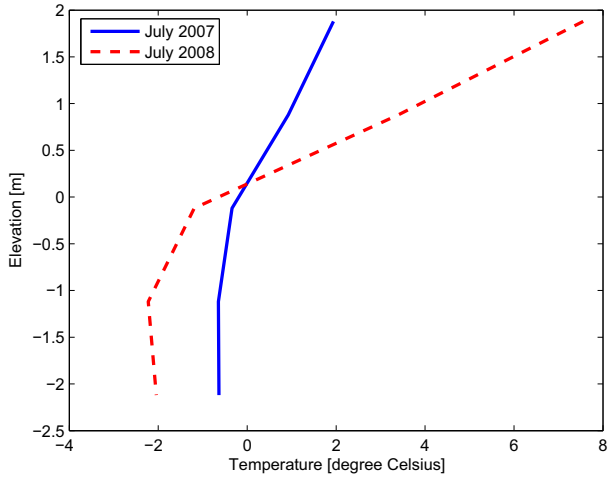

Figure 5.35: Comparison of the temperature profiles along thermistor cable C5 in July 2007 and July 2008

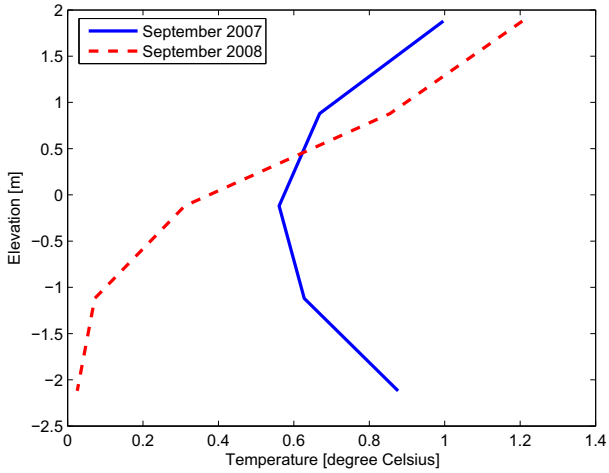

Figure 5.36: Comparison of the temperature profiles along thermistor cable C5 in September 2007 and September 2008

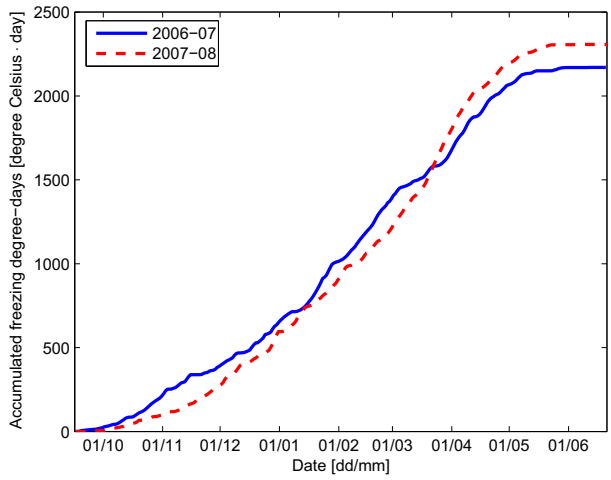

Figure 5.37: Comparison between the AFDD in 2006–07 and in 2007–08

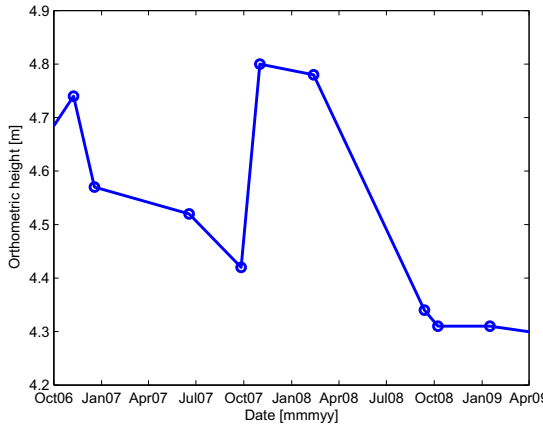

Figure 5.38: Vertical movement of the top of the breakwater

5.14 Ground resistivity

We performed two series of measurements: on 2 September 2006 and on 17 May 2007.

The breakwater tip was not built to full height at the time of the first measurement series. The length of the measurement line was 80 m and the electrode spacing 1 m. The results are shown in Figures 5.39 and 5.39.

The second measurement series was done along a 200-m-long line with electrodes every metre. The 0 metre mark is at the tip of the breakwater. Therefore, points with negative values on the abscissa are on the sea ice.

Both series show that the resistivity of the dumped masses is high. These masses extend over a distance of 100 m: 50 m of access road and 50 m of breakwater. The difference in resistivity is due to the water and salt content: the dumped masses have remained dry, while the natural land consists partly of salty moraine remains.

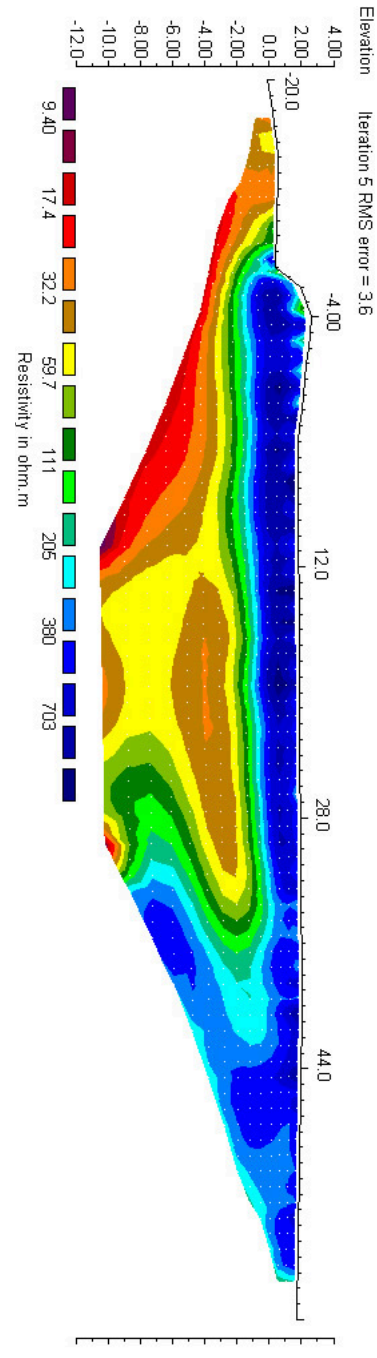

Figure 5.39: Ground resistivity along the breakwater. All distances in metres. Looking from north-east: the sea is on the left side – 2 September 2006

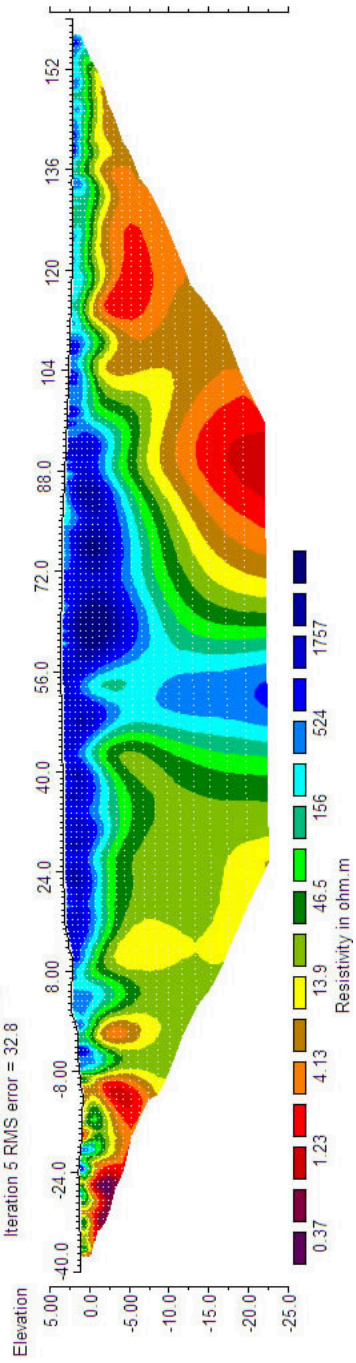

Figure 5.40: Ground resistivity along the breakwater. All distances in metres. Looking from north-east: the sea is on the left side – 17 May 2007 – NOTE: the colour and distance scales on the figures are different from Figure 5.39

5.15 Tide

5.15.1 Harmonic tide constants

Einar Kvale (Norwegian Hydrographic Service—Sjøkartverket) calculated the harmonic constants for 2006–07 and 2007–08 (Tables 5.6 and 5.7). The tables contain the harmonic constants with an amplitude greater than 1 cm. The phase is corrected to take into account the fact that the timestamp of the sea level means recorded by the tide gauge is at the start of the averaging period instead of in the middle.

Harmonic constant	H (amplitude in m)	G (phase in °)
Q1	0.0132	48.55
O1	0.0329	110.33
P1	0.0240	236.38
K1	0.0713	239.78
MU2	0.0273	76.74
N2	0.0979	22.21
NU2	0.0196	11.07
M2	0.5156	42.63
LDA2	0.0114	16.69
L2	0.0276	14.73
S2	0.1890	96.49
K2	0.0542	94.48
M6	0.0194	133.01
2MS6	0.0202	188.35

Table 5.6: Harmonic constants of the tide in Sveasundet, measurement period: 21 October 2006 to 10 September 2007

Harmonic constant	H (amplitude in m)	G (phase in °)
Q1	0.0103	46.57
O1	0.0328	108.95
P1	0.0217	230.01
S1	0.0129	315.79
K1	0.0701	238.75
MU2	0.0267	78.09
N2	0.0967	24.50
NU2	0.0191	13.13
M2	0.5109	43.51
LDA2	0.0114	16.98
L2	0.0180	33.19
S2	0.1867	96.95
K2	0.0541	94.84
M6	0.0175	136.49
2MS6	0.0202	190.30

Table 5.7: Harmonic constants of the tide in Sveasundet, measurement period: 10 September 2007 to 29 October 2008

5.15.2 Orthometric height vs. height over mean sea level

Since there were no permanent tide measurements in Svea, the altitude difference between the orthometric height and the height over MSL were unknown.

I calculated the MSL as the mean value of the tidal elevation data.

Moreover, I computed the orthometric height of the sea surface at different points in time based on freeboard and ice top surveys.

The comparison of the orthometric height from the surveys and the height over MSL from the tide gauge shows that the map datum is 0.32 m above the MSL, with a standard deviation of 0.06 m (Table 5.8).

Due to a data processing mistake, however, the height difference used in this thesis is 0.28 m instead of 0.32 m. The difference was not considered significant enough to reprocess all the data.

When taking into account the timestamp delay mentioned in 5.15.1, the difference becomes 0.33 m (instead of 0.32 m), with a standard deviation of 0.03 (instead of 0.04). Since the data is more accurate, the reduction in the standard deviation was expected.

In Table 5.8 the following notations are used:

h_{MSL}: height relative to MSL

h_o: orthometric height

σ: standard deviation of $h_{MSL} - h_o$

Date	$h_{MSL} - h_o$ [m]	σ [m]	Number of measurement points	Point names
week 4	0.33	0.04	9	i1.t.01.05 to i1.t.01.13
week 4	0.35	0.03	9	i1.t.02.05 to i1.t.02.13
week 4	0.35	0.02	10	i1.t.03.04 to i1.t.03.13
week 5	0.29	0.02	29	fs1 to fs29
week 8	0.27	0.01	9	h.ice
week 16	0.33	0.04	54	02, 04, 05 and 06
All data	0.28	0.06		

Table 5.8: Difference between the orthometric height and the height relative to MSL

5.15.3 Tide predictions based on the Longyearbyen tide table

In Longyearbyen the LAT is the reference water level and the MSL is 1.05 m above. When using the Longyearbyen tide table to predict the tide in Svea, 1.05 + 0.33 = 1.38 m must be subtracted from the predicted value in Longyearbyen. Also, the tide in Svea is delayed by approximately 40 minutes compared to Longyearbyen.

5.15.4 Seasonal tidal analysis

I studied the influence on the tide of the ice cover in parts or all of Van Mijenfjorden. It certainly has a dampening effect on the swell and modifies the flow profile through friction. Einar Kvale at the Hydrographic Service of the Norwegian Mapping Authority (Sjøkartverket) calculated the harmonic tide constants for April–May—the period when the ice cover is thickest—and July–August—a period with no ice cover—, and compared 2007 and 2008 values. M_2 is almost unchanged both in phase and in amplitude. The amplitude of S_2 changed by 2–3 cm, which is not significant compared to natural variations. The phase of S_2 changed more appreciably—over 30°—but that is because the period over which the harmonic analysis is done is too short to calculate all constants and K_2, which was not calculated, influences the phase of S_2 (Tables 5.9 and 5.10). Therefore, the ice cover does not seem to have a significant effect on the tide.

	April–May		July–August	
Constant name	Amplitude [m]	Phase [°]	Amplitude [m]	Phase [°]
M_2	0.5173	37.04	0.5114	38.88
S_2	0.2180	78.59	0.2013	108.96

Table 5.9: Harmonic tide constants – Sveasundet, 2007

	April–May		July–August	
Constant name	Amplitude [m]	Phase [°]	Amplitude [m]	Phase [°]
M_2	0.5195	38.04	0.5166	39.45
S_2	0.2122	77.81	0.1800	112.33

Table 5.10: Harmonic tide constants – Sveasundet, 2008

Chapter 6

Discussion

6.1 Ice thickness

The location of the maximum measured ice thickness—12.3 m seaward of crack 1—may be explained by the formation of superimposed ice at that precise location, as described pages 174–176 (observations for weeks 10 and 11).

Local thickness maxima seem to have occurred at the location of the tide cracks. This trend was observed at crack 1 in week 4, at crack 2 in weeks 7 and 8 and at crack 4 in weeks 16 and 20. It is possible that the hinge movement created a horizontal compressive load and, in turn, vertical tensile strain due to Poisson's effect. Aleksey Shestov (UNIS) witnessed this when he installed a stress sensor close to one of the quay piles in the harbour of Longyearbyen in the winter of 2008–09: he made sure the sensor head was several centimetres above the ice but when he returned to the site the ice had grewn so much that it had popped off the sensor head.

From the thin-sections presented in Section 5.11 it appears that, within 6 m of crack 1, at least the highest 50 cm of the coastal ice consist of snow ice. At 15 m from crack 1, the thickness of the snow ice is less than 50 cm. It is probably not much less that 50 cm, however, since the 30–40 cm-long wood sticks I placed around the surface water pond in week 10 (week-10 Section, page 174) were completely frozen in snow ice later on.

Due to a lack of data, several unexpected phenomena are delicate or pointless to analyse and explain:

- a large amount of ice melted away between week 16 and week 20 in a zone extending from crack 3 to 7 m seaward, while the water temperature did not start to get warmer before week 20 (Figure 5.2);

- in week 16, the ice thickness varied greatly in space;
- the ice thickness decreased from week 5 to week 8 in the zone 10 to 15 m from crack 1.

It is unfortunate that I did not perform more frequent ice measurements data. As the phenomena described above are a reminder of, such measurements are important because in the coastal zone, ice conditions change more than what surface observations may suggest.

Regarding the quality of ice thickness data, the measurements may be invasive by letting sea water flow to the surface (week-4 Section, page 166). In addition to modifying the boundary conditions over the flooded area, it may lead to the formation of several-centimetres-high ice mounds around the measurement holes, a phenomenon I observed when performing repeated thickness measurements throughout a tidal cycle in –15 °C air temperature.

6.2 Snow thickness

There are mainly two reasons why the snow layer seldom got thicker than 0.25 m. First, the combination of little precipitation and windy weather. Secondly, the presence of a thick snow layer weighs on the sea ice and leads to surface flooding and, consequently, to the formation of snow ice. In fact, the maximum snow layer thickness may be calculated. Assuming a snow density of 380 kg m^{-3}, an ice density of 900 kg m^{-3} and a sea water density of 1000 kg m^{-3}, Archimede's law states that:

$$1000 \cdot h_w = 380 \cdot h_s + 900 \cdot h_i, \tag{6.1}$$

where h_i is the ice thickness, h_s the snow thickness and h_w the water level relative to the bottom of the sea ice. Flooding occurs whenever the water level is bigger than the ice thickness, i.e.

$$h_w - h_i > 0, \tag{6.2}$$

which leads to

$$h_s > \frac{0.1 \cdot h_i}{0.38} \tag{6.3}$$

For an ice thickness of 1.0 m, the calculation above shows that the ice is flooded if the snow layer is thicker than 0.26 m, which is in perfect accordance with the observations.

The calculation above does, however, not fully apply for nearshore coastal ice, which is not floating completely freely. This concerns at least the 10 first metres seaward of crack 1. Therefore, it is probable that, in that zone, wind and precipitation are the main factors of the snow thickness.

6.3 Break-up

Although seasons 2004–05 and 2006–07 were comparable in AFDD, according to Høyland (2009), the ice was thicker in 2004–05 than in 2006–07, which explains why the break-up occurred two weeks earlier in 2007 than in 2005.

People with local knowledge of Svea claim that the break-up occurs simultaneously with spring tides. That proves not to be completely correct: all three years the break-up occurred in a period of rising tidal range and in all cases the range was higher than 1 m (Table 5.2). Therefore, the break-up date is probably better predicted by monitoring the water temperature (Section 5.1).

6.4 Vertical tidal ice movement

6.4.1 Movement in the course of a tidal cycle

For weeks 4, 8 and 16 it is possible to read the exact position of the most seaward tide crack directly on the plots in Figure 5.11 since the ratio of the amplitude of the vertical movement of the ice to the amplitude of the tide is increasing linearly shoreward of the crack while it is almost constant on its seaward side. This feature confirms the presence of the unsurveyed fifth crack, mentioned in the week-16 Section, page 182, about 16 m from crack 1. In addition, the fact that the amplitude ratio varies linearly means that crack-delimited zones of ice are rotating around a shore-parallel axis.

In week 4, the amplitude of the movement of the free-floating ice in the first six metres seaward of the hinge zone was dampened by 10–20 % compared to that of the sea level, probably because the free-floating ice was thin (about 0.5 m) and could, therefore, bend close to the tide crack.

The measurements show that the coastal ice is not in hydrostatic equilibrium with the sea water. This is a consequence of the friction forces along the tide cracks.

6.4.2 Hysteresis

I found no satisfactory explanation of the hysteresis described in Section 5.6.2.

6.4.3 Spatial variability of the vertical tidal ice movement

The measurements presented in Section 5.6.3 confirmed the dampening of the tidal movement with the proximity to the shore and the rotational movement of the ice around a shore-parallel axis. I have not found a reason why rotation also occurs, although in a smaller extent, around an axis perpendicular to the shore (Figure 5.15).

6.5 Horizontal ice movement

6.5.1 Throughout the tidal cycle

As opposed to the vertical movement, the horizontal movement between cracks 1 and 4 decreased with the distance from the shore (Figure 5.16), which suggests that the ice may be hinged along the bottom of the cracks. Indeed, in that case, the closer to the crack, the greater the horizontal component of the tidal movement of the top of the ice is. Another possible reason may be that the coastal ice is confined between the free-floating ice sheet and land, and is not allowed to expand horizontally.

6.5.2 Throughout the season

According to Carstens et al. (1979), the horizontal displacement is an order of magnitude higher at Kapp Amsterdam, which is only a few kilometres further south-west: they measured 1.5 m displacement during a period of two weeks. The validity of these measurements is, however, uncertain, since Biedorf (2002) did not measure any displacement at Kapp Amsterdam between 27 February and 24 April 2002.

Reports of horizontal displacement of coastal ice are found several places (Frederking and Nakawo, 1984; Stander et al., 1988; Frederking et al., 1986; Sayed et al., 1988). They are explained either by the dilation of the tide cracks due to adfreezing of sea water or by the wind conditions. The direction of the movements observed at Barryneset—more or less perpendicular to the shore—suggest that tide crack dilation is preponderant.

6.6 Tide cracks

Since the ice was almost certainly bottom-frozen shoreward of crack 1, crack 0 probably formed in a different way than the other tide cracks. A possible explanation is that the ice consisted of several layers and that the top, snow-ice layer yielded under compression loads applied along crack 1. Another explanation is that the crack formed under thermal contraction.

As pointed out by Stander (2006), in the beginning of the ice cover period, the ice is thin and warm, therefore, "pliable enough to bend with changing water levels without fissuring." As the cover thickens and becomes more brittle, shore-parallel cracks form.

The distance between the cracks grew with time as a the ice thickened and its bending strength, in turn, increased.

According to Carter et al. (1998), the theory of beams on elastic foundations (Hetenyi, 1946) predicts that the location of a maximum bending moment for a thin floating ice plate is:

$$L_{max} = \frac{\pi}{4} l, \tag{6.4}$$

where

$$l = \left[\frac{E h^3}{12 \rho g (1 - \nu^2)} \right]^{\frac{1}{4}} \tag{6.5}$$

and E is the elastic modulus of the ice, h its thickness, ρ its density and ν its Poisson ratio.

Theoretical values of L_{max} are calculated in Table 6.1 using values from the ice core analyses for E and ρ (Section 5.11), from Løset et al. (2006) for ν and from the assumed date of crack formation for h (Table 6.1).

Carter et al. (2001) point out that at a distance $L_{90} = \frac{5.6}{8.8} L_{max}$ the bending moment is 90 % of the maximum moment, and irregularities in the ice may cause it to crack at that distance. The comparison of the theoretical L_{90} with the measured length between cracks, L_{obs}, shows that the model has a high error margin ($\pm$ 30 %), which may be due, in part, to the side-effects at the corners. Besides, equations 6.4 and 6.5 apply to a beam with a free end, while the coastal ice is confined.

Parameter	Crack 1–2	Crack 2–3	Crack 3–4	Crack 4–5
E [GPa]	1.06	1.10	1.20	1.33
ρ [kg m^{-3}]	720	785	810	865
ν	0.3	0.3	0.3	0.3
h [m]	0.5	0.7	0.6	0.8
L_{max} [m]	5.1	6.4	5.8	7.4
L_{90} [m]	3.3	4.1	3.7	4.7
L_{obs} [m]	2.5	3.5	3.5	6.4
$\frac{L_{90}}{L_{obs}}$	1.3	1.2	1.1	0.7

Table 6.1: Ice parameters and theoretical distances between tide cracks

6.7 Ice foot and coastal ice

6.7.1 Conditions of coastal-ice formation, growth and decay

The mechanisms described in Section 5.10 occur under the influence of varying meteorological and geographical conditions. In this section, we will discuss how such conditions determine the morphology and structure of the coastal ice. A similar discussion about the parameters that affect the formation of the ice foot is found in (Wiseman Jr. et al., 1981).

Wind and waves Wind prevents the formation of a continuous ice cover: under windy conditions, pancakes form on the surface of freezing waters. If the wind blows towards land, pancakes are pushed ashore and pile up into a berm.

Waves have a similar effect as the wind in that they break up the ice cover and push pancakes ashore. The size of the waves determines how far ashore pancakes are stranded and, therefore, is an major factor of the size of the ice foot.

Waves and wind generate spray and swash. Spray and swash freeze on land if the soil is cold enough, forming an ice cap. If a pancake berm has formed, they consolidate it.

During break-up, waves increase the amount of water washed over the ice foot and, thus, the melting. They also exert a mechanical load on the ice foot, accelerating its decay.

Sea ice regime Sea ice conditions vary in space and in time. When it comes to coastal-ice conditions, one critical aspect is how long it takes between the first sea ice appears until the sea freezes over, if it ever does. During this period, drift ice is subjected

to the influence of wind and waves as described above. Therefore, the longer this period, the bigger the ice foot.

The type of drift ice also has an importance: it may be anything from frazil to cakes, floes and even icebergs.

Temperature The ground temperature, which is influenced by the air temperature, determines whether spray, swash and moisture freeze on land or not. In the tidal zone, the ground is intermittently above and under water. When it is above water, an ice cap is forming, but when is is under water, it is melting. Therefore, the lower limit of this ice cap is a function both of the ground temperature and the duration of water coverage during the tidal cycle.

At Barryneset, warm weather during the ice cover period seemed to increase the amount of water flooding the ice cover. The surface water may freeze and, therefore, influence the structure of the coastal ice.

During break-up the air and ground temperatures have a direct effect on the ice foot melting. Ice resting over warm ground may detach from it more easily under the action of the waves.

Coast morphology and current Drift ice may be forced into specific places depending on the shape of the coastline and the current distribution. In such places, the formation of berms and the stranding of cakes and floes is likely.

The beach slope has an influence on the wave regime and, thereby, on the coastal-ice morphology.

In addition the beach slope has an influence on the tidal bending of the coastal ice and, thus, on the tide cracks. On gentle slopes, the ice is grounded over a long distance and many cracks appear (Dionne, 1994). Along vertical walls, on the other hand, a single crack separates an ice bustle from the free-floating ice (Løset and Marchenko, 2008).

The influence of the coast morphology was already pointed out in Charlesworth (1957).

Tide The tide controls the height of the ice foot. The altitude of the top of the ice foot seems, indeed, to coincide with the MHW mark.

The tide is also what causes the coastal ice to crack up. It seems that, depending on the ice thickness and the tidal amplitude, the transition between the free-floating ice and the hinge zone may be either smooth, like at Barryneset, or discontinuous, like in the St Lawrence estuary (Dionne, 1994).

During break-up, the tide generates vertical forces on the remaining ice on land.

The tidal range also determines the amount of time when this ice is flooded, which, in turn, influences the melting process.

Precipitation The presence of snow on top of the ice may weigh on the coastal ice and lead to surface flooding and the formation of snow ice.

During break-up, precipitation in the form of rain accelerates the melting process.

Groundwater Groundwater seepage is a known mechanism of ice foot creation (Prowse and Gridley, 1993, p. 7), but I did not observe any seepage at Barryneset.

6.7.2 Ice foot: definition

The description of the ice foot processes at Barryneset (Section 5.10) are a relevant input to the discussion on the definition of the ice foot started in Section 2.2.3.

Dionne rightly points out that the morphology of the ice foot may vary considerably from one location to another (Dionne, 1994). He, therefore, proposes the generic definition mentioned in Section 2.2.3: "a fringe of ice of varied width at the edge of the shores in cold regions, entirely or partially attached to the shore (at the bottom or by the side) and affected or unaffected by the vertical movements of the water surface." When applied to Barryneset, though, this definition turns out to be both ambiguous, unpractical and non-intuitive.

The ambiguity comes from the fact that Dionne qualifies coastal ice as ice foot if it is at least partially attached to the shore, either at the bottom or by the side, but does not mention tide cracks. One possibility is to consider that tide cracks divide the coastal ice into separate zones and that, for a zone to be a part of the ice foot, it has to be attached to the ground at least in one point. In that case, at Barryneset, the ice foot extends to crack 1. Due to the high friction along the cracks, the movement of the ice on one side of a crack strongly affects the movement of the ice on its other side and, therefore, it would also be possible to consider the ice in the tide crack zone as a whole, in which case the ice foot at Barryneset would extend to crack 4—the most seaward tide crack.

The reason why Dionne's definition is not practical is because it is not possible to determine the extension of the ice foot with the naked eye during the ice cover period. In fact, not even a survey of the movement of the ice top is enough, since the fact that ice is not affected by the tide does not imply that it is attached to the ground. The only ways to determine whether ice is attached to the ground are probably either to measure the temperature at the interface between the ice and the ground or to dig trenches.

A last problem that arises with Dionne's definition is illustrated during break-up at Barryneset. The ice between crack 1 and crack 2 was not directly attached to the ground

(Section 5.10) and, therefore, not a part of the theoretical ice foot. When looking at Figure B.92, however, it feels intuitive to consider that zone as a part of the ice foot.

The issues above raise the question of whether it is necessary to define the ice foot throughout the whole season. Although in the St-Lawrence-Estuary locations described by Dionne (Dionne, 1994), the upper-strand and lower-strand ice feet are easily identifiable throughout the whole season, at Barryneset, the ice foot merged with the sea ice into a continuous, albeit cracked zone—the *hinge zone*—with no clear features to help identify the ice foot. Comparable situations are described in Greene (1970) and Charlesworth (1957, pp. 174–175). Of course, it is still possible to define a theoretical ice foot but I can not see what would be gained from that, at least not at Barryneset. Yet, if there should appear to be a good reason to define an ice foot during the ice cover period, the discussion above is a reminder that this definition needs to be precise, especially when it comes to the delimiting role of the tide cracks. Otherwise it may be better to consider the zone shoreward of the most seaward tide crack—the *hinge zone*—as a whole. If desirable, one may then divide the *hinge zone* into sections based on the locations of the shore-parallel tide cracks.

6.7.3 Environmental influence of the ice foot

Geomorphology Most ice foot studies are concerned with geomorphological coastal processes (Dionne, 1994; Owens, 1976; Allard et al., 1998).

The ice foot has a dual influence on the shore: during the open-water period, it prevents wave erosion, while during break-up, it may carry away shore masses. According to Owens (1976), this latter effect is negligible.

Ice movement in the hinge zone displaces underlying masses. At Barryneset it changed the shape of the geosynthetic bags and, on the east side, left a ditch, which was, however, rapidly levelled out after the ice had disappeared.

Engineering Few engineering studies of the ice foot were ever done. This very fact was actually a major motivation for the work presented in this thesis. The effect of the ice foot depends on ice conditions:

- During the freeze-up, the ice foot prevents erosion of gravel slopes, as mentioned above. I have, however, not found any study of the impact of the ice foot on protected slopes (rip-rap, bags, tetrapods). I assume that it rigidifies the structure and, in addition, reduces its porosity, and, thus, its ability to dissipate wave forces. Therefore, it should probably be taken into consideration when designing a shore protection layer.

- During the ice cover period, the rotation of the ice in the hinge zone may lift protection elements. Again, I have not found any study on this for sea ice. It is probably even a bigger issue in reservoirs, where the water level may fluctuate with many metres and rotate the coastal ice extensively.

6.8 Ice properties

6.8.1 Ice texture analysis

The size and orientation of the crystals have an influence on the results from the mechanical tests. For samples Pt5-H2 and Pt5-H3, the crystal size was comparable to the sample size, and the 45° angle between the loading direction and the basal plane direction caused the maximum shear stresses to act along one single basal plane. When the strength of the basal plane was reached through a stress build-up, the sample failure was brittle.

For samples where crystals have a predominant direction, Peyton (1966) showed that the strength will be lowest when this direction is 45° to the direction of compression and that it reaches local maxima at 0 or 90°. As seen in Lainey and Tinawi (1984), ice loaded in compression perpendicular or parallel to the C-axis is 2 to 3 times stronger than ice loaded at 45°. Therefore, since the direction was 45° in the ice cores, higher strengths would have been obtained if the cores had been taken in any other direction.

In the coastal ice, due to the way the ice was formed, the size of the crystals compared to the diameter of the samples varied from very small (factor 100) to small (factor 10), as seen in Figures 5.30 and 5.33. Core Pt4-H3 contained ice formed directly from sea water while core Pt1-H1 contained ice formed by snow that was soaked with sea water at high tide. Because the brine was drained at low tide, the ice at Pt1-H1 was porous and had a low salinity.

6.8.2 Residual stresses

In Figure 6.1 the residual stresses are plotted against the brine content. The two lowest residual stresses were found in Pt5-H2 and Pt5-H3. Like for the strength, the residual stresses would probably have been higher if the samples had been taken with the predominant crystal orientation parallel with or perpendicular to the direction of compression. The residual stress tended to decrease with the brine content, in accordance with (Cole, 1997).

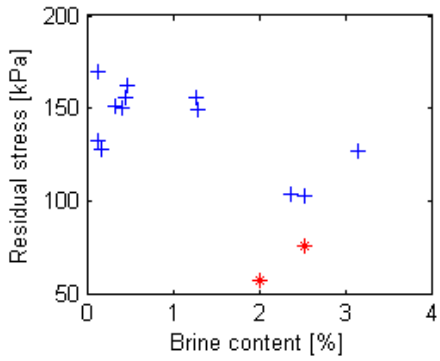

Figure 6.1: Residual stress vs. brine content – Coastal ice with crosses, free-floating ice with stars

6.8.3 Salinity

The salinity measurements contradict those of (Frederking and Nakawo, 1984), where the salinity was higher on flooded ice than on free-floating ice. I have not found any explanation for this contradiction.

6.8.4 Young's modulus

As seen in Figure 6.2, the Young's modulus is decreasing with porosity in accordance with (Moslet, 2007b) and (Timco and Frederking, 1990). The physical mechanism for elastic deformation is, in fact, strain of the atomic structure. The smaller the porosity, the denser that structure is.

6.8.5 Strength

In Figure 6.3, the data is split in 3 groups: free-floating ice (star), Pt3-H1 (circle) and the rest of the coastal ice (cross).

The reason why Pt3-H1 was plotted differently is that it was the only coastal-ice core that failed brittlely. That was interpreted as a sign that its structure was different from that of the other coastal-ice cores where, based on the four thin-sections, the crystal orientation was random. One reason why the structure of the ice in Pt3-H1 would be different is that Pt3 was located in a place that remained flooded in weeks 10 and 11 (pages 174 and 176).

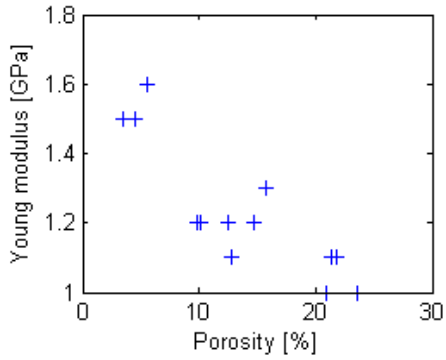

Figure 6.2: Young modulus vs. porosity

The strengths of the free-floating ice cores were a bit lower than the porosity alone would indicate, possibly due to the presence of large grains (Lee and Shulson, 1986).

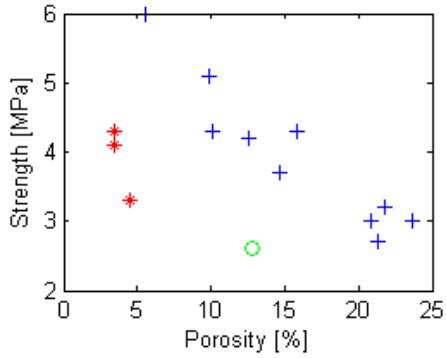

Figure 6.3: Strength vs. porosity – coastal ice with crosses, free-floating ice with stars and Pt3-H1 with a circle

6.8.6 Data quality

We only analysed the properties of one sample per location, but the strong geographical data dependency is coherent with on-site observations of the structure of the ice and the way it forms. In addition, strength tests of the samples that had gone through creep tests showed a satisfactory consistency.

The storage duration varied because not all tests were done the same day. We did not assess the effect of storage duration.

Finally, it should be noted that the coastal-ice cores were taken in the top 50 cm while the coastal ice was up to 1.6 m thick (Pt1). Therefore, the results are not fully representative.

6.9 Ice stresses in the hinge zone

Previous studies in Sveabukta showed that the wind does not affect ice stresses below 20 m s^{-1} (Teigen et al., 2005). In the early winter of 2008, Aleksey Marchenko (UNIS) measured the tidal current close to the breakwater and found a maximum value of 30 cm s^{-1}. It is unlikely that such a small current would have a major effect on the stresses in the ice cover.

Although there were no thermal stresses in the free-floating ice, the inside of the cracks was intermittently in contact with air and water. Therefore, it is reasonable to assume that some of the measured stresses were thermally-induced.

The 20-kPa peak of the stresses perpendicular to the cracks is likely due to the opening and closing of the crack depending on the tide, which is a discontinuous process involving both friction and mechanical yielding.

We did not expect to measure the highest stresses in the direction parallel to the crack. The literature lead us to think that *tidal jacking*, caused by the freezing of water in the tide cracks (Section 2.2.5), would produce sizeable stresses in the direction perpendicular to the stress. We also thought that, given the length of the front of the breakwater (25 m), it was reasonable to assume plane strain conditions.

It is possible that tidal jacking contributed to the stresses perpendicular to the cracks. When it comes to the direction of the stresses, however, it seems that the invalidity of the plane-strain hypothesis might be explained by the presence of a rubble accumulation in the west corner of the breakwater. In fact, the rubble might have caused the ice to bend in the direction parallel to the cracks, which would produce bending stresses in same direction.

The observed stress variations were within the range of values found in the literature. Frederking et al. (1986) measured 70 kPa off the Coast of Adams Island, where the tidal range is up to 2 m, while Sayed et al. (1988) measured 500 kPa there. Moslet (2001) found 25 kPa in Svea and Nikitin et al. (1992), 500 kPa in the active zone of the Okhotsk Sea, with a tidal range of 1.25 m. As in Svea, they all found that the highest stresses were in antiphase with the tide. However, the ice around the breakwater was not translating away

from the shore as Frederking and Nakawo (1984) observed around the Nanisivik wharf piles, where they measured horizontal displacements of several metres throughout the season. Stander et al. (1988) also recorded horizontal displacements, of several centimetres per day.

Measured stresses were small compared to stresses measured on offshore structures. As Brian Morse (University of Alberta) rightly made me aware of, for large structures like dams, the total force may, however, be considerable. Ice forces on reservoirs are discussed in Carter et al. (1998, 2001) among others.

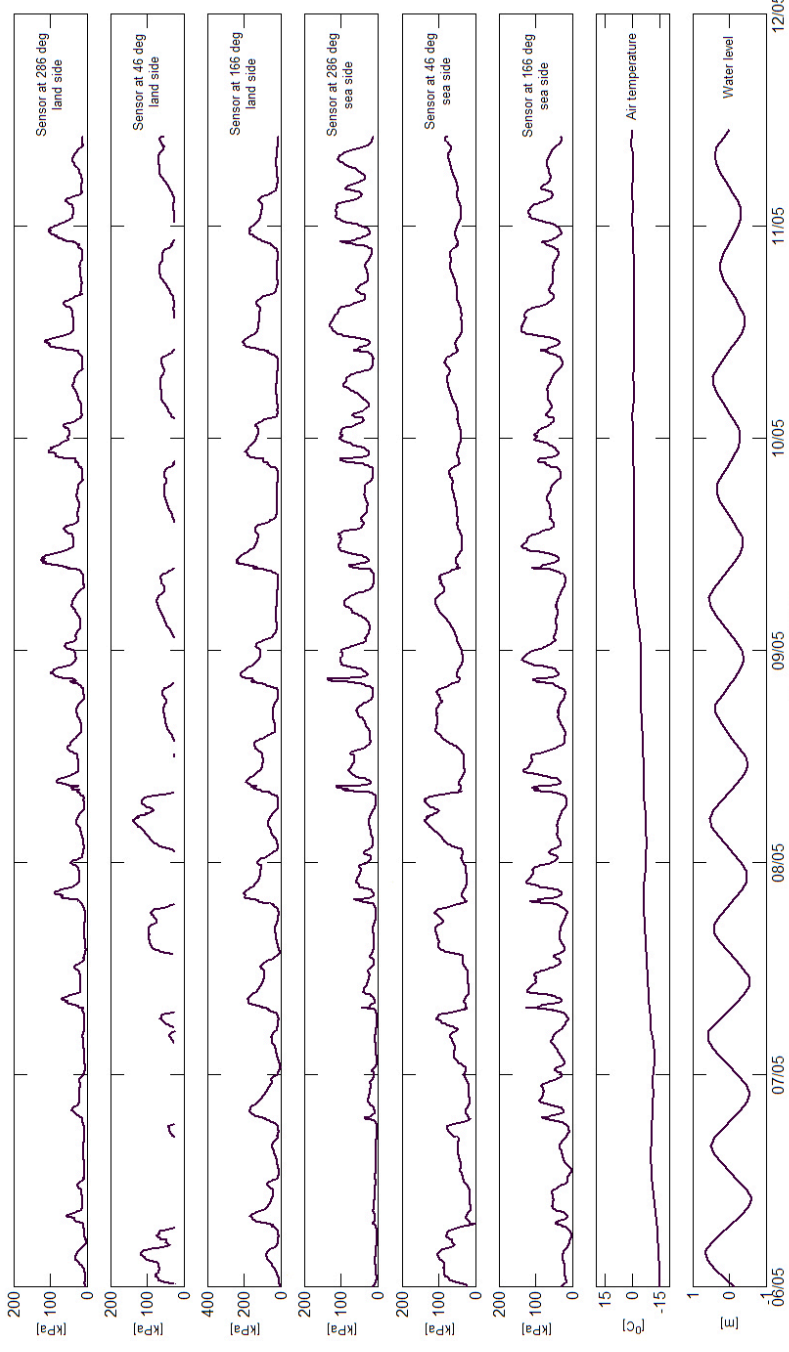

Figure 6.4: Air temperature, sea level and stress intensities in the two rosettes on both sides of the crack – full measurement period

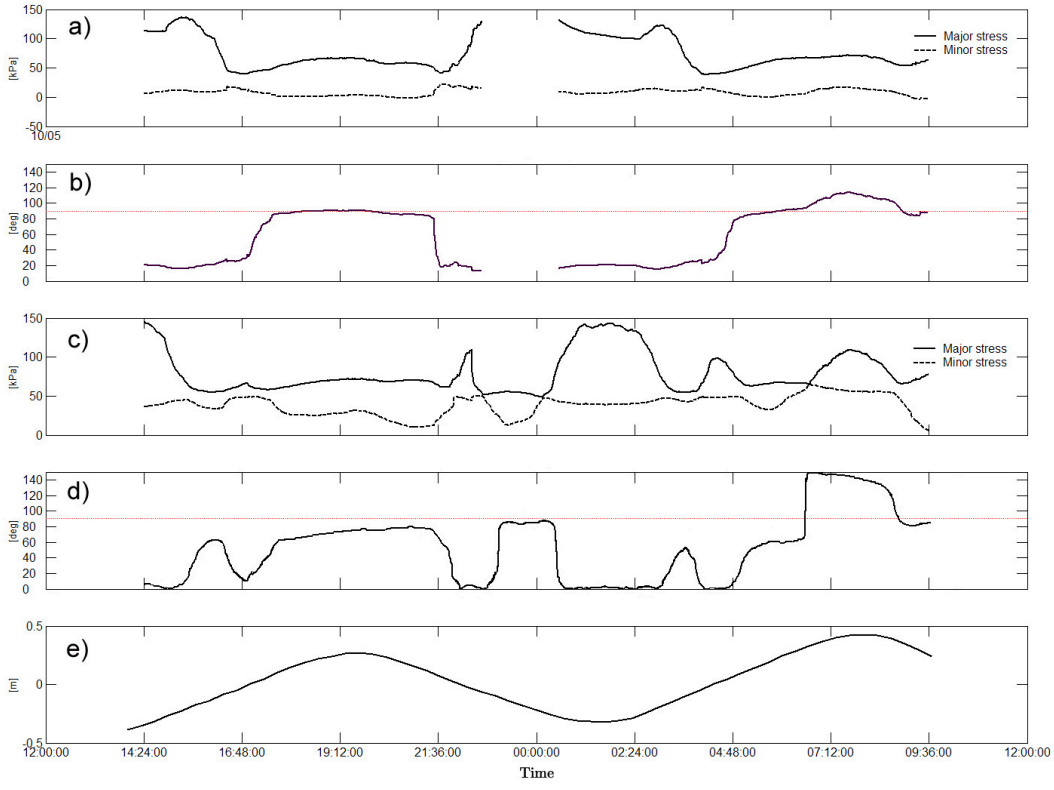

Figure 6.5: Principal stresses and direction on the land side (a and b) and on the sea side (c and d) from 10 to 11 May. The sea level is shown on e). In this figure, the 0° does not correspond to north as elsewhere in this thesis, but to the direction parallel to the tide crack (46° to the north).

6.10 Thermal regime and frost heave

The cooling of the breakwater with time may be due to the fact that the AFDD was 5 % higher in 2007–08 than in 2006–07 (Figure 5.37). Another possible explanation is that the breakwater was gradually cooling down toward a state of thermal equilibrium.

Ideally, a numerical model should be developed. A simple, plane heat flux numerical model—the plane being vertical and orthogonal to the direction of the breakwater—would give a rough estimate of the thermal flux in the undisturbed seabed. A more precise, 3-dimensional model would require to make assumptions on the horizontal thermal flux from land in the direction of the breakwater.

6.11 Ground resistivity

A striking feature is the vertical high-resistivity zone at the base of the breakwater—around the 44-m mark for the 2006 measurement and around the 52-m mark for the 2007 measurement. We did, unfortunately, not find a good explanation for it.

A problem with the ground resistivity measurements is that saline clayey permafrost has a lower resistivity than the dry, dumped masses. Therefore, it is difficult to conclude anything on the state of the permafrost at a given point in time. By repeating the measurements along the same profile, however, it would be possible to detect the possible formation of permafrost in the dumped masses.

Chapter 7

Conclusion

7.1 Coastal-ice properties

The inhomogeneity of the coastal ice was reflected in the values of the physical and mechanical properties of the cores, which were taken in the top 50-cm-layer. The salinity changed from about 0.4 to 4.5 psu and the relative air volume from 21 to less than 1 % from the shore to the free-floating ice. Creep, stiffness and strength increased with the distance from the shore. The elasticity ranged from 1 to 1.5 GPa and the strength from about 3 to 4 MPa.

7.2 Stresses along tide cracks

Measuring stresses in metre-thick, inhomogeneous, coastal ice is a challenge of which my colleagues and I barely scratched the surface. We installed pressure sensors both in the upper ice-foot and in the free-floating sea ice. There were almost no stresses in the free-floating sea ice while stresses up to 150 kPa were measured in the ice foot. Contrary to what one might think, the highest stresses were measured in the direction parallel—not perpendicular—to the tide cracks.

7.3 Ice foot

Dionne's definition of the ice foot succeeds, all in all, in generalising the definition of the ice foot. Dionne is right that the definition of the ice foot should not be linked to specific

tide levels as there are a multitude of other parameters that affect the morphology of the ice foot. In addition, it seems correct to distinguish between a higher part, the *upper-strand ice foot*, and a lower part, the *lower-strand ice foot*.

Based on the observations from Barryneset I would, instead, suggest a temporal approach by defining a *freeze-up ice foot* corresponding, in effect, to Dionne's *upper-strand ice foot*, and a *break-up ice foot* that, in the case of Barryneset, would include the ice zone between crack 1 and crack 2. The *freeze-up ice foot* may be defined as the ice building up on the shore before the surrounding waters freeze over. It would require observations from more sites to define the *break-up ice foot* in a generic way. Along rivers, the *break-up ice foot* seems to correspond to the *ice ledge*. During the ice cover period, the distinction between an *upper-strand* and a *break-up* ice foot may still be possible in some places, like the in St Lawrence Estuary, but at Barryneset it makes more sense to consider the *hinge zone*, which is possible to identify to the naked eye, as opposed to either ice foot.

The discussion around the ice foot and, more generally, the review of the literature testify to the dependence of the morphology of coastal ice on the environment.

With today's limited knowledge, it is difficult to predict ice conditions at a given site. The researchers at UNIS whom I consulted at the beginning of the study had been working with sea-ice at Kapp Amsterdam, only a few kilometres from Barryneset, and mistakenly assumed the conditions at Barryneset would be similar. Indeed, at Barryneset, there were no ridges, unsignificant horizontal displacement and certainly no encroachement during the ice cover period.

One achievement of this thesis has been to thorougly describe processes at a given site and try and relate them to the underlying environmental causes. By performing similar studies in different environments, we may reach the level of knowledge required for making reliable predictions.

7.4 Ice loads

The nature of the ice loads varied throughout the season.

During freeze-up, drifting pancakes were scrubbing against the shore, causing limited damage on the soft, geosynthetic-bag protection-layer. As the ice foot formed, it increasingly protected the shore against scrubbing.

During the ice cover period, the horizontal movement of the ice was negligible and, therefore, there occurred no ice encroachment, which is what generally damages shore protection layers. Under the influence of the tide, the ice was, however, rotating and, in doing so,

displacing underlying masses. Neither the tide nor thermal expansion caused significant horizontal stresses on the structure.

During break-up, the shore was gradually more exposed to scrubbing from drifting cakes as the protective ice layer was decaying and detaching. Pile-ups occurred at the end of the break-up but they were small compared with pile-ups described in the literature (Baltic Sea, Beaufort Sea) and perpertrated little damage because, that late in the season, the ice was rotten and soft. Since these were the most destructive events, the ice conditions may be characterised as mild.

The pile-ups may still cause damages. Therefore, it makes sense to take them into account when designing a structure. First, the locations exposed to pile-up loads should be identified. On the Barryneset breakwater, only the east corner was exposed. It may be possible to design the structure so as to reduce the area and number of exposed locations. Once this has been done, it may be wise to reinforce the protection layer in these locations, either with sacrificial geosynthetic bags or with armour rocks.

7.5 Further work

7.5.1 Coastal-ice processes

The multitude of processes observed at Barryneset and their unpredictability made it difficult to study them in detail. The processes that I have identified require further investigation.

Of special interest is the mapping of the properties of the ice in the hinge zone, for which sampling over the full thickness instead of just the upper layer is desirable.

The results from the stress measurements in the hinge zone indicate that it is necessary to measure the stresses in more locations and depths and to develop a finite element model in order to understand the stress distribution. It implies installing stress sensors deep in the ice and under the water, which is a technical and practical challenge. It also requires a thorougher investigation of the tide cracks. The first task is to understand where and how they occur. Then to include them in the finite element model of the coastal ice. This latter task requires assessing friction forces along the cracks.

Finally, observations from two consecutive break-ups indicates that the pile-up intensity is stochastic. Therefore, it would be interesting to create a pile-up model that could predict a 10- or 50-year intensity.

7.5.2 Thermal regime and geotechnical consequences

Temperature measurements below the surface and vertical displacement of the breakwater suggest that a combination of long-term cooling and seasonal, freeze-thaw cycles take place. These mechanisms are poorly understood.

A thermal model should be created in order to check the hypothesis that permafrost is forming inside the breakwater. Most parameters may be found in this thesis and in (Gregersen et al., 1983) and (Caline, 2000). There is, however, some uncertainty as to the composition of the seabed.

Further, the effect of the thermal regime of the seabed and the breakwater on the stability of the breakwater has not been studied.

Bibliography

M. Allard, Y. Michaud, M.-H. Ruz, and A. Héquette. Ice foot, freeze-thaw of sediments, and platform erosion in a subarctic microtidal environment, Manitounuk Strait, northern Quebec, Canada. *Canadian Journal of Earth Sciences*, 35:965–979, 1998.

O. Artières, M. G. G. Bæverfjord, F. Caquel, P. Delmas, L. Grande, A. Langeland, I.-L. Solberg, and A. Watn. Geosynthetics for innovative sustainable solutions in arctic climate, SINTEF-report SBF IN F09404. Technical report, SINTEF, Trondheim, Norway, 2009.

M. G. G. Bæverfjord and V. Thakur. A geotechnical evaluation of embankment construction in the Braganza bay, Svalbard. Technical report, SINTEF, 2006.

S. Barrault and K. V. Høyland. Mechanisms and measurements of generation of stresses in first-year landfast sea ice. In *19th International Conference on Port and Ocean Engineering under Arctic Conditions (POAC)*, pages 685–694, Dalian, China, 2007.

R. Biedorf. Loads on structures exerted by sea ice in arctic regions. Master's thesis, The University Centre in Svalbard (UNIS) and Technical University Bergakademie Freiberg, 2002.

F. Caline. Modelling permafrost temperature response to variations in meteorological data. Master's thesis, The University Centre in Svalbard (UNIS) and Ecole Nationale des Ponts et Chaussées (ENPC), 2000.

F. Caline and S. Barrault. Measurements of stresses in the coastal ice on both sides of a tidal crack. In *19th IAHR International Symposium on Ice*, Vancouver, British Columbia, Canada, 2008.

T. Carstens, K. Karal, and J. H. Kjeldgaard. Svea kaiprosjekt – isundersøkelser (in Norwegian), technical report SINTEF STF60 A79006. Technical report, Vassdrags- og havnelaboratoriet, NTH, Norway, 1979.

D. Carter, D. S. Sodhi, E. Stander, O. Caron, and T. T. Quach. Ice thrust in reservoirs. *Journal of Cold Regions Engineering*, 12:169–183, 1998.

D. Carter, E. Stander, O. Caron, J. P. Tournier, and C. Pek. Poussées statiques des glaces. In *11th Workshop on River Ice. River ice processes with a changing environment*, 2001.

J. K. Charlesworth. *The quaternary era: with special reference to its glaciation*. Edward Arnold, London, 1957. Cited in (Dionne, 1994).

D. M. Cole. Modeling the cyclic loading response of sea ice. *International Journal of Solid Structures*, 35, 31–32:4067–4075, 1997.

G. F. N. Cox and W. F. Weeks. Equations for determining the gas and brine volumes in sea ice samples, crrel report 82-30. Technical report, CRREL, 1982.

K. Croasdale. Ice forces on fixed, rigid structures. Technical report, International Association for Hydraulic Research, 1980.

R. A. Davis Jr. *Encyclopædia Britannica*, chapter Coastal Landforms. Encyclopædia Britannica Online, 16 March 2009. URL `http://www.britannica.com`.

J.-C. Dionne. L'action des glaces sur les littoraux. In *POAC 81: the 6th international conference*, pages 955–973, Québec, Canada, 1981.

J.-C. Dionne. *Cold Climate Landforms*, chapter 16. The notion of icefoot with special reference to the St Lawrence Estuary, pages 325–349. John Wiley & Sons, New York, 1994. ISBN 0471940437.

eKlima. Meteorological and climatological database. The Norwegian Meteorological Institute, 2009. URL `http://eklima.met.no`.

J. Finseth. Laboratorieforsøk hull 31, Kapp Amsterdam, Svea. Technical report, NTNU, 2002a.

J. Finseth. Laboratorieforsøk hull 11, 21 og 31 Sveasundet og Kapp Amsterdam (hull 31). Technical report, NTNU, 2002b.

J. Finseth, R. Sandven, and P. O. Moslet. Grunnundersøkelser for ny vegfylling, Braganzavågen, Svea. Technical report, NTNU, 2002.

D. L. Forbes and R. B. Taylor. Ice in the shore zone and the geomorphology of cold coasts. *Progress in Physical Geography*, 18:59–89, 1994. Cited in (Schwartz, 2005).

R. M. Frederking. Sea ice management - coastal structures. In *Sea Ice Management Seminar, St. John's, Newfoundland*, 1983.

R. M. Frederking, E. Wessels, J. B. Maxwell, S. Prinsenberg, and M. Sayed. Ice pressures and behaviour at adams island, winter 1983/1984. *Canadian Journal of Civil Engineering*, 13:140–149, 1986.

R. M. W. Frederking and M. Nakawo. Ice action on Nanisivik Wharf, winter 1979–1980. *Canadian Journal of Civil Engineering*, 11:996–1003, 1984.

M. Gabrielsen, S. Barrault, F. Caline, and K. V. Høyland. Comparison of physical and mechanical properties of coastal ice and level ice. In *19th IAHR International Symposium on Ice*, Vancouver, British Columbia, Canada, 2008.

M. Gary, R. McAfee, and C. L. Wolf, editors. *Glossary of Geology*. American Geological Institute, Washington, D.C., 1972. ISBN 0913312002. Cited in (Dionne, 1994).

K. D. Gawne. Assessing the susceptibility of shorelines to inundation by ice: a practical approach. In *10th Workshop on river ice*, Winnipeg, Manitoba, 1999.

J. C. C. George, H. P. Huntington, K. Brewster, H. Eicken, D. W. Norton, and R. Glenn. Observations on shorefast ice dynamics in Arctic Alaska and the responses of the Iñupiat hunting community. *Arctic*, 57:363–374, 2004.

T. S. Glickman. *Glossary of Meteorology, Second Edition*. American Meteorological Society, Boston, MA, 1999. URL `http://amsglossary.allenpress.com/glossary/`.

M. A. Granskog, M. Leppäranta, T. Kawamura, J. Ehn, and K. Shirasawa. Seasonal development of the properties and composition of landfast sea ice in the Gulf of Finland, the Baltic Sea. *Journal of Geophysical Research*, 109, 2004.

H. G. Greene. Microrelief of an Arctic beach. *Journal of Sedimentary Research*, 40, 1970.

O. Gregersen and T. Eidsmoen. Permafrost conditions in the shore area at Svalbard. In *Proceedings of the 5th International Conference on Permafrost*, pages 933–936, Trondheim, Norway, 1988. Tapir Publishers, Trondheim.

O. Gregersen, A. Phukan, and T. Johansen. Engineering properties and foundation design alternatives in marine svea clay, svalbard. In *Proceedings of the Fourth International Conference on Permafrost*, pages 384–388, Fairbanks, Alaska, 1983.

M. Hetenyi. *Beams on elastic foundation*. University of Michigan Press, Ann Arbor, Michigan, 1946. ISBN 0472084453. Cited in (Carter et al., 1998).

P. Hoekstra and D. McNeill. Electromagnetic probing of permafrost. In *2nd International Conference on Permafrost*, pages 517–526, Washington, D.C., 1973.

K. V. Høyland. Ice thickness, growth and salinity in the Van Mijen fjord on Svalbard, Norway. *Polar Research*, 2009.

IAHR. Multilingual ice terminology. Technical report, International Association for Hydraulic Research, 1980.

IHB. Hydrographic dictionary, fifth edition. International Hydrographic Bureau, Monaco, 2009. URL `http://www.iho-wms.net:8080/hydrodic/en/`.

B. Instanes. Coal loading pier in Svea, Svalbard. In *International Conference on Port and Ocean Engineering and Arctic Conditions (POAC)*, pages 217–232, Trondheim, Norway, 1979.

J. A. Jackson and R. L. Bates. *Glossary of Geology*. American Geological Institute, 1990.

E. K. Kane. *Arctic Explorations: The Second Grinnell Expedition in Search of Sir John Franklin, 1853–1855*. Childs and Peterson, Philadelphia, 1856. Cited in (Dionne, 1994).

A. Kovacs and D. S. Sodhi. Shore ice pile-up and ride-up — field observations, models, theoretical analyses. *Cold Regions Science and Technology*, 2:209–298, 1980.

A. Kovacs and D. S. Sodhi. Sea ice piling at fairway rock, bering strait, alaska: observations and theoretical analyses. In *POAC 81*, 1981.

A. Kovacs, D. S. Sodhi, and G. F. N. Cox. Bering Strait sea ice and the Fairway Rock icefoot, CRREL report 82-31. Technical report, U.S. Army Cold Regions Research and Engineering Laboratory, Hanover, NH, USA, 1982.

L. Kristensen. *Glacier surges and landforms in a permafrost environment, inner Van Mijenfjorden, Svalbard*. PhD thesis, University of Oslo (UiO) and the University Centre in Svalbard (UNIS), 2009.

L. Kristensen, H. Christiansen, and F. Caline. Temperatures in coastal permafrost in the Svea area, Svalbard. In *Ninth International Conference on Permafrost*, pages 1005–1010, Fairbanks, Alaska, 2008.

L. Kristensen, H. Juliussen, H. H. Christiansen, and O. Humlum. Structure and composition of a tidewater glacier push moraine, svalbard, revealed by dc resistivity profiling. *Boreas*, 38(1):176–186, 2009.

L. Lainey and R. Tinawi. The mechanical properties of sea ice – a compilation of available data. *Canadian Journal of Civil Engineering*, 11:119–127, 1984.

O.-A. Larsen. Forprosjekt – vei til Ispallen. Technical report, Barlindhaug Consult AS, 2004.

T. S. Ledley. Sea ice: multiyear cycles and white ice. *Journal of Geophysical Research*, 90:5676–5686, 1985.

R. W. Lee and E. M. Shulson. The strength of ductile ice under tension. *Journal of Offshore Mechanics and Arctic Engineering*, 110:187–191, 1986.

I. O. Leont'yev. Coastal profile modeling along the Russian Arctic coast. *Coastal Engineering*, 51:779–794, 2004.

P. Liferov. *First-year ice ridge scour and some aspects of ice rubble behaviour*. PhD thesis, The Norwegian University of Science and Technology, NTNU, 2005.

M. H. Loke and R. D. Barker. Rapid least-squares inversion of apparent resistivity pseudosections by a quasi-newton method. *Geophysical Prospecting*, 44(1):131–152, 1996.

S. Løset and A. Marchenko. Ice bustles on quay piles: field studies and numerical simulations. In *19th IAHR International Symposium on Ice*, Vancouver, Canada, 2008.

S. Løset, K. N. Shkhinek, O. T. Gudmestad, and K. V. Høyland. *Actions from Ice on Arctic Offshore and Coastal Structures*. LAN, 2006.

A. K. Lund. Estimering av vannføring i Kjellstömelva på Svalbard, project thesis, 2005.

A. Marchenko and A. Shestov. Personal communication, 2007.

G. Melland. Personal communication, 2009.

B. Michel. Winter regime of rivers and lakes. Technical report, U.S. Army Cold Regions Research and Engineering Laboratory, 1971.

B. Michel and R. O. Ramseier. Classification of river and lake ice. *Canadian Geotechnical Journal*, 8:36–45, 1971.

A. Morang and L. E. Parson. *Coastal Engineering Manual. Engineering Manual 1110-2-1100*, chapter Coastal terminology and geologic environments (IV-1). U.S. Army Corps of Engineers, Washington, D.C., 2002.

B. Morse and F. Hicks. Advances in river ice hydrology 1999–2003. *Hydrological processes*, 19:247–263, 2005.

B. Morse, B. Burrell, A. S. Hilaire, N. Bergeron, D. Messier, and T. T. Quach. River ice processes in tidal rivers: research needs. In *10th Workshop on River Ice. River Ice Management with a Changing Climate: Dealing with Extreme Events*, pages 388–399, 1999.

B. Morse, D. Messier, and T. T. Quach. Le savoir écologique local de la dynamique des glaces dans l'estuaire Portneuf. In *11th Workshop on River Ice. River ice processes with a changing environment*, pages 247–265, 2001.

B. Morse, B. Ringo, E. Stander, J.-L. Robert, D. Messier, and T. Thanh-Quach. Growth and decay of estuary ice cover. *Journal of Cold Regions Engineering*, 20:70–94, 2006.

P. O. Moslet. Estimation of loads exerted by sea ice on the quay at Kapp Amsterdam, the

Van Mijen Fjord. Master's thesis, The Norwegian University of Technology (NTNU) and The University Centre in Svalbard (UNIS), 2001.

P. O. Moslet. *In-situ measurements of sea-ice parameters that affect the loads on coastal and offshore structures*. PhD thesis, Norwegian University of Science and Technology (NTNU) and The University Centre in Svalbard (UNIS), 2007a.

P. O. Moslet. Field testing of uniaxial compression strength of columnar sea ice. *Cold Regions Science and Technology*, 48:1–14, 2007b.

P. O. Moslet and K. V. Høyland. Ice stress measurements adjacent to a wide structure in land-fast ice. In *International Conference on Port and Ocean Engineering under Arctic Conditions (POAC)*, Trondheim, Norway, 2003.

V. A. Nikitin, A. I. Shushlebin, and I. B. Sheikin. In-situ stress measurements in fast ice and possible tidal loads on structures. In *Proceedings of the second International Offshore and Polar Engineering Conference*, pages 696–702, San Francisco, USA, 1992.

NOAA, editor. *Tide and Current Glossary*. National Oceanic and Atmospheric Administration, Silver Spring, MD, 1999.

NPI. *The Place Names of Svalbard*. Norwegian Polar Institute, Tromsø, Norway, 2003. URL `http://miljo.npolar.no/placenames/pages/searchE.asp`.

D. Ottesen, J. A. Dowdeswell, D. J. Benn, L. Kristensen, H. H. Christiansen, O. Christensen, L. Hansen, E. Lebesbye, M. Forwick, and T. O. Vorren. Submarine landforms characteristic of glacier surges in two spitsbergen fjords. *Quaternary Science Reviews*, 27:1583–1599, 2008.

E. H. Owens. Effects of ice on the littoral zone at Richibucto Head, Eastern New Brunswick. *Revue Géographique de Montréal*, pages 95–104, 1976.

H. R. Peyton. Sea ice strength. final report of Naval Research Arctic Project, 1958–1965, UAG R–182102. Technical report, University of Alaska, Fairbanks, 1966.

K. W. Pilarczyk. *Geosynthetics and Geosystems in Hydraulic and Coastal Engineering*. Taylor Francis, 2000. ISBN 9058093026.

T. D. Prowse and N. C. Gridley, editors. *Environmental Aspects of River Ice*. National Hydrology Research Institute, Saskatchewan, Canada, 1993.

J. C. Reed and J. E. Sater, editors. *The Coast and Shelf of the Beaufort Sea*, chapter Sea ice geomorphology and ice as a geologic agent in the northern Beaufort Sea, pages 113–162. Arctic Institute of North America, Arlington, VA, 1974.

A. G. Rike. Permafrost response to environmental and industrial loads. final Report Strate-

gic Institute Programme 1999–2003 - NGI SIP:1-93. Technical report, Norwegian Geotechnical Institute, Oslo, Norway, 2003.

D. T. Røsvik Andreassen. Stability of test embankment in Svea, Project Thesis, 42 p. The University Centre in Svalbard (UNIS) and the Norwegian University of Science and Technology (NTNU), 2006.

M. Sayed, R. M. Frederking, and E. Wessels. Field measurements of stresses and deformations in a first-year ice cover adjacent to a wide structure. *Canadian Geotechnical Journal*, pages 726–734, 1988.

M. L. Schwartz, editor. *Encyclopedia of Coastal Science*, chapter Beach features, pp. 145–147. Springer Netherlands, 2005. ISBN 1402019033.

A. D. Short and W. J. Wiseman Jr. Freezeup processes on Arctic beaches. *Arctic*, 27: 215–224, 1974.

D. S. Sodhi, S. L. Borland, and J. M. Stanley. Ice action on riprap. Technical report, CRREL, 1996.

E. Stander. Ice stresses in reservoirs: effect of water level fluctuations. *Journal of Cold Regions Engineering*, 20:52–67, 2006.

E. Stander, R. M. Frederking, and J. P. Nadreau. The effects of tidal jacking on ice displacement and strain in the nearshore environment. In *9th International Symposium on Ice*, Sapporo, Japan, 1988.

S. H. Teigen, K. V. Høyland, and P. O. Moslet. Thermal stresses in first-year sea ice. Technical report, The University Centre in Svalbard (UNIS), 2005.

G. W. Timco and R. M. W. Frederking. Compressive strength of sea ice sheets. *Cold Regions Science and Technology*, 17:227–240, 1990.

USACE. *Coastal Engineering Manual. Engineering Manual 1110-2-1100*. U.S. Army Corps of Engineers, Washington, D.C., 2002a.

USACE. *Engineering and Design – Ice Engineering. U.S. Army Engineer manual 1110-2-1612*. U.S. Army Corps of Engineers, 2002b.

D. G. Vaughan. Tidal flexure at ice shelf margins. *Journal of Geophysical Research*, 100: 6213–6224, 1995.

Vegvesen. Korrelasjon av vinddata Kinsarvik–Hellesøy fyr. Notat av 1981-08-31 fra Norges Hydrodynamiske Laboratorier til Statens Vegvesen. Technical report, Directorate of Public Roads (Vegdirektoratet), Oslo, Norway, 1981.

W. F. Weeks and S. F. Ackley. The growth, structure, and properties of sea ice, CRREL Monograph 82–1. Technical report, U.S. Army Cold Regions Research and Engineering Laboratory, Hanover, New Hampshire, 1982.

W. J. Wiseman Jr., E. H. Owens, and J. Kahn. Temporal and spatial variability of ice-foot morphology. *Geografiska Annaler*, 63:69–80, 1981.

WMO. Sea ice nomenclature, draft version 1.1. Technical report, World Meteorological Organisation, Geneva, Switzerland, 2007.

C. S. Wright and R. E. Priestly. *Glaciology, British (Terra Nova) Antarctic Expedition 1910-1913*. Harrison and Sons, London, 1922. Cited in (Dionne, 1994).

J. I. Wuebben. *Ice Effects on Riprap*, chapter 31, pages 513–530. John Wiley Sons Ltd, 1995.

Appendix A

Data

A.1 Equipment

A.1.1 Thermistor cables

The ground temperature was recorded with 5 thermistor cables (C1, C2, C3, C4 and C5) from EBA Engineering Consultants Ltd.

C1, C2 and C3 each contained 6 thermistors with 12 cm spacing. Cable 4 (C4) contained 16 thermistors spaced with 1.5 m. Cable 5 (C5) contained 16 thermistors spaced with 1.0 m.

The measurement period started 22 September 2006 and ended 20 December 2008. The data were recorded every hour.

The cables were originally designed with a different set-up in mind, therefore, only the data from some of the thermistors were analysed (Table A.1).

A.1.2 Tide and wave gauge

The sea level and the waves were recorded with a SBE 26plus SEAGAUGE wave and tide recorder from Sea-Bird Electronics, Inc. The instrument serial number was 26P40013-1094. The sea level was measured continuously and an average recorded every 20 minutes.

The approximative position of the gauge is given in Table A.2

Cable name	Serial number	Comments
C1: Upper row	1955	4 last sensors inside the bag (assumption)
C2: Lower row	1954	Penetrating the bag 1 m from the bottom 4 last sensors inside the bag.
C3: Middle row	1956	Penetrating the bag 1 m from the top 4 last sensors inside the bag.
C4: Along slope, below the bags	1953	9 last thermistors are along the slope.
C5: Hole	1952	5 last thermistors are in the hole.

Table A.1: Thermistor cables set-up

UTM zone 33X [WGS84]	
Northing [m]	8647026
Easting [m]	541044
Orthometric height [m]	-2.71

Table A.2: Approximative position of the tide and wave gauge

A.2 Complementary data

A.2.1 Seabed elevation

Distance from Barryneset [m]	Seabed elevation [m]	Hard layer elevation [m]	Soft layer thickness [m]
0	-1.33	-1.33	0
40	-3.2	-3.2	0
50	-4.19	-4.19	0
60	-4.42	-4.42	0
70	-3.81	-4.26	0.45
80	-3.32	-3.92	0.60
90	-2.88	-3.68	0.80
100	-2.85	-3.75	0.90
110	-2.83	-3.48	0.65
120	-2.9	-4.6	1.70

Table A.3: Seabed elevation and thickness of the soft layer along a line perpendicular to the tip of the breakwater – winter 2005

A.2.2 Vane test data

Elevation [m]	Vane shear strength [kPa]	Remoulded strength [kPa]
–3.48	11	5
–3.67	10	5
–4.14	8	5
–4.83	6	5
–5.31	8	5
–5.81	20	3
–6.23	N/A	N/A

Table A.4: Vane test data

A.2.3 NP150-position

The position data of the NP150 topographic point are found in A.5.

UTM zone 33X [WGS84]	
Northing [m]	8647481.348
Easting [m]	540769.443
Orthometric height [m]	9.081
Geoid height [m]	31.778
Ellipsoid height [m]	40.859
Geographical coordinates [WGS84(Euref89)]	
Latitude	77° 53’ 49.21429
Longitude	16° 44’ 31.48512

Table A.5: Position of the NP150 reference point

A.2.4 Wind in the direction of longest fetch

Wind speed [m s^{-1}]	Wind direction [°]	
	187–197	197–207
0–1	44	43
1–2	5	6
2–3	115	131
3–4	86	124
4–5	52	72
5–6	15	36
6–7	17	25
7–8	4	12
8–9	1	12
9–10	1	1
10–11	0	1

Table A.6: Frequency of the daily maximum hourly mean wind speed in the direction ranges 187–197° and 197–207° in Svea – 1996-2005

A.2.5 Wind calculations

The frequency of the daily maximum hourly mean wind speed in the wind range of longest fetch is found in Table A.6.

The data are fitted to a Weibull distribution with
$\gamma = 2.192$
and
$F_c = 4.206\,\mathrm{m\,s^{-1}}$

Hence, the cumulative distribution function of the wind speed may be written as:
F(f) = 1-e$^{-(f/4.206)^{2.192}}$

There are 803 observations in the course of 10 years. Hence the mean distance between the observation is:
$\tau = 10/803 = 1.245.10^{-2}\,\mathrm{year}$

The value of the return period R_p of the significant daily maximum mean wind speed is calculated for 10 years:
$F(f_{10}) = 1 - \tau/R_p = 9.988.10^{-1}$
$f_{10} = 10.0\,\mathrm{m\,s^{-1}}$

and for 50 years:
$F(f_{50}) = 1 - \tau/R_p = 9.998.10^{-1}$
$f_{10} = 11.0\,\mathrm{m\,s^{-1}}$

A.2.6 Temperature at the top of the bags

The temperature at the top of the second row of bags (0.8 m elevation) is strongly affected by the air temperature while the temperature at the top of the third and fourth rows (respectively 0.3 and 0.1 m elevation) are closer to the water temperature, with the temperature at the third row up to about 1 degree Celsius colder that the temperature at the fourth row (Figure A.1).

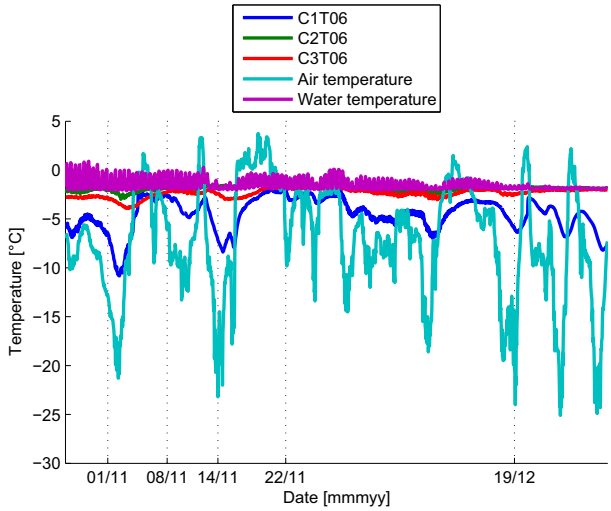

Figure A.1: Comparison between C1T06, C2T06, C3T06 and the air and water temperatures from 27 October to 30 December 2006

A.2.7 Ground properties at Barryneset

On 1 May 2006 a 10-m-deep hole was drilled at the beginning of the 2005 breakwater at Barryneset in order to analyse the soil composition, state—frozen or not—and salt content. Unfortunately, we were not able to take soil cores. The position of the hole was measured with a handheld GPS with 20 m precision (Table A.7). The qualitative results are found in Table A.8. There was a high water content at all depths and no salt in the top 9 m.

WGS84, UTM zone 33X	
Northing [m]	8647189
Easting [m]	540972

Table A.7: Location of the drilled hole at Barryneset

Depth [cm]	Observations
0 - 75	sea ice
75 - 225	fill material, contains ice
225 - 400	mix of clay, stones, gravel and ice
400 - 450	lighter colour and coarser material
450 - 650	finer material: more clay
650 - 850	coarser again
850 - 900	almost only stones
900 - 1000	clay with low frozen water content, salt

Table A.8: Soil stratigraphy down to 10 m at Barryneset

Appendix B

Chronological observations from fall 2006 to summer 2007

In this appendix, the nomenclature given in Figure 1 is used when referring to the different parts of the breakwater.

The paragraphs correspond to each time I went to Svea and start with a summary of the weather conditions since the previous visit: air temperature, wind and tide.

The wind data is plotted as arrows showing the hourly wind direction and its intensity. This way of plotting the wind works well as long as the time period is limited to less than 2 weeks but not as well in the few cases where the period is longer.

I summed up the air temperature in words in the beginning of each paragraph but did not do it for the tide and wind data because, in general, they have a smaller influence on the ice conditions.

B.1 Freeze-up

B.1.1 Week 43 – 27 October 2006

Air temperature (Figure B.1): during the month of October the daily air temperature varied between –10 and 0 °C, with an average of –5.7.

Sea ice: (Figure B.2): the fjord was almost entirely ice-free except the parts close to land in Braganzavågen, which were covered partly with grease ice and partly with

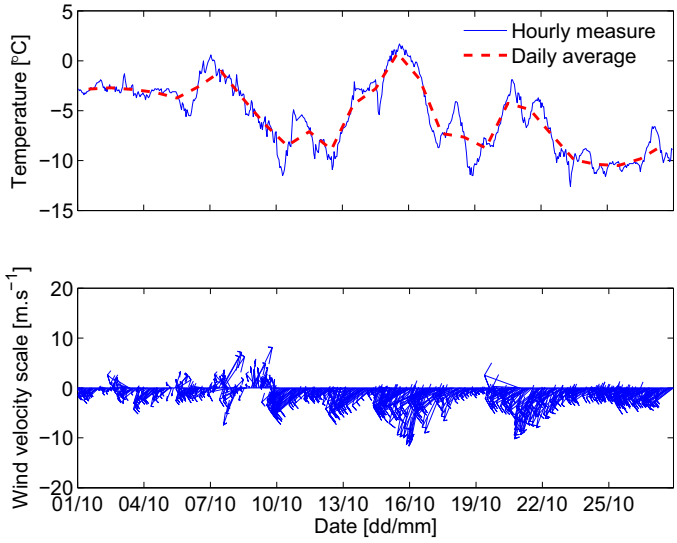

Figure B.1: Air temperature and wind data from 1 to 27 October 2006

pancake ice. The maximum extension of the frazil-covered zone was occurring at low tide and reaching the tip of the breakwater.

Ice foot: on the east side, deposited pancakes were stacked up into a berm (Figure B.3) and sea water spray was cementing them together. The pancakes were formed at the surface of the sea surrounding the breakwater. On the west side of the breakwater there was a stranded ice cake of 4.7 x 2.0 m (Figure B.4). Along the tip of the breakwater an ice cap had grown on the bags and was covering the second row of bags, i.e. a 40 cm-high zone above MHW (Figure B.5). Stranded cakes were integrated into this ice cap in the form of scattered lumps of ice.

Bags: (Figure B.5): The first row of bags was frozen and covered with a thin layer of snow. The second row was completely covered with ice. On the third row there was some ice rubble resulting from the abrasion of the ice pancakes on the bags. The third and fourth rows were frozen but not covered with ice.

Figure B.2: Pancake ice to the left and strip of grease ice in the middle, looking toward the east corner – 27 October 2006 (week 43)

Figure B.3: Ice foot, east side, looking toward Svea, sea height = –0.1 m — 27 October 2006 (week 43)

Figure B.4: Stranded ice cake, west side, looking toward Ispallen, sea height = –0.1 m – 27 October 2006 (week 43)

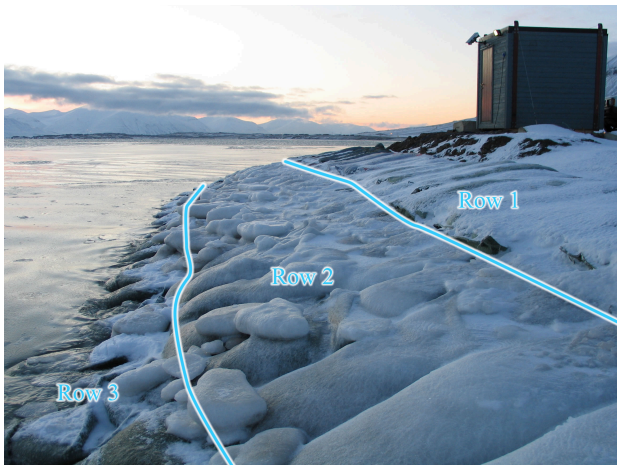

Figure B.5: Bags at the tip of the breakwater, looking toward west, sea height = –0.1 m – 27 October 2006 (week 43)

B.1.2 Week 44 – 1 November 2006

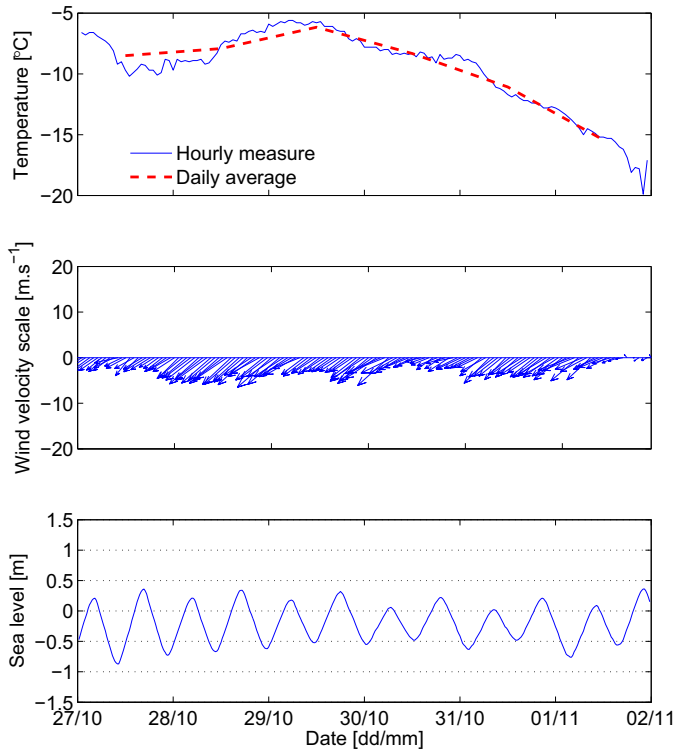

Figure B.6: Air temperature, wind and sea height data from 27 October to 1 November 2006

Air temperature (Figure B.6): the daily air temperature stayed between –5 and –10 °C from 27 to 30 October then decreased to –15 °C on 1 November. The mean temperature during this period was –9.6 °C.

Sea ice (Figure B.8): the pancake ice on the east side of the breakwater had coalesced into a continuous sheet of young ice. On the east side the shore was bare approximately below the mean sea level close to the breakwater tip. Further away from the tip on the east side, the shore was covered with the sheet of young ice.

Ice foot (Figure B.9): on the east side of the breakwater the ice foot consisted of two steps. The lower step was 0.6 to 1.0 m high and the upper step 0.2 to 0.5 m high (Figure B.7). The voids between the stacked-up cakes described in week 43 on page 131 were filled with ice resulting in a stronger ice foot.

Bags: The state of the bags was similar to that of the previous week (Figure B.10) but the ice foot was looking more and more like a step.

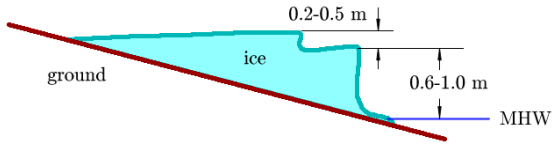

Figure B.7: Sketch of the ice foot shape on the east side of the breakwater — 1 November 2006 (week 44)

Figure B.8: Pancake ice, east side, looking toward Braganzavågen – 1 November 2006 (week 44)

Figure B.9: Ice foot, east side, looking toward Svea, sea height = –0.5 m — 1 November 2006 (week 44)

Figure B.10: Bags at the tip of the breakwater, looking toward west, sea height = –0.5 m – 1 November 2006 (week 44)

B.1.3 Week 45 – 8 November 2006

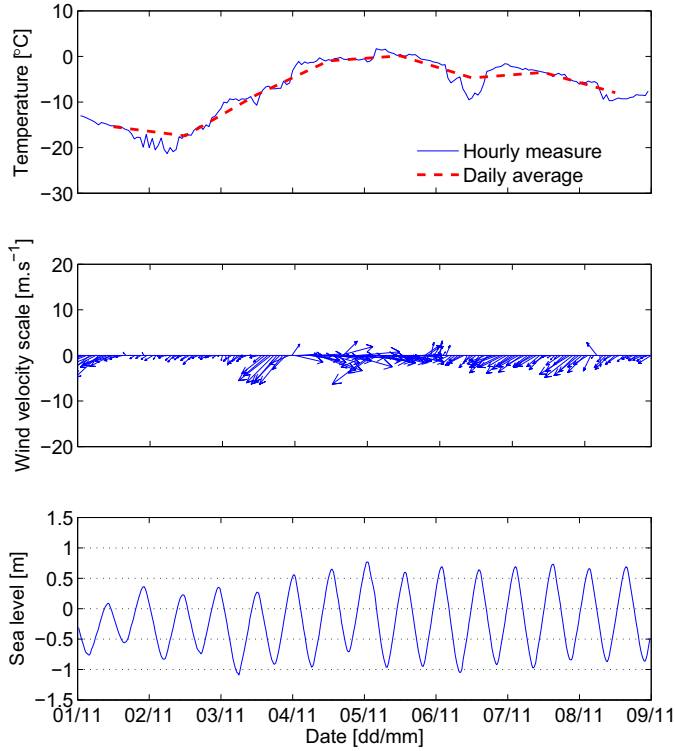

Figure B.11: Air temperature, wind and sea height data from 1 to 8 November 2006

Air temperature (Figure B.11): the daily air temperature stayed around –15 °C on 1 and 2 November before increasing to 0 °C by 5 November and then dropping gradually to –8°C on 8 November. The mean temperature during this period was –7.3°C.

Sea ice: Although I did not make any observation of the sea ice on the east side of the breakwater, pictures taken on 8 November suggest that the young ice that was covering the shore the previous week had been washed away. It is possible that the sheet of young ice covering the sea was split during the same time. The rest of the fjord was still ice-free. There was a sizeable amount of ice rubble on the shore below the ice foot. It was a result of the abrasion of the sea ice, which was swept along the shore by the tidal current and grinding against it.

Ice foot: as the lower step of the ice foot gradually grew upwards, the ice foot transformed into a single step (Figure B.14). The upward growth took place in periods

of spring tides when the ice foot was flooded on high tide. When snow was present, it became saturated and froze into snow ice during ebb, when it was above the water level. On the west side, the stranded ice cake was gradually being integrated in the ice foot (Figure B.13). The lower boundary of the ice cap along the tip of the breakwater has moved higher upwards as a result of mild weather (Figure B.14).

Bags: The amount of ice rubble, described in week 43, had increased, and it extended to the fourth row of bags.

Figure B.12: Ice foot (left) and ice rubble (middle), east side, looking toward Svea, sea height = –0.3 m – 8 November 2006 (week 45)

Figure B.13: Ice foot, west side, looking toward Ispallen, sea height = –0.3 m – 8 November 2006 (week 45)

Figure B.14: Bags at the tip of the breakwater, looking toward west, sea height = –0.3 m – 8 November 2006 (week 45)

B.1.4 Week 46 – 14 November 2006

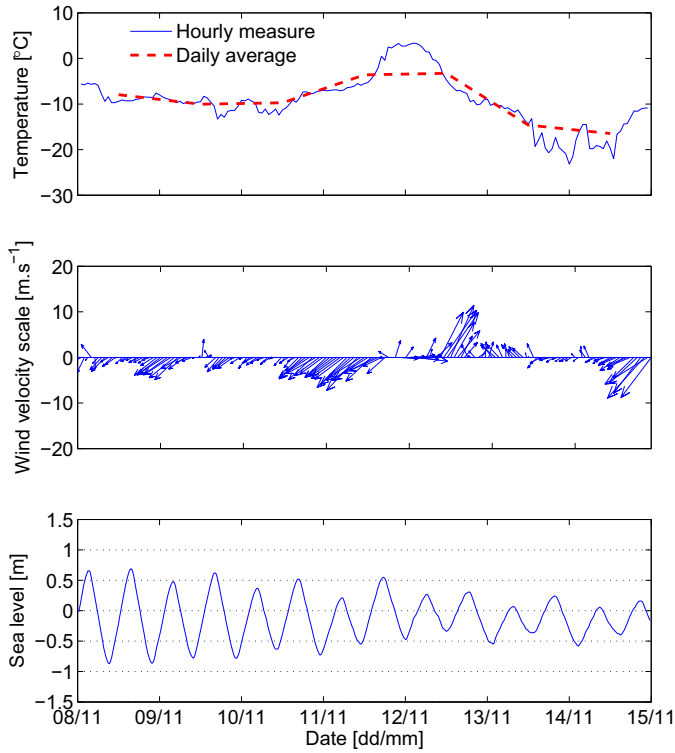

Figure B.15: Air temperature, wind and sea height data from 8 to 14 November 2006

Air temperature (Figure B.15): the daily air temperature oscillated between –3.3 and –16.5 °C with an average of –9.8. The higher temperatures occurred on 11 and 12 November and the lower on 13 and 14 November.

Sea ice (Figure B.16): the sea had frozen over. There was a 40 m-long, 10 m-wide channel lead situated 10 m from the breakwater tip and oriented with the direction of the water flow. The panorama in Figure B.16 is put together from several pictures, therefore, the view is distorted. The channel was maintained ice-free by the tidal current.

Ice foot (Figure B.17): at that point, the ice foot consisted of only one step. Below the ice foot the shore was covered with 6 cm-thick young ice. As opposed to the ice foot, which was fixed to the ground, the cover of young ice was moving with the tide, floating when the sea level was high and resting on the ground when it was

low. This vertical movement bends the ice and cracks were forming parallel to the shore (Figure B.18).

Bags: All the bags were covered with ice. On the second row of bags the ice foot was fixed to the bags while on the lower rows there was a cover of young ice moving up and down with the tide and that was not fixed to the bags.

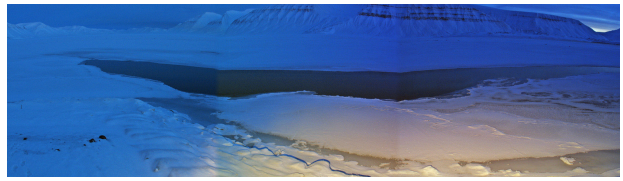

Figure B.16: Channel lead along the breakwater tip, sea height = –0.4 m — 15 November 2006 (week 46)

Figure B.17: Ice foot and shore ice, east side, looking toward Svea, sea height = –0.5 m – 15 November 2006 (week 46)

Figure B.18: Bending cracks in the sea ice due to the tide – 15 November 2006 (week 46)

Figure B.19: Bags at the tip of the breakwater, looking toward west, sea height = –0.5 m – 15 November 2006 (week 46)

B.1.5 Week 47 – 22 November 2006

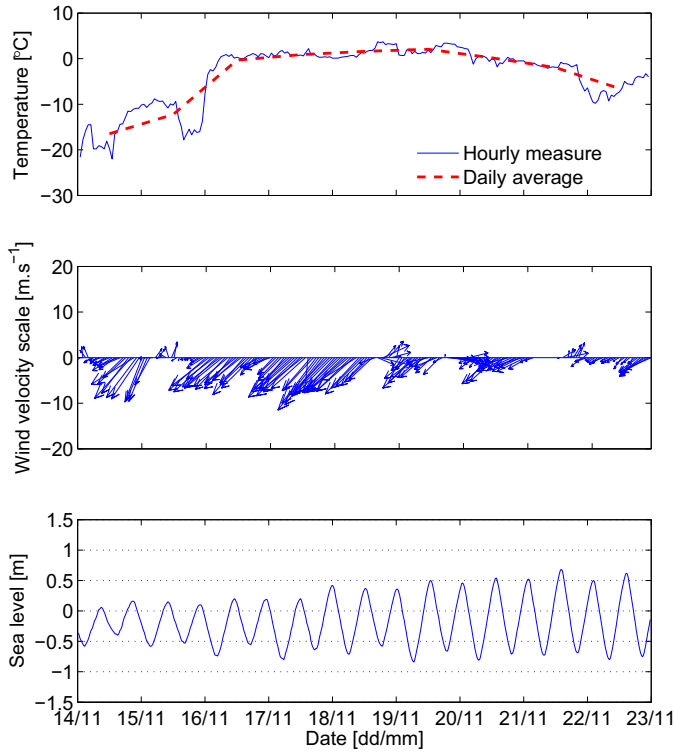

Figure B.20: Air temperature, wind and sea height data from 14 to 22 November 2006

Air temperature (Figure B.20): the daily air temperature surged from below –15 to 0 °C between the 14 and the 16 November. It stayed above 0 until the 20th then gradually dropped to –5 °C by the 23rd. The mean temperature for this period was –3.3 °C.

Sea ice (Figure B.21): several days with mild weather caused the sea ice to break up. There remained ice pancakes and frazil at the tip of the breakwater but most of the fjord was ice-free. The pancakes were 3 cm thick and about 30 cm in diameter. They were moving with the tidal current as can be seen in Figure B.26, which was photographed with slow shutter speed. The maximum surface current velocity was of the order of 1 m s^{-1} on the east side of the breakwater but was slower along its tip as the streamlines are pushed away. During flow (respectively ebb) there was an eddy at the east (respectively west) corner of the breakwater with water flowing along the side of the breakwater and the tip toward west (respectively east) and turning around as it met the flowing water (Figure B.22).

Ice foot: the ice foot was still growing on the west side of the breakwater: above a certain water level ice pancakes were piling up into a 60 cm-high wall (Figure B.23). It was quite soft: a person walking on top would leave 10 cm-deep footprints. With time this lump will consolidate and stick to the underlying bags. At the tip of the breawater the ice foot was 40 cm high and extended approximately to the top of the third bag row (Figure B.24). On the east side the ice foot was 1 m high and growing in overhang (Figure B.25). As opposed to the west side, along the tip and on the east side, the ice foot had consolidated.

Bags: Due to a period of mild weather the young ice that was covering the lower bags had been washed away. Ice abrasion against the bags was occurring again, with increased intensity (Figure B.27). In addition to generating ice rubble the abrasion was wearing the bags by brushing the fibres in the direction of the flow as seen in Figure B.28. The fabric of the net-covered bags seemed to be less affected by the abrasion.

Since the bags were never perfectly full and the fill material settles with time, the top of the bags was loose and the ice rubble was accumulating beneath the top of some bags (Figure B.28).

Shrimp-looking amphipods (Themisto abyssorum) and isopods (Sagitta elegans (Verril, 1837)) were observed attached to the fabric of some bags (Figure B.30).

Figure B.21: Pancakes and frazil at the breakwater tip, looking toward south – 22 November 2006

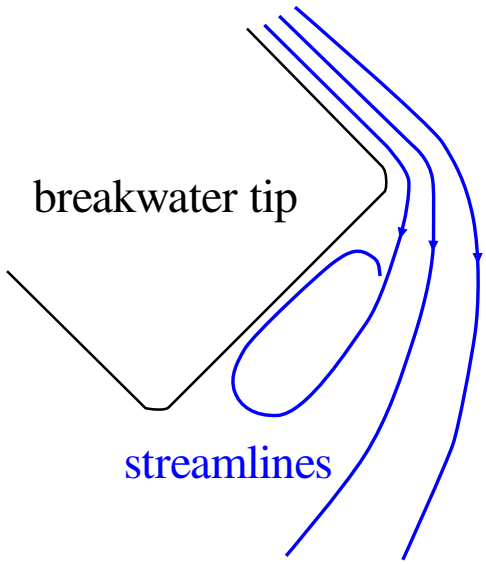

Figure B.22: Streamlines around the tip of the breakwater during ebb

Figure B.23: Ice foot, west side, looking toward Ispallen, sea height = –0.7 m – 22 November 2006 (week 47)

Figure B.24: Along the breakwater tip the ice foot was 40 cm high, looking toward Kapp Amsterdam, sea height = –0.6 m – 23 November 2006 (week 47)

Figure B.25: On the east side the ice foot was 1 m high, looking toward Svea, sea height = –0.6 m – 22 November 2006 (week 47)

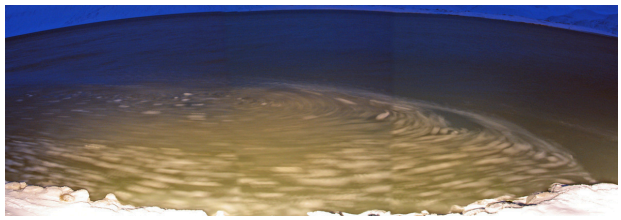

Figure B.26: Eddy in front of the breakwater tip during flow visualised through moving ice panckes (slow shutter speed) – 23 November 2006 (week 47)

Figure B.27: Ice rubble on the bags, sea height = –0.6 m – 22 November 2006 (week 47)

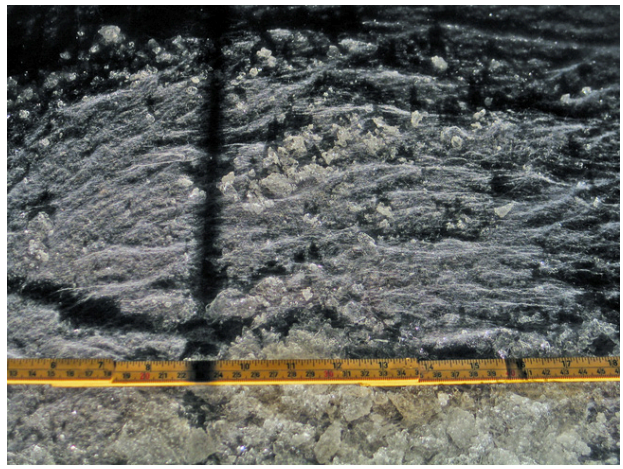

Figure B.28: Brushed bag fabric – 23 November 2006 (week 47)

Figure B.29: Ice rubble accumulation beneath the bags tops – 22 November 2006 (week 47)

Figure B.30: “Shrimps” on the bags – 23 November 2006 (week 47)

B.2 Ice cover period

B.2.1 Week 51 – 19 December 2006

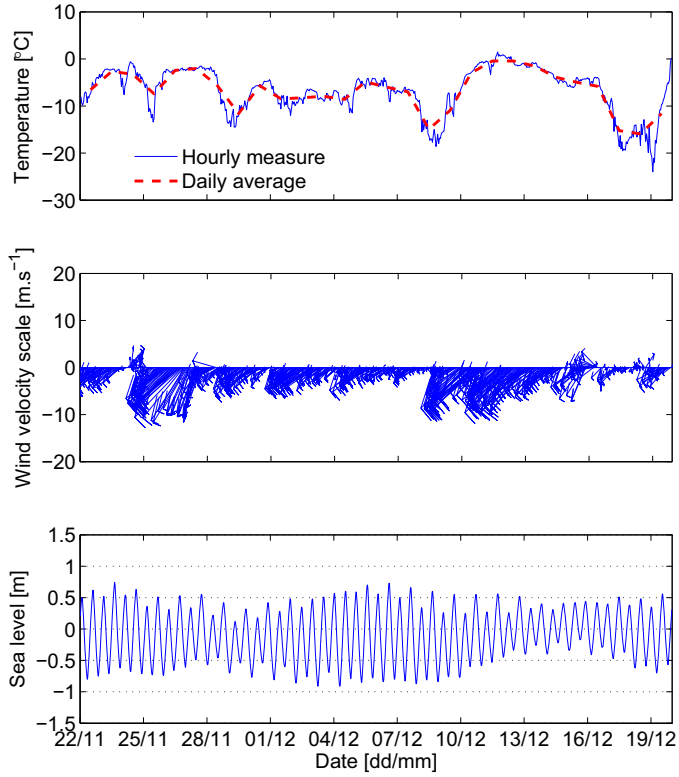

Figure B.31: Air temperature, wind and sea height data from 22 November to 19 December 2006

Air temperature (Figure B.31): the daily air temperature oscillated between –2 and –12 °C until 7 December, dropped to –15 °C on 8 December, then surged to 0 °C on 11 December. Between 13 and 18 December it decreased from –2 to –16 °C. The mean temperature during this period was –6.5 °C.

Sea ice: the sea ice had frozen over again. There was ice all around the breakwater (Figure B.32) except for a channel lead about 10 m from the tip, in the direction of water flow. The channel was smaller than the one observed in week 46. From the air, in the darkness the sea ice seemed to extend a couple of kilometres to the west,

as drawn on the map in Figure B.32. The sheet of young ice covering the lower part of the foreshore was up to 50 cm thick.

Tidal movement: Figure B.34 illustrates the tidal movement of the ice sheet covering the lower shore with pictures at different sea heights. At high tide the gap between the ice sheet and the ice foot was filled with water. The picture series shows that, as opposed to the ice foot, the ice sheet was not fixed to the shore.

Ice Foot: the shore ice had a different profile depending on the side of the breakwater. Along the tip it consisted of a cap of spray ice on the backshore and of young ice on the foreshore. Both zones had approximately the same thickness (Figure B.35). On the east side cakes were stacked up on the backshore into a berm while the foreshore was covered with a 50-cm thick sheet of sea ice (Figure B.36). The elevation of the berm top was 1.21 m, which is close to the HOW mark (1.13 m (Table 3.4). The profile on the west side is similar in shape to that on the east side, but the berm is not as high and the ice thickness along the foreshore is only about 5 cm thick (Figure B.37).

Tide cracks: The tidal movement of the ice created cracks parallel with the water surface. The biggest crack ran along the junction of the sea ice and the ice foot (Figure B.33).

Bags: the lower bags were again covered with young ice. There was a hole in the ice cover at the west corner of the breakwater. The bags located in that hole were covered with a thin layer of ice (Figure B.38). In the west corner ice cakes had piled up and created a less even surface than on the rest of the breakwater (Figure B.39).

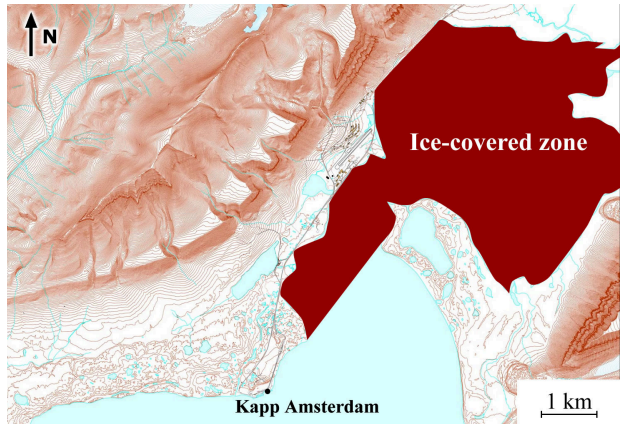

Figure B.32: Extent of the sea ice – 19 December 2006 (week 51) – Background map: SNSG

Figure B.33: Ice cover along the tip of the breakwater, sea height = –0.4 m – In red: tide cracks – 20 December 2006 (week 51)

(a) sea height = –0.5 m

(b) sea height = 0.3 m

(c) sea height = 0.5 m

Figure B.34: Tidal movement, ice foot in the foreground, shore ice in the background – 19 December 2006 (week 51)

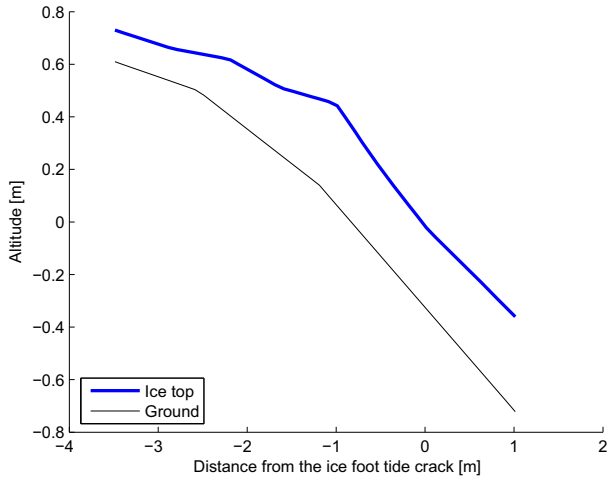

Figure B.35: Profile of the shore ice along the breakwater tip of the breakwater – 20 December 2006 (week 51)

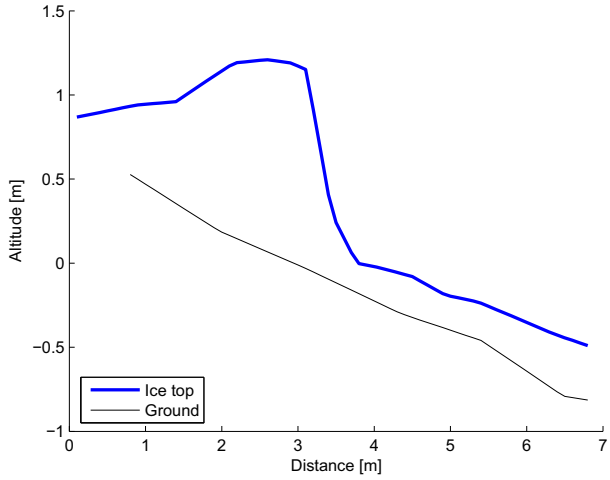

Figure B.36: Profile of the shore ice along the east side of the breakwater – 20 December 2006 (week 51) – Unlike at the tip of the breakwater, there is no ice foot tide crack, therefore, the origin of the abscissa is chosen arbitrarily

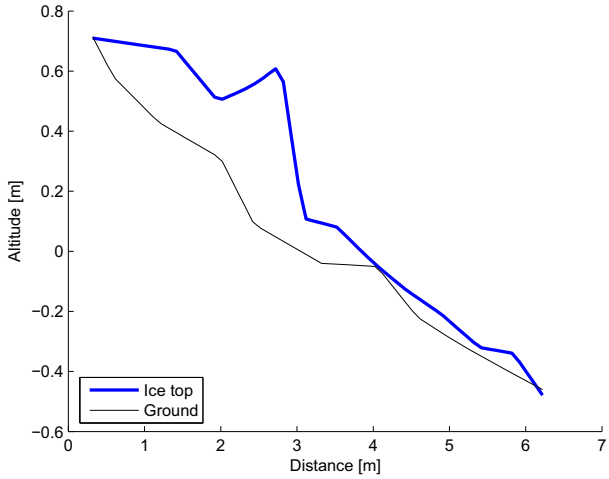

Figure B.37: Profile of the shore ice along the west side of the breakwater – 20 December 2006 (week 51) – Unlike at the tip of the breakwater, there is no ice foot tide crack, therefore, the origin of the abscissa is chosen arbitrarily

Figure B.38: Hole in the ice cover at the west side of the breakwater, sea height = –0.4 m – 20 December 2006 (week 51)

Figure B.39: Piled-up sea ice cakes at the west corner of the breakwater, sea height = –0.4 m – 20 December 2006 (week 51)

B.2.2 Week 52 – 30 December 2006

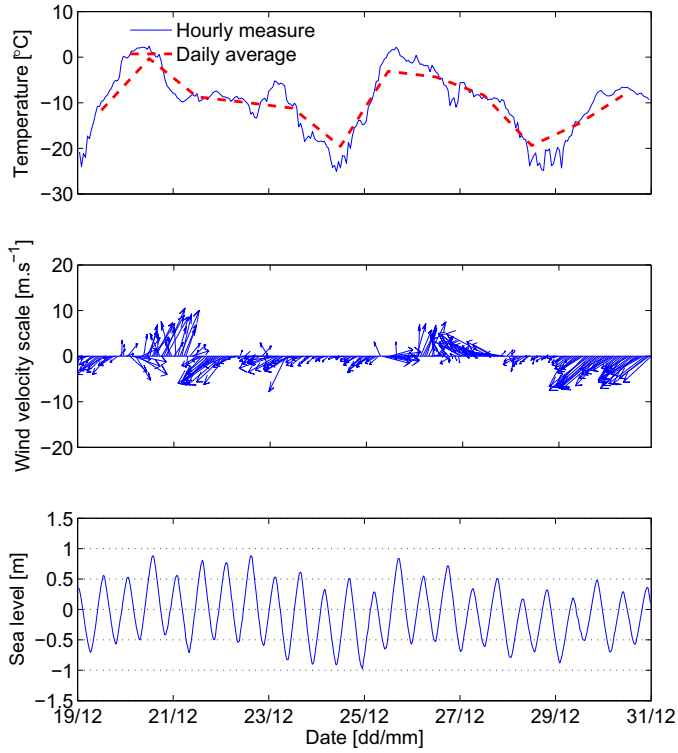

Figure B.40: Air temperature, wind and sea height data from 19 and 30 December 2006

Air temperature (Figure B.40): the daily air temperature oscillated twice between warm (above –5 °C) and cold (–20 °C). The mean temperature for this period was –10.2 °C.

Sea ice: the sea seemed to be still covered with ice. I did not take any note about the channel lead observed the week before, therefore, I do not know whether it still was there. The shore ice had been growing to 45 cm thickness on the west side and 60 cm on the east side.

Ice foot (Figure B.41): with the shore ice growing, the transition with the ice foot was smoother.

Tidal movement: cracks resulting from the tidal movement of the sea ice were developing in a parallel pattern above and outside of the breakwater.

Figure B.41: Ice foot at the breakwater tip, looking toward west, sea height = –0.5 m – 30 December 2006 (week 52)

B.2.3 Week 1 – 6 January 2007

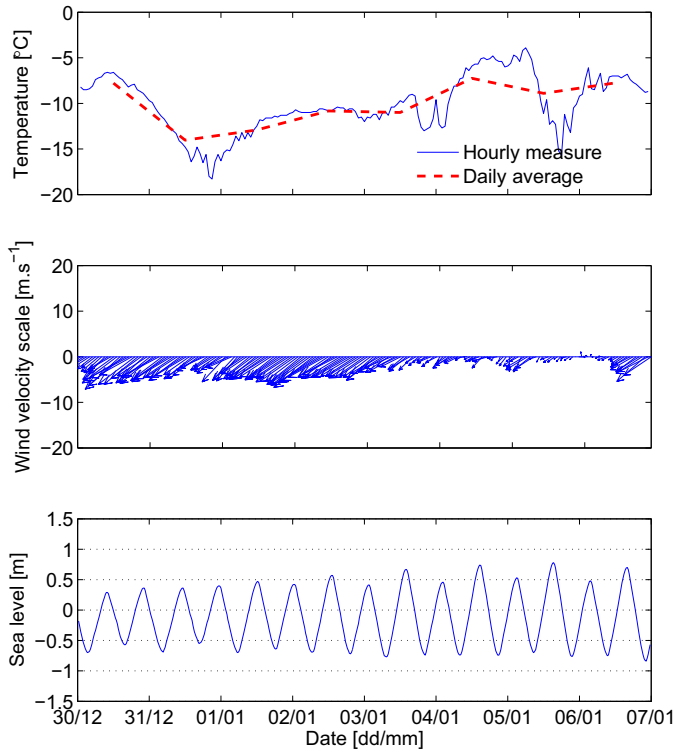

Figure B.42: Air temperature, wind and sea height data from 30 December 2006 to 6 January 2007

Air temperature (Figure B.42): the daily air temperature stayed between –7 and –14 °C during this period, with an average at –10.1 °C.

Sea ice: for the first time, it was possible to walk on the sea ice. As shown in Figure B.44 the shore ice had a steeper slope in the west corner of the breakwater, probably due to the absence of bags on the lower slope (Figure B.23).

Ice foot: small ice cakes had piled up on the end bags of the west side (Figure B.43(a)). Due to the presence of the breakwater built in 2005 (Section 4.1), the slope was more gradual in the pile-up zone than elsewhere around the breakwater. As a result, the bottom of the bag section was higher than elsewhere and, more importantly, than low sea levels. Therefore, on low sea levels, when the sea ice was grounded, it had a tendency to break up at the bottom of the bag section, which formed a 40 cm-thick

step. Consequently, on high sea levels, pictures taken by the video camera pointed towards the west side reveal that there was a small zone of open water between the bags and the sea ice, where the broken pieces of ice were floating. During spring tides, as those occurring from 3 to 6 January, where the tidal range varied between 111 and 151 cm, these pieces were stranded and piled up.

Tidal movement: Figure B.43 illustrates the effect of the tide on the west side of the breakwater. At high sea levels the sea ice is flooded and the current is visible with the naked eye. As opposed to the picture series from week 51 (Figure B.34), the sea ice cover had frozen fast to the ice foot and did not float up at high tide.

The sea ice was also flooded in front of the breakwater tip at high sea levels (Figure B.45). Because of the narrowness of the tide crack through which the surface water penetrates, some of it becomes trapped at low sea levels, and create surface water ponds (Figure B.45). The extent of surface water ponds changed every day. During the period of observations (5 to 7 January) the width of the water pond photographed in Figure B.45 varied between 2 and 5 m. Some of the surface water froze to the top of the sea ice layer and formed a growing layer of snow-ice.

Tide cracks: The tide cracks are seen at high sea height (0.7 m) in Figure B.46 and at low sea height (–0.7 m) in Figure B.47. The pictures show the east corner of the breakwater. The ice was fixed to the ice foot, resulting in bending stresses at high water levels and the creation of cracks at some distance from the ice foot. The cracks were developing parallel to the shore.

In addition to the cracks parallel to the shore, there were radial cracks in the corners of the breakwater. Figure B.48 shows the radial crack in the east corner. It also shows the continuation of cracks 2 and 3 along the east side of the breakwater while crack 1 stopped close to the radial crack (the crack numbering is explained in the Conventions).

(a) sea height = –0.75 m

(b) sea height = –0.1 m

(c) sea height = 0.3 m

Figure B.43: Tidal movement, west side – 7 January 2007 (week 1)

Figure B.44: Steep shore ice in the west breakwater corner, sea height = –0.7 m – 5 January 2007 (week 1)

Figure B.45: Pond of surface water along the tip of the breakwater, sea height = –0.7 m – 5 January 2007 (week 1)

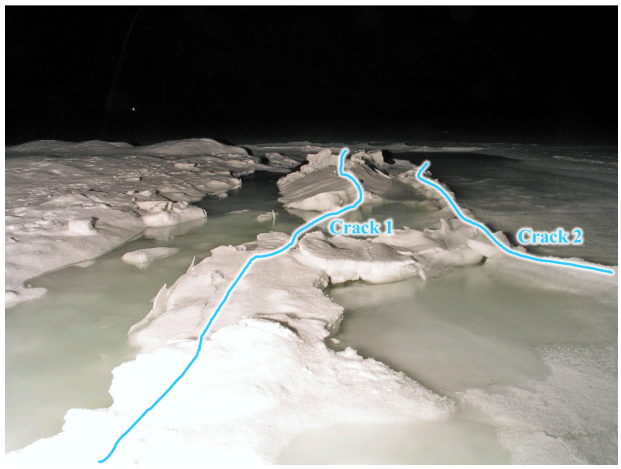

Figure B.46: Tide crack in the coastal ice along the tip of the breakwater, looking toward east, sea height = 0.7 m – 6 January 2007 (week 1)

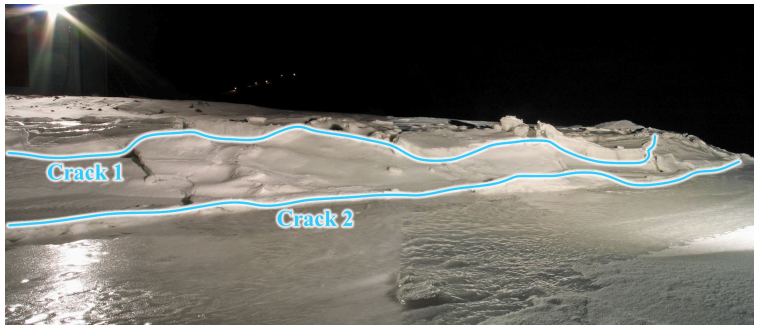

Figure B.47: Tide cracks at the eastern part of the breakwater tip, sea height = –0.7 m – 5 January 2007 (week 1)

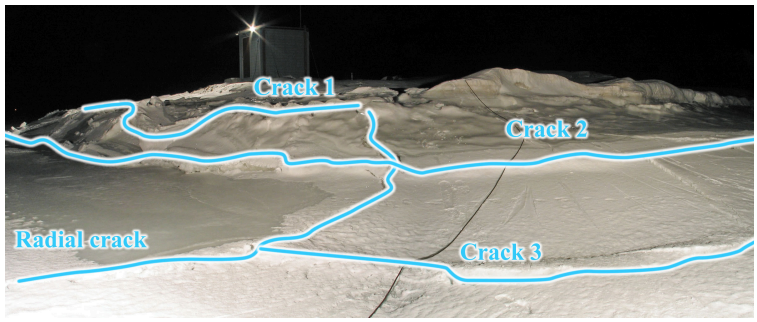

Figure B.48: Radial crack at the east corner of the breakwater, sea height = –0.1 m – 9 January 2007 (week 1)

B.2.4 Week 41 – 22 January 2007

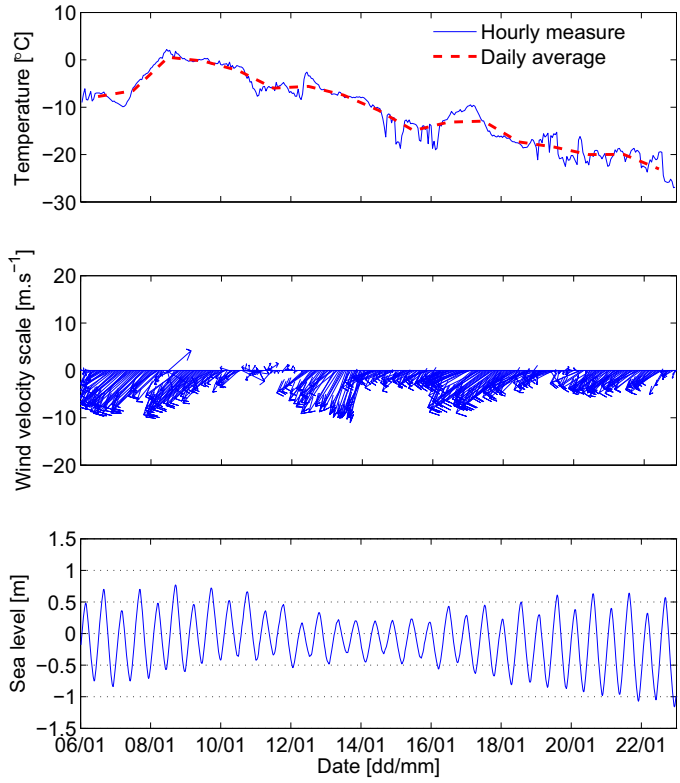

Figure B.49: Air temperature, wind and sea height data from 6 to 22 January 2007

Air temperature (Figure B.49): the daily air temperature rose to 0.5 °C on 9 January then was decreasing quite linearly the rest of the period and ended at –23 °C. The mean temperature for this period was –10.9 °C.

Sea ice: the profiles of the coastal ice at low tide and high tide are plotted in Figures B.50 and B.51 along the line shown in Figure B.52. The ice thickness was decreasing from more than 1 m close to the ice foot to 30 cm offshore. There was an appreciable amount of snow ice on top of the sea ice.

Tide cracks: two to three shore-parallel tide cracks ran around the breakwater and there was a radial crack in each corner (see Figure B.52).

Ice foot: there was no ice growth shoreward of the tide crack 1 (crack numbering convention explained in the Conventions).

Tidal movement: the ice was not flooded at high tide anymore (Figure B.53). As seen in B.51 the ice top was below sea level in a 3 m-wide area close the ice foot at high tide and, therefore, that area was flooded when I drilled holes on 23 January 2007 to measure the ice thickness (Figure B.54). In order to avoid such artificial flooding a good solution is to install tubes around the drilled holes (Figure B.73).

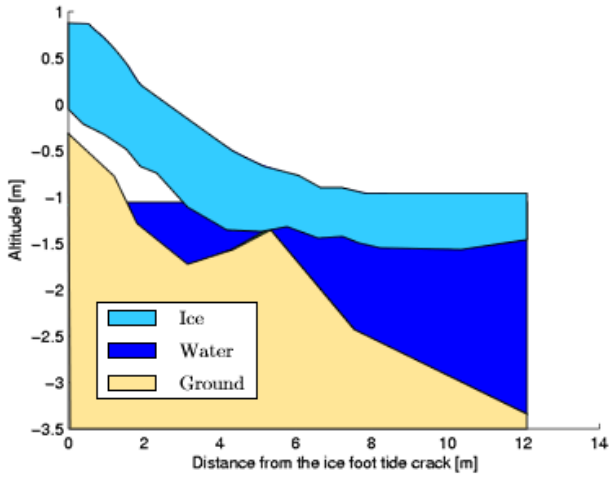

Figure B.50: Profile of the coastal ice at low tide, sea height = –1.09 m — 22 January 2007 (week 4)

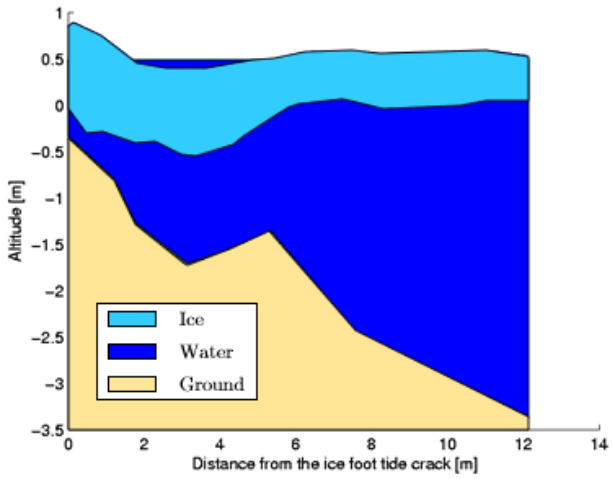

Figure B.51: Profile of the coastal ice at high tide, sea height = –0.50 m — 22 January 2007 (week 4)

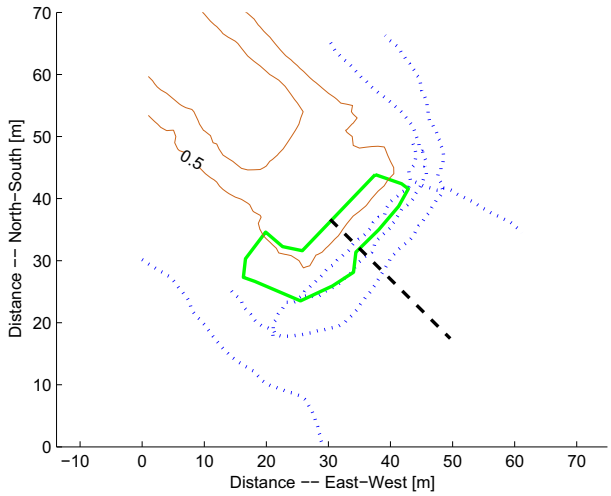

Figure B.52: Tide cracks around the breakwater in blue, dotted lines. The zone covered with bags is delimited by a green, solid line. The black, dashed line is the line along which the profile measurements were done. The brown, thin contour lines show the topography of the breakwater – 22 January 2007 (week 4)

Figure B.53: Hinge zone without surface water (normal conditions), breakwater tip, looking toward the east corner, sea height = 0.3 m – 22 January 2007 (week 4)

Figure B.54: Surface water on top of the hinge zone after holes were drilled, breakwater tip, looking toward the east corner, sea height = 0.5 m – 23 January 2007 (week 4)

B.2.5 Week 5 – 30 January 2007

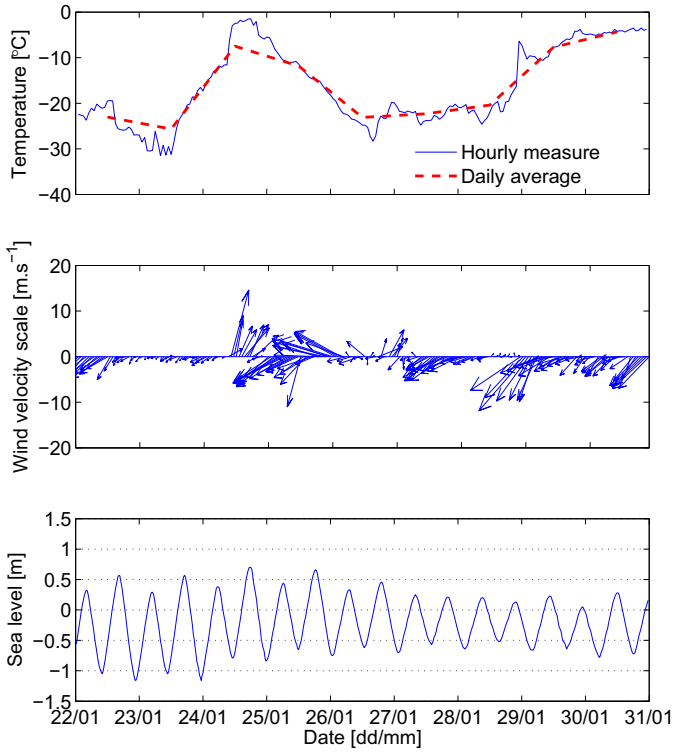

Figure B.55: Air temperature, wind and sea height data from 22 to 30 January 2007

Air temperature (Figure B.55): the air temperature alternated between 2-3 day-long cold and warm periods, starting the week with a daily average below –20 °C, increasing to above –10, decreasing back to below –20 and finally ending at –4. The mean temperature during the period was –16.2 °C.

Sea ice and snow cover: I measured up to 30 cm ice growth since the previous week between 3 and 12 m seaward of the ice foot (Figure 5.3).

There is some wet snow close to the breakwater. The snow cover is about 20 cm thick on the free-floating ice (Figure 5.5). In the hinge zone it varies between 10 and 30 cm between the cracks 2 and 3.

B.2.6 Week 8 – 22 February 2007

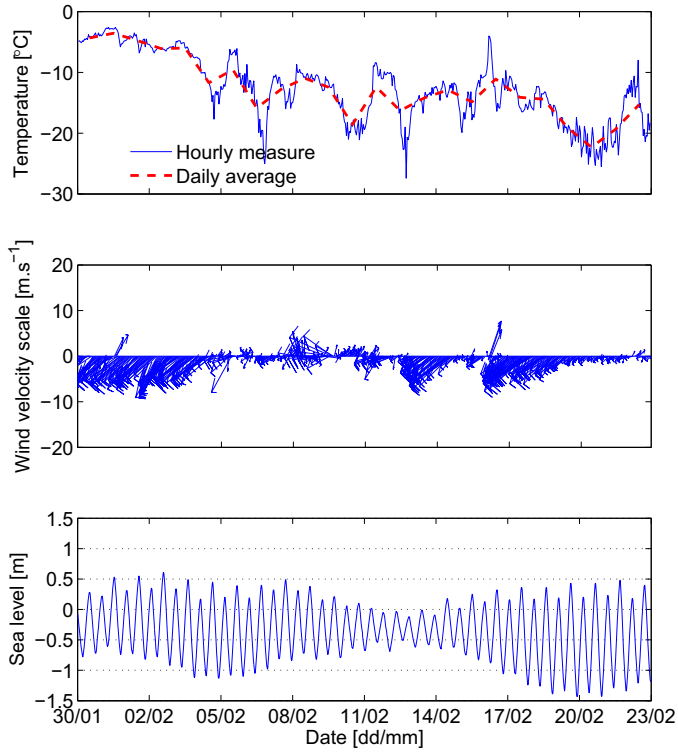

Figure B.56: Air temperature, wind and sea height data from 30 January to 22 February 2007

Air temperature (Figure B.56): the air temperature oscillated between –20 and –10 °C. The mean temperature during the period was –12.6 °C.

Tide cracks: a fourth shore-parallel tide crack had formed since the surveys done one week earlier (Figure B.57). Additional, minor cracks had also formed along the tip close to the west corner.

Crack 1 was opening up several decimetres at low tide and was completely closed at high tide.

Sea ice and snow cover: I measured the ice thickness between 3 and 11 m seaward of the breakwater. Compared with week 5, the ice had only grown in the zone between 3 and 5 m. Between 5 and 11 m it had become up to 0.25 cm thinner.

Compared to week 5 the snow cover between cracks 2 and 3 was mostly between 10 and 20 cm thicker, with a maximum of 40 cm at crack 3. Seaward of crack 3 the snow cover thickness was decreasing, and 4.4 m away it was 1 cm. For comparison, it was 15 cm in week 5.

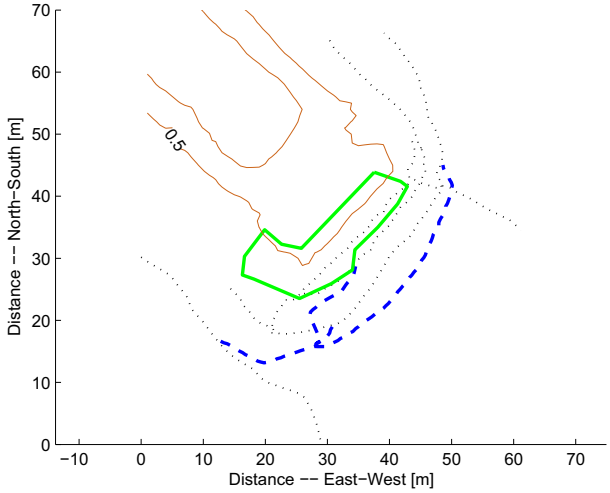

Figure B.57: Tide cracks formed between weeks 7 and 8 in thick, blue, dashed lines. In thin, black, dashed lines, the tide cracks already present in week 4. The zone covered with bags is delimited by a green, solid line. The brown, thin contour lines show the topography of the breakwater – 22 February 2007 (week 8)

Figure B.58: Crack 1 opening at high tide (10-20 cm) – 22 February 2007 (week 8)

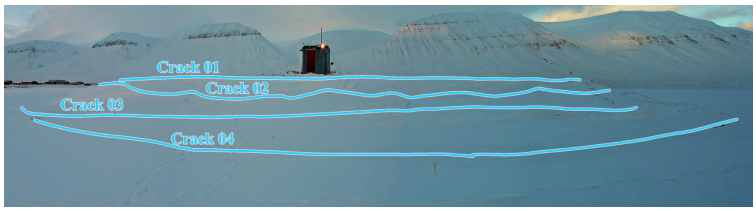

Figure B.59: Crack pattern at the tip of the breakwater, sea height = –1.1 m – 22 February 2007 (week 8)

B.2.7 Week 10 – 9 March 2007

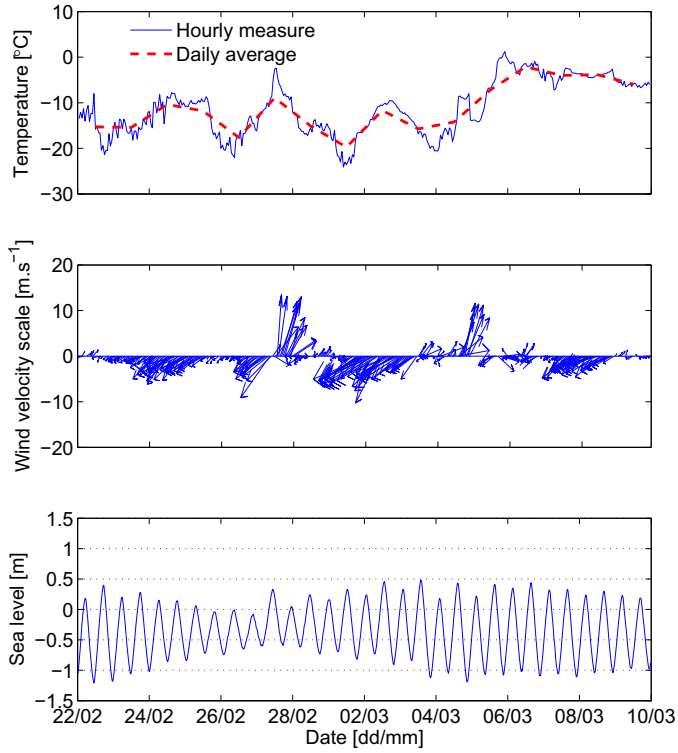

Figure B.60: Air temperature, wind and sea height data from 22 February to 9 March 2007

Air temperature (Figure B.60): the daily mean temperature stayed stable between –20 and –10 °C until 5 March then rose to about –5 °C. The mean temperature during this period was –11.2 °C.

Sea ice and snow cover: a pond of seawater had formed on the surface of the hinge zone along the breakwater tip (Figures B.61 and B.62). The pond was 15 m long and 5 m wide on 11 March 2007. It started to form at approximately 06:00 on 6 March 2007. Actually, a whole area around the pond was covered with slush from sea water flowing through the ice cover. The pond was only the part of the submerged area where the water level was higher than the snow top.

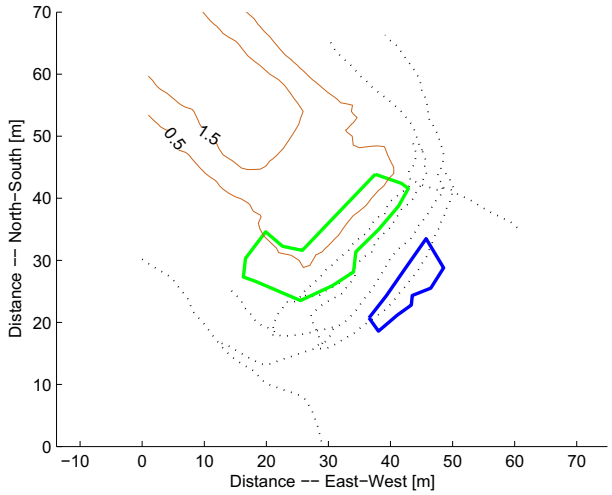

Figure B.61: Delimited by a thick, blue, solid line, the pond of surface seawater along the tip of the breakwater. The zone covered with bags is delimited by a green, solid line. In thin, black, dashed lines, the tide cracks and in thin, brown, the contour lines of the breakwater – 11 March 2007 (week 10)

Figure B.62: Pond of surface seawater along the tip of the breakwater, sea height = –0.1 m – 9 March 2007 (week 10)

B.2.8 Week 11 – 14 March 2007

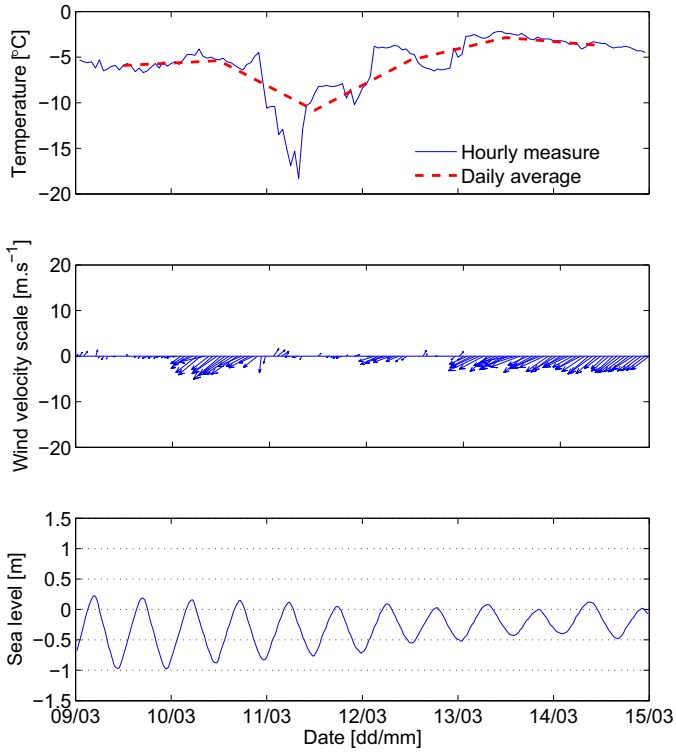

Figure B.63: Air temperature, wind and sea height data from 9 to 14 March 2007

Air temperature (Figure B.63): the daily air temperature stayed warm, between –11 and –3 °C, with an average of –5.7 °C.

Sea ice: The pond of surface seawater was still present although it had shrunk (Figure B.64).

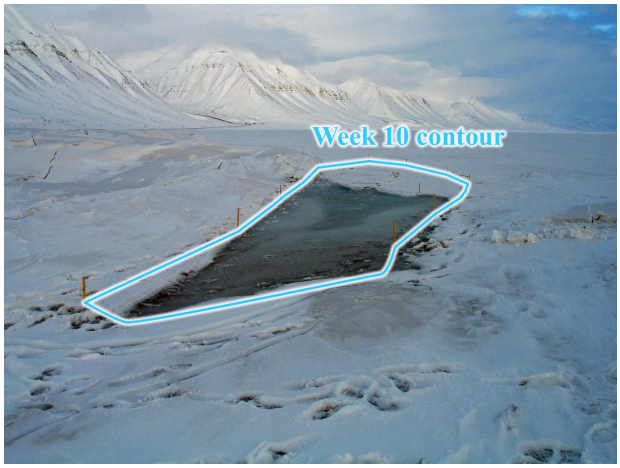

Figure B.64: Pond of surface seawater along the tip of the breakwater, sea height = –0.4 m – 14 March 2007 (week 11)

B.2.9 Week 13 – 26 March 2007

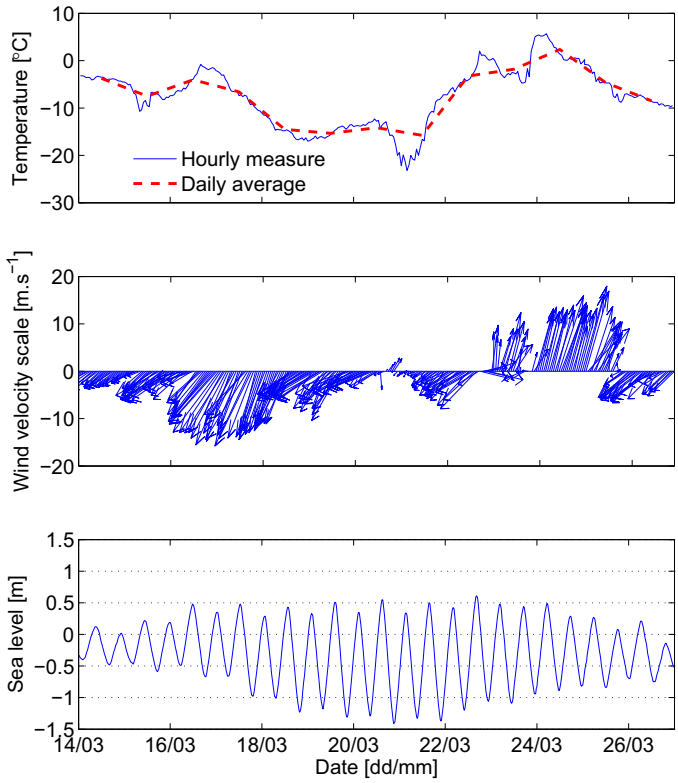

Figure B.65: Air temperature, wind and sea height data from 14 to 26 March 2007

Air temperature (Figure B.65): the daily air temperature stayed around –5 °C until 18 March then around –15 until 22 March. Between 23 and 26 March the weather was warm and there were strong, westerly winds. During this period it was raining.

Sea ice: The pond described in weeks 10 and 11 had frozen over (B.69.

There was 17 cm of slush on top of the ice separated from the dry snow by a thin layer of snow ice. The slush water was probably a combination of sea and rain water. Under such conditions it was necessary to wear waterproof clothes when working on the ice (Figure B.67). In some places the snow ice layer is strong enough to support a person.

Snow: Figure B.68 shows snow drifts on the lee of the cabin.

Bags: All but a few of the upper bags were covered either with snow or ice (Figure B.69).

Figure B.66: Coastal ice along the tip of the breakwater, sea height = –0.1 m – 27 March 2007 (week 13)

Figure B.67: Due to the presence of surface water it was necessary to wear waterproof clothes – 28 March 2007 (week 13)

Figure B.68: Two snowdrifts had formed on the lee side of the cabin during the winter – 27 March 2007 (week 13)

Figure B.69: Backshore and cabin – 27 March 2007 (week 13)

B.2.10 Week 15 – 10 April 2007

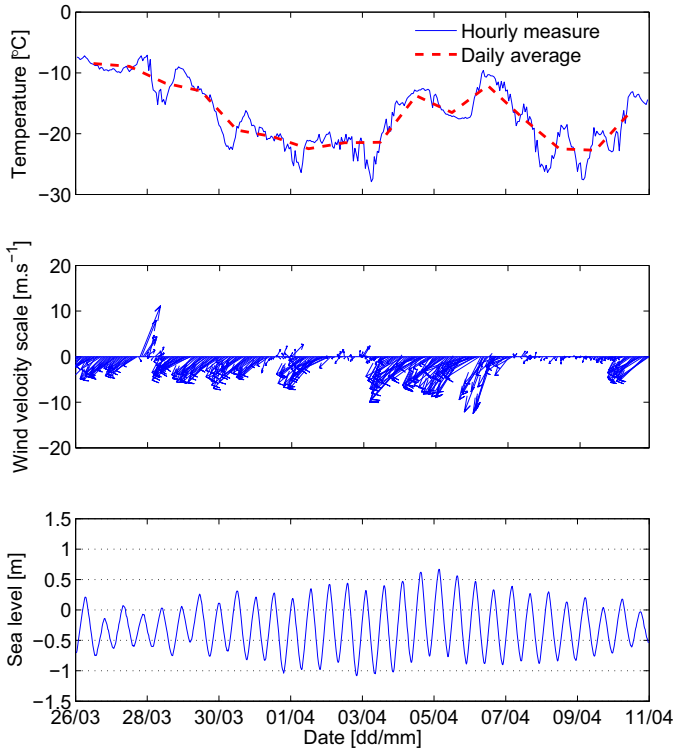

Figure B.70: Air temperature, wind and sea height data from 26 March to 10 April 2007

Air temperature (Figure B.70): the daily air temperature fell quite linearly to about –20 °C on 31 March and stayed mostly below –15 °C until 10 April. The mean temperature for this period was –16.8 °C.

Snow: Most of the snow had blown away.

B.2.11 Week 16 – 20 April 2007

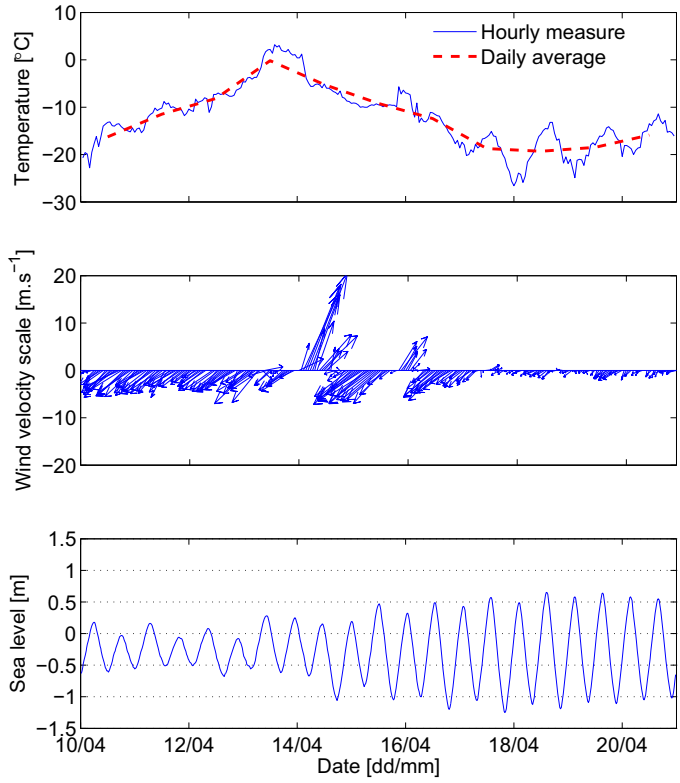

Figure B.71: Air temperature, wind and sea height data from 10 to 20 April 2007

Air temperature (Figure B.71): the daily air temperature gradually increased to 0 °C on 13 April then decreased to about –20 °C on 17 April and stayed fairly constant until 20 April. The mean temperature for this period was –12.3 °C.

Tide cracks: a new shore-parallel crack had appeared landward of the existing cracks, approximately 1.5 m apart from crack 1.

Seaward of crack 4 another shore-parallel crack had appeared (Figures B.72 and B.73). Unfortunately I did not survey its position.

Snow: at 4.5 m from the ice foot the snow thickness was about 40 cm. Seaward of crack 3 the snow thickness on the ice was varying between 10 and 25 cm. I measured it up to 17 m seaward of the ice foot and it seemed as is the snow thickness of the free-floating ice was around the same.

The snow density varied between 340 and 420 kg m^{-3}, with an average of 380.

Figure B.72: New shore-parallel crack seaward of crack 4, sea height = –0.7 m – 18 April 2007 (week 16)

Figure B.73: Tubes placed around drilled holes avoid the sea water from flooding the ice when performing freeboard measurements in the hinge zone. In the foreground, tube 5. There is a tide crack between tube 5 and the next tube, tube 4. Ice core "graveyard", on the left, from the coring campaign described in Section 4.2.11 – 21 April 2007 (week 16)

B.2.12 Week 16 – 25 April 2007

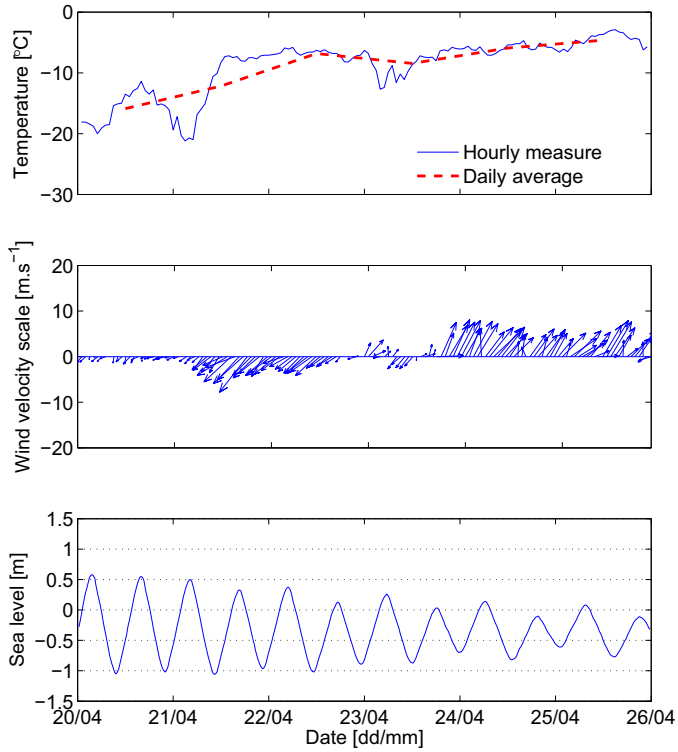

Figure B.74: Air temperature, wind and sea height data from 20 to 25 April 2007

Air temperature (Figure B.74): the daily air temperature increased linearly from –16 to –7 °C between 20 and 22 April and stayed at around –5 °C for the rest of the period. The mean air temperature for this period was –9.0 °C.

Ice foot: While digging a hole to install stress sensors on both sides of crack 2 I noticed that the ice consisted of several several-centimetres-thick, inhomogeneous layers and that it contained numerous, sizeable cavities.

B.2.13 Week 20 – 17 May 2007

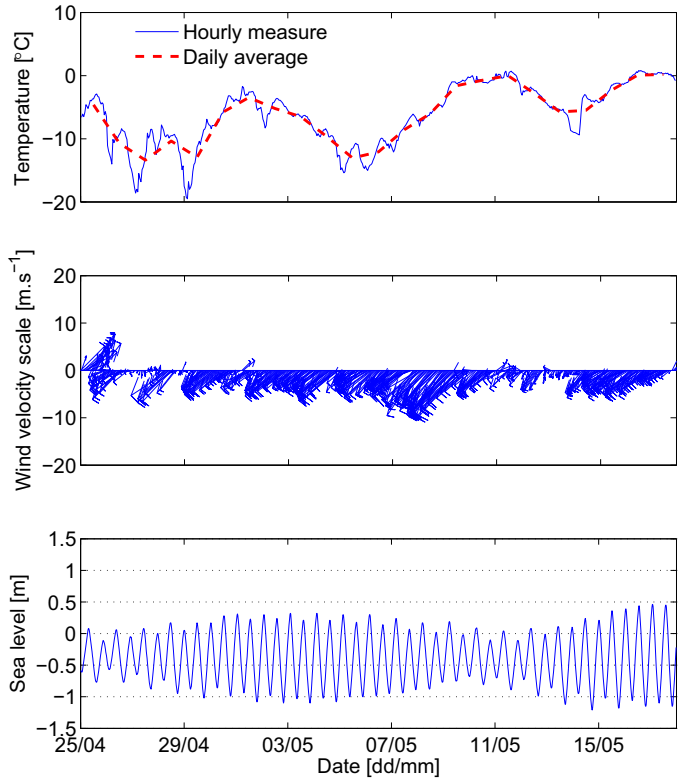

Figure B.75: Air temperature, wind and sea height data from 25 April to 17 May 2007

Air temperature (Figure B.75): the air temperature was warming up, with an average of –6.1 °C. Apart from the period between 26 and 29 April and 5 and 6 May, the daily temperature stayed above –10 °C and even above 0 °C during the last couple of days.

Snow: the snow started to melt around mid-May as can be seen by comparing Figures B.76 and B.77. By 18 May it was already quite rotten and the first ponds of melt-water started to form (Figures B.77). Ponds were observed on the west side of the breakwater but they were caused by sea water flooding at high sea levels (Figure B.77).

Sea ice: the sea ice was 85 cm thick 50 m from the breakwater.

Bags: from the beginning of May the air temperature got closer to 0 °C and the snow

cover was slowly melting. By 17 May almost all the snow had melted from the upper row of bags (Figure B.79).

Figure B.76: Still winter: sea ice at the breakwater tip, sea height = –0.7 m – 11 May 2007 (week 19)

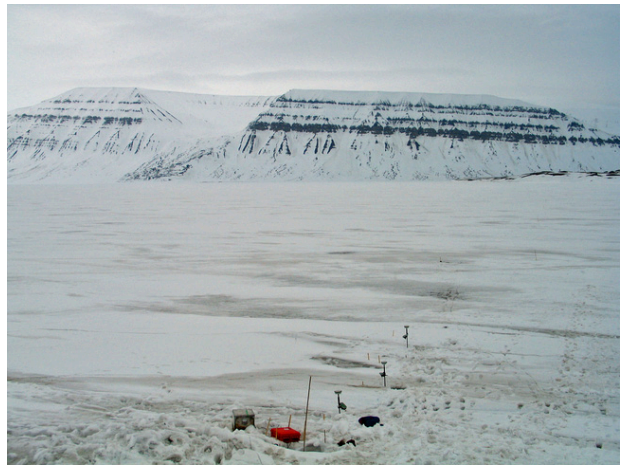

Figure B.77: The snow layer was rottening and the first meltwater ponds are starting to form. In the foreground the stress sensors with battery and logger. The three poles on the ice are DGPS rovers. The picture was taken from the cabin in the direction of Ispallen – 17 May 2007 (week 20)

Figure B.78: Sea water ponds on the west side of the breakwater, sea height = –0.3 m – 18 May 2007 (week 20)

Figure B.79: The upper row of bags was almost free of snow – 17 May 2007 (week 20)

B.2.14 Week 21 – 21 May 2007

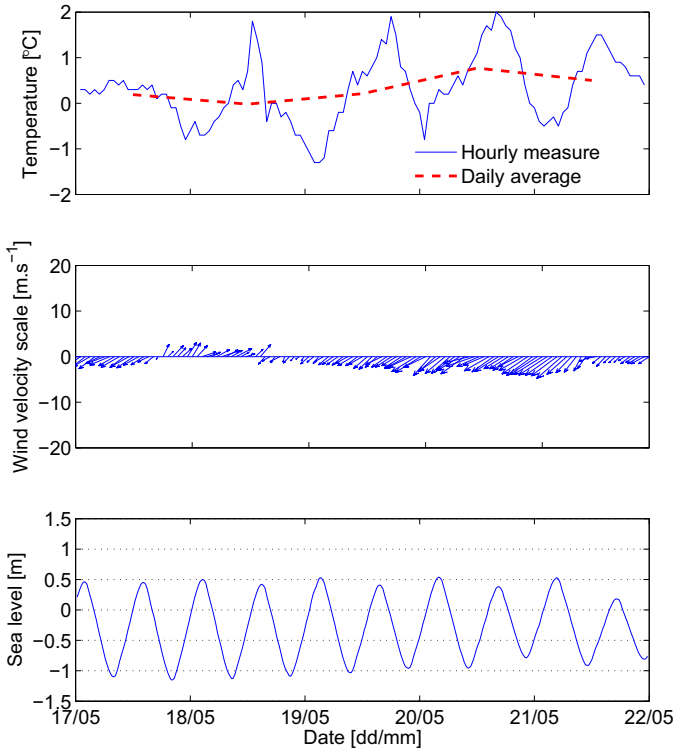

Figure B.80: Air temperature, wind and sea height data from 17 to 21 May 2007

Air temperature (Figure B.80): the daily air temperature stayed fairly constant for the whole period with an average of 0.3 °C, however the hourly temperature varyied between –1 °C during the night and 2 °C during the day.

Snow: most of the snow on land had melted. There was still snow, albeit rotten, on the ice foot and the sea ice (Figures B.81 and B.82).

Sea ice: the sea ice was covered with interconnected water ponds of up to 30 cm depth. The ice was 75 cm thick 50 m seaward of the breakwater. It was the start of what can be called the pre-break-up.

Figure B.81: Ice covered with rotten snow and meltwater at the tip of the breakwater, sea height = –0.3 m – 22 May 2007 (week 21)

Figure B.82: View of Sveasundet and Braganzavågen from Liljevalchfjellet. The ice was covered with ponds of meltwater – 22 May 2007 (week 21)

B.2.15 Week 22 – 31 May 2007

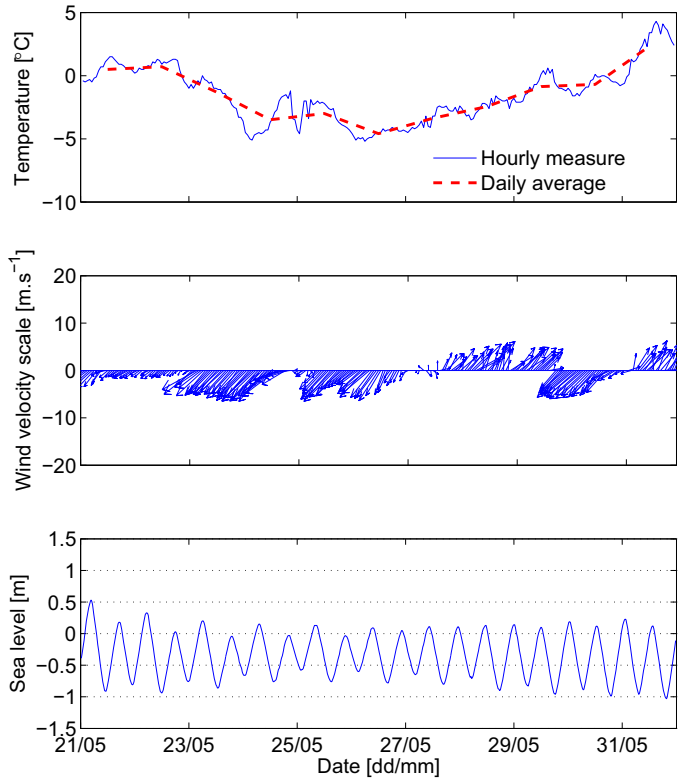

Figure B.83: Air temperature, wind and sea height data from 21 to 31 May 2007

Air temperature (Figure B.83): the daily air temperature was negative for most of the period, with a minimum of –5 °C. On 31 May it was over 2 °C. The mean temperature was –1.5 °C.

Sea ice: the water temperature is –0.1 °C at the ice bottom and –0.3 °C 20 cm right below the ice. The appearance of the sea ice was similar to what it had been 10 days earlier (Figures B.84 and B.85).

Figure B.84: State of the ice at the tip of the breakwater. A tide crack is crossing the picture in the foreground. Sea height = 0.1 m – 31 May 2007 (week 22)

Figure B.85: View of Sveasundet and Braganzavågen from Liljevalchfjellet — 1 June 2007 (week 22)

B.2.16 8 June 2007 (week 23)

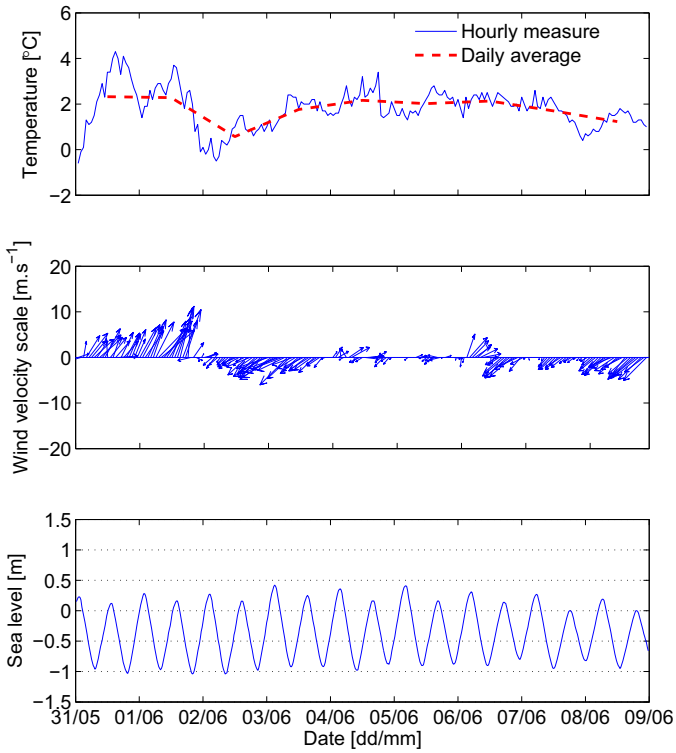

Figure B.86: Air temperature, wind and sea height data from 31 May to 8 June 2007

Air temperature (Figure B.86): The daily air temperature stayed fairly constant, between 0 and 2 °C, with an average of 1.8 °C.

Sea ice: the sea ice 50 m away from the breakwater was 43 cm thick. The ice was melting up in situ from the top, the bottom and along the tide cracks, which were widening (Figure B.87). The meltwater ponds were continuing to develop and were merging into small lakes close to the shore (Figure B.88).

Bags: the snow was continuing to melt on the bags and a meltwater pond had formed on top of the ice foot (Figure B.89).

Figure B.87: State of the ice at the tip of the breakwater. The tide crack in the foreground was getting wider. Sea height = –0.7 m – 8 June 2007 (week 23)

Figure B.88: View of Sveasundet and Braganzavågen from Liljevalchfjellet – 8 June 2007 (week 23)

Figure B.89: Meltwater pond on top of the ice foot at the breakwater tip, picture taken from the roof of the cabin - 8 June 2007 (week 23)

B.3 Thaw-up and break-up

Due to the rapid evolution of the sea ice during the thaw-up period I made daily observations from 12 to 21 June 2007.

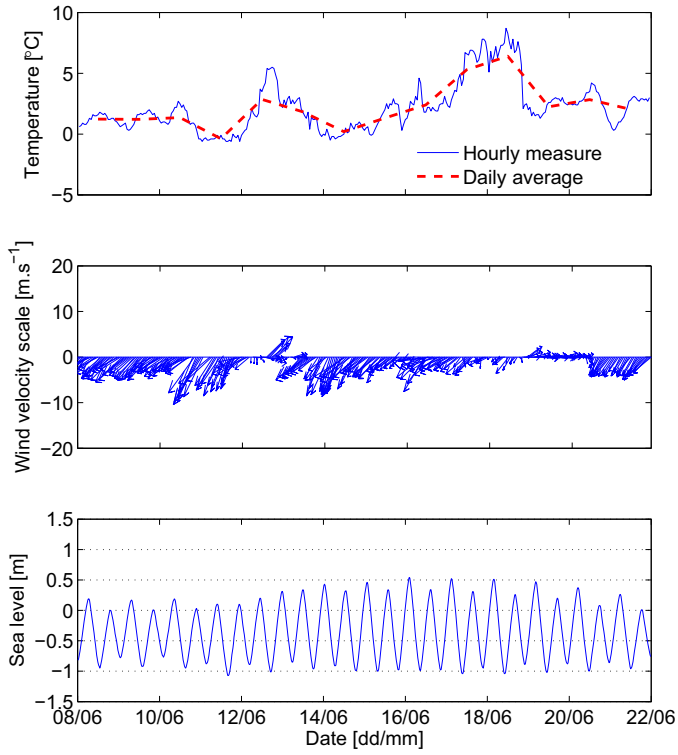

Figure B.90: Air temperature, wind and sea height data from 8 to 21 June 2007

Air temperature (Figure B.90): The daily air temperature stayed fairly constant, between 0 and 3 °C until 14 June then increased linearly to 6.4 °C (18 June) and decreased to 2.0 °C on 21 June. The mean temperature was 2.2 °C during the whole period.

The maximum daily tidal range increased from 1.32 m on 12 June to 1.52 m on 15 June.

12 June 2007 (week 24):

The sea ice was 41 cm thick 50 seaward of the breakwater. The sea water temperature was still –0.1 °C at the ice bottom but +1.1 °C 10 cm below the ice bottom. There were some thaw holes close to the breakwater. The ice had started to break up along the shore in Braganzavågen between the breakwater and Svea. Between the breakwater and Kapp Amsterdam the sea ice was breaking up in situ along the coast. At the tip of the breakwater it remained fast.

Figure B.91: State of the ice at the tip of the breakwater, sea height = –1.0 m – 12 June 2007 (week 24)

13 June 2007 (week 24):

The ice seaward of tide crack 2 broke loose and drifted away during flow, at 10:05 (Figure B.92). Although the ice had broken up around the breakwater most of the ice in Sveasundet was still fast. The zone of unconsolidated ice extended along land in Braganzavågen and stopped at the west corner of the breakwater. Within that zone ice cakes were drifting back and forth with the tide. On the opposite side of Sveasundet a meltwater river was starting to form along Crednermorenen (Figure B.93).

The bags were starting to become apparent (Figure B.95).

Figure B.92: State of the ice at the tip of the breakwater, sea height = –0.8 m – 13 June 2007 (week 24)

Figure B.93: View of Sveasundet and Braganzavågen from Liljevalchfjellet – 13 June 2007 (week 24)

14 June 2007 (week 24):

On the east side of the breakwater ice cakes were stranded on the ice foot at high tide (Figure B.94). The ice in the hinge zone was continuing to break apart from the ice foot. Figure B.95 shows the difference between the fixed ice foot (to the left) and the moving sea ice (in the middle). The moving sea ice was melting both from the top and from below.

Figure B.94: Stranded ice cakes, east side of the breakwater, sea height = –0.9 m – 14 June 2007 (week 24)

Figure B.95: Ice still attached to the breakwater and crack 1, sea height = –0.9 m – 14 June 2007 (week 24)

15 June 2007 (week 24):

The meltwater river seen in Figure B.93 and the zone of drift ice in Braganzavågen were extending (Figure B.96). There was also a sizeable area of open water along the northern shore of Sveabukta. The fast ice in Sveasundet was, however, still attached to land at the west corner of the breakwater. Figures B.97 and B.98 illustrate the back-and-forth movement of the drift ice: at ebb the sea was covered with drift ice retained by fast ice at the west corner of the breakwater while at flow the sea was ice-free as the drift ice was pushed into Braganzavågen. At the breakwater tip, the drift ice moved along the shore and, consequently was not stranded, contrary to what happened along the east side of the breakwater (Figure B.94).

Figure B.96: View of Sveasundet, Sveabukta and Braganzavågen from Liljevalchfjellet – 15 June 2007 (week 24)

Figure B.97: Drift ice stuck in front of the breakwater during ebb, sea height = –0.5 m – 15 June 2007 17:16 (week 24)

Figure B.98: The area east of the breakwater was ice-free during flow, sea height = –0.3 m – 15 June 2007 14:22 (week 24)

16 June 2007 (week 24):

During ebb, ice cakes were drifting out of Braganzavågen, around the breakwater, and being pushed against the last zone of fast ice in Sveasundet, breaking it eventually up sometimes between 05:00 and 05:30 (Figures B.100 and B.101). Further west, however, the fjord was still covered with fast ice. In the east corner the current tended to drive the drift ice away from the tip of the breakwater. Depending on the drift ice density, however, some cakes got squeezed and pushed on land at the corner when the ice was moving out of Braganzavågen. For the first time, a few cakes were stranded along the tip of the breakwater.

The cakes were about 30 cm thick and while some were soft, others were hard. As seen in Figure B.99 the ice on the east side of the breakwater had completely melted away.

On the east side of the breakwater I observed a peculiar geomorphological feature in the form of a track left on the shore by the ice foot crack (Figure B.102). The track was levelled out after a few tidal cycles though.

The ice foot was continuing to melt but it was still acting, to some extent, as a protection layer against drift ice impacts (Figure B.105). At low tide the drift ice was scouring at the lower part of the lowest row of bags, below the ice foot (Figure B.107). On the west side the lower bags of rows 3 and 4 (see Figure C.10) were ice-free and subjected to abrasion from the drift ice. The polypropylene fibres were untwined and brushed from the abrasion (Figure B.104). Some of the exposed bags were covered with sediments (Figure B.105). In the west corner of the breakwater it appears that the bag protection nets were caught into the ice and deformed (Figure B.106).

Figure B.99: Stranded ice blocks on the east side of the breakwater, sea height = –0.6 m – 16 June 2007 (week 24)

Figure B.100: View of Sveasundet and Braganzavågen from Liljevalchfjellet — 16 June 2007 05:00 (week 24)

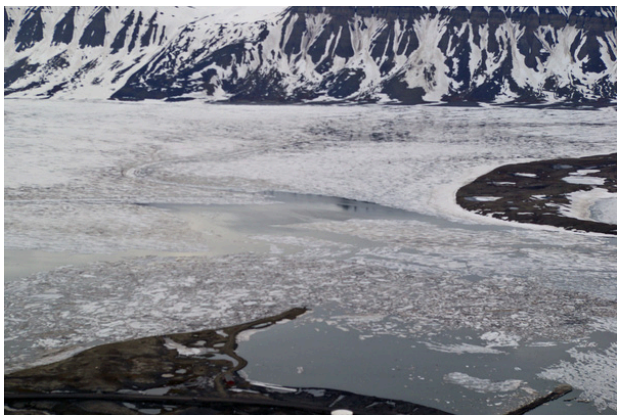

Figure B.101: View of Sveasundet and Braganzavågen from Liljevalchfjellet — 16 June 2007 05:30 (week 24)

Figure B.102: Track left by the ice foot crack on the shore – 16 June 2007 (week 24)

Figure B.103: Bags exposure following the melting of the ice foot, eastern part of the breakwater tip, sea height = –0.9 m – 16 June 2007 (week 24)

Figure B.104: Elongated fibres on the lower bags on the west side – 16 June 2007 (week 24)

Figure B.105: Bag covered with sediments – 16 June 2007 (week 24)

Figure B.106: Deformed protection net at the west corner of the breakwater – 16 June 2007 (week 24)

Figure B.107: Drift ice scouring against the lower bags at low tide, sea height = –0.6 m – 16 June 2007 (week 24)

17 June 2007 (week 24):

During ebb the floating ice cakes moved further west for each tidal cycle as the ice was gradually breaking up toward west (Figure B.108). During flow the cakes moved back into Braganzavågen.

On the west side of the breakwater the bags were completely ice-free (Figure B.109).

Figure B.108: View of Sveasundet and Braganzavågen from Liljevalchfjellet – 17 June 2007 (week 24)

Figure B.109: Bags on the west side of the breakwater, sea height = –1.0 m – 17 June 2007 (week 24)

18 June 2007 (week 25):

Except for a 6 x 2 m section close to the west corner of the breakwater (dark, rotten ice in Figure B.110), the ice foot had melted away at the tip of the breakwater. An approximately 15 x 5 m piece of ice remained frozen to land on the west side of the breakwater, next to the bags (Figure B.110). Several ice cakes were stranded, mostly on the east side of the breakwater, but also at its tip. The cakes on the tip reached up to the second row of bags and were about 5 x 5 m. Figures B.111 and B.112, taken at 05:13 and 06:13 respectively, show what happened: a sizeable area of ice of about 500 x 1000 m broke loose from the ice cover in Braganzavågen and drifted westwards with the tidal current. As it was wider than Sveasundet, ice cakes on its periphery were pushed ashore.

As a result of the cross-section narrowing at the breakwater, the tidal current was pushing the drift ice against the corners of the breakwater but away from the tip. A drifting ice cake created a 60 x 40 cm hole in the bag closest to the east corner (bag #150). That was the only visible damage (Figure B.113, which also shows how the lower bags were covered with sediments).

Masses in the bags from the lower row had moved from the center of the bags to their bottom under the action of the ice rotating along crack 1. Therefore, the bags had become peanut-shaped: both ends were thicker than the middle, the lowest one being the thickest. The shape was so pronounced that the fabric in the middle of the bag was streched like a drumhead. Bags on the third row were deformed as well, albeit in a different manner: while the lowest bags were thinnest in the middle, the bags in the third row had more of a pear shape with the thickness linearly increasing from the top to the bottom.

As seen in Figure B.113 the ice foot was sticking strongly to the bags and when bigger blocks of the ice foot broke loose the bags were stretched in the points where the ice foot stuck the most.

Figure B.110: Aerial view of the breakwater. Photo: Lene Kristensen. Sea height = –0.4 m – 18 June 2007 (week 25)

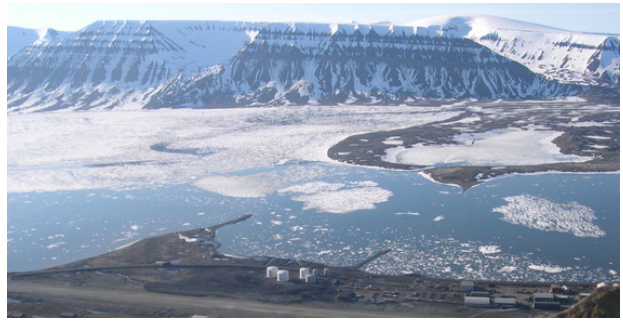

Figure B.111: View of Sveasundet and Braganzavågen from Liljevalchfjellet – 18 June 2007 05:13 (week 25)

Figure B.112: View of Sveasundet and Braganzavågen from Liljevalchfjellet – 18 June 2007 06:13 (week 25)

Figure B.113: Damage on bag #150 at the east corner of the breakwater, looking toward west, sea height = –1.0 m – 18 June 2007 (week 25)

Figure B.114: Ice foot ice stuck to a bag at the breakwater tip – 18 June 2007 (week 25)

19 June 2007 (week 25):

Drift ice had piled up at the east corner of the breakwater (Figure B.115). The weather was unfortunately foggy while the pile-up was taking place, therefore, it is not possible to use the pictures from the cameras on Liljevalchfjellet in the same manner as on 18 June. Pictures taken by one of the video cameras show, however, that the same type of mechanism was responsible for the pile-up and that it started at 06:24, which is 2 hours after high tide. The pictures in Figure B.118 were taken from the video camera and give an idea of how the ice piled up. The biggest piled-up cakes were about 3.6 x 1.2 m in horizontal dimenstions and 30 cm in thickness.

Figure B.115: Ice pile-up in the east corner of the breakwater, sea height = –0.8 m – 19 June 2007 (week 25)

Figure B.116: Ice pile-up at the tip of the breakwater, sea height = –1.0 m – 19 June 2007 (week 25)

Figure B.117: Ice pile-up at the tip of the breakwater, sea height = –1.0 m – 19 June 2007 (week 25)

(a) time: 06:28:02

(b) time: 06:28:07

(c) time: 06:28:12

Figure B.118: Ice pile-up at the eastern corner of the breakwater, sea height = 0.0 m – 19 June 2007 (week 25)

21 June 2007 (week 25):

The piled-up ice was washed away at high tide up to the top of the third row of bags (Figure B.119). During the pile-up bag #150 was damaged further, probably by stones displaced by the ice from the corner of the breakwater (Figure B.119).

The return of the eider ducks marked the summer (Figure B.120).

Figure B.119: Breakwater tip, looking toward west, sea height = –0.9 m – 21 June 2007 (week 25)

Figure B.120: Eider ducks on the first day of summer – 21 June 2007 (week 25)

Figure B.121: Deformed bags in the third row – 21 June 2007 (week 25)

22 June 2007 (week 25):

By 22 June most of the ice has drifted away and Sveabukta is ice-free (Figure B.120).

Figure B.122: Ice-free sea except for a small ice patch in Braganzavågen – 22 June 2007 (week 25)

Appendix C

Geosynthetic bags for shore protection in the Arctic

The breakwater was used as a test structure for a parallel project, which goal was to assessing the resistance to ice loads of an erosion protection system consisting of geosynthetic bags filled with local masses. This appendix contains background and practical information about the project. A separate report with full results is available (Artières et al., 2009).

C.1 Introduction

My supervisor was approached at the beginning of my PhD by TenCate Geosynthetics, who wanted to develop products adapted to cold climates. The demand for such products was expected to grow rapidly due to:

- the increased accessibility of arctic coasts to shipping, as the sea ice is gradually retreating;
- the extreme levels of coast erosion in the Arctic, only reinforced with the extension of the ice-free period and the increased thawing rate of the permafrost (Leont'yev, 2004).
- in most of the Arctic, there is a shortage of natural rock. Soft structures built with geosynthetics—geosystems—are, therefore, an alternative to traditional, hard structures that is cheaper and more respectful of the environment. Half the cost of a causeway across Sveasundet were estimated to come from the erosion protection layer (Larsen, 2004).

Geosystems have been used for coastal engineering for many years (Pilarczyk, 2000) but their usage along the coasts of ice-infested waters is scarce and poorly documented.

Store Norske and TenCate agreed to a partnership and the decision was made to test geosynthetic bags on the breakwater created to study the coastal ice.

The advantage of a soft solution is that the bag envelope simply deforms when the ice foot is rotating, as opposed to hard structures where whole elements may displaced. The question we started investigating is how resistant to ice loads bags are.

Figure C.1: Shore protection attempt with low-quality, local rocks at Kapp Amsterdam – 17 July 2007

C.2 Longyearbyen experiment

C.2.1 Description

In February 2005 I hired LNS Spitsbergen (LNSS), a contractor, and got help from UNIS student Alf Kristian Lund to fill 8 geosynthetics bags with local masses and place them on the beach close to the harbour of Longyearbyen. The goal was to test the construction method and observe the sea ice loads applied to the bags. 5 different types of non-woven polypropylene fabrics were used.

I sewed the bags from trapezoidal sheets of geosynthetics of dimensions: H = 3.0 m, B = 3.3 m, b = 2.3 m and folded in to along the middle (Figure C.2). I used a Fischbein Portable F sewing machine. The volume of the sewn bags was around 0.6 m^3 and the fill weight around 1000 kg. The large base side was left open to fill the bags. I sewed a 0.2-m-wide hem along the opening, passed a 20 mm polyester rope inside and tied a loop at each end for easy lifting.

We filled the bags through an elevated funnel placed on a self-designed steel frame (Figure C.3). The top of the bag was folded over the top of the frame and hold in place by the

funnel. When the bag was full we pulled the funnel away, attached the bag rope to the excavator shovel and, by lifting the shovel, put the lifting rope under enough tension to maintain the bag in a stable vertical position. The frame was built with vertical hinges so I folded it open and removed it from around the bag. With the bag still maintained vertical, I closed it by tightening a 8 mm polypropylene rope several times around its top. Finally we lifted the bag by the top rope and put in place (Figure C.4). During the lifting operation the bottom of the bags suffered great elongation from the weight of the fill masses. That lead to designing trapezoidal bags: after elongation they had an almost constant cross-section perpendicular to their length.

The beach slope on site is 1V:6H. The maximum ice thickness during the winter was about 50 cm. The bags were rapidly completely covered with ice. The ice started to break up on 21 April. On 1 May the fjord was still covered with ice but 4 days with near gale blew away the ice within 4 May. The maximum wind gust was measured at 18 m s^{-1} on 4 May. During the following week the fjord was covered with drifting ice cakes. A gale on 14 May blew several cakes toward the bags. They stayed next to the bags for one week and were completely blown away by 20 May.

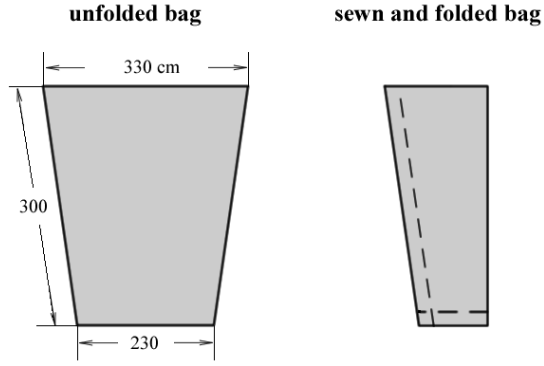

Figure C.2: Sketch of the bags used in Longyearbyen

C.2.2 Results

In the construction phase, one bag burst open at the bottom during the lifting operation. Apparently the seam was cut by a sharp rock.

I was on sick leave for most of the winter due to a back injury and could, therefore, not document the ice conditions properly.

Figure C.3: Filling of a bag in Longyearbyen

After the gale on 14 May the bottom seams of three bags were unpicked. Initially the openings were only 10 cm wide but the ice and waves eventually unpicked the seams completely. Since the seams were intact before the storm the damage was most probably caused by the drifting ice cakes.

In addition to the seam damages, the bags were punctured in several places and surface fibres were loose. All the punctures occurred around sharp stones on the inside of the bags.

C.2.3 Lessons learnt

The sewing machine was not adapted to the fabric thickness, therefore, it was almost impossible to sew the bags.

The seams are the weakest point of the bags, especially because if they are damaged in one spot, they are easily completely unpicked. Seams should, therefore, at least be doubled and, if possible, protected on installed bags, for example by placing the bags close to each other.

The lifting mechanism with a rope passed in a sewn hem worked well but was time-consuming both during bag construction and after placement, when the ropes were removed.

The puncture holes showed the importance of filling the bags with masses at least smaller than 100 mm in diameter.

The filling method needed improvement. It was difficult to remove the frame from the bag. It is also important to avoid sharp edges: the section of the funnel was square and its corners perforated some of the bags.

We need some kind of scaffolding to stand on while closing the bags. It is preferable to have two people close the bags: that would ensure a tighter closing and it would probably be quicker.

Figure C.4: Placement of a bag in Longyearbyen – 2 March 2005

C.3 Barryneset bags

C.3.1 Design

I redesigned the bags based on the experience acquired during the Longyearbyen experiment. Since the bags were going to be carried in a bucket, it was possible to sew them from a rectangular sheet of 1.2 x 5 m instead of a trapezoidal sheet. The sheet was folded in two along the short side and sewn along both long sides. That way there was no seam along the bottom of the bags. The opening of the bags was approximately 0.6 m in diameter, their volume 0.6 m^3 and their mass 1000 kg when filled to 80 % with materials of 1900 kg m^{-3} density.

The pieces of fabric were cut out of a 6-m-wide roll of geosynthetics. The preconstruction of a bag, including the cutting and the sewing takes 10 minutes for a single operator. The sewing was done with a Union Special 2200 portable sewing machine and a Gruschwitz

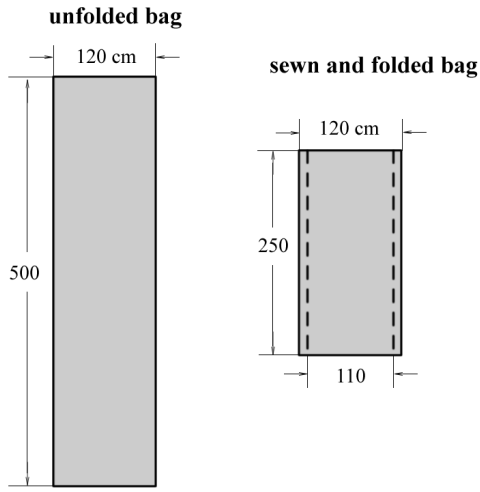

Figure C.5: Sketch of the bags used at Barryneset

Polypropylen Et.15 thread. The seam design was such that it may unravel in the direction opposite to the sewing direction, therefore, it was necessary to always tie a knot at the end of the seam. The seam strength was 33–35 kN m^{-1}, which is comparable to the strength of the fabrics used.

The bags were built with three different types of fabrics: F80, P50UV and P80UV. All three fabrics are two-layer, non-woven geosynthetics. F80 is a filter fabric used in coastal structures instead of a graded filter layer. It consists of a grey filter layer and a blue layer protecting against overlying armour rocks. The P50UV and P80UV are a bicolour (green and grey) fabric used to protect watertight geomembranes barriers in landfills. The UV suffix means that one layer is UV-resistant. The thicknesses of the P80UV and the F80 are in the upper range of the sewing machine, therefore, we had to modify the factory settings.

A protection net was sewn around several bags. Two types of nets were used. FC011 is a UV-resistant polyethylene 10 mm net weighing 190 g.m-2. It is usually used for erosion protection and has a green colour. The other type of net is a black and green net—*filet*, in French—with small curls—*bouclettes*, in French—, which I, therefore, abbreviated *FB*. Finally, I built some bigger bags with sewn sizes of 1.4 x 3 and 1.1 x 3 m. The overview over the different types of bags is found in Table C.1. The bags with nets took twice as much time to build as the normal bags. The structure of the net and the added thickness made the sewing more difficult.

When lying on the ground, filled, standard bags are approximately 0.6 m thick and 0.8 m wide.

Bag type	Quantity
P50UV	32
P80UV	41
F80	27
F80 + FC011	20
F80 + FB	4
P50UV 1.4 x 3 m	4
P80UV 1.1 x 3 m	5
TOTAL	133

Table C.1: Quantity of bags of each type

C.3.2 Construction

We used the finest masses available locally. They were extracted from the bed of a melt river on Liljevalchfjellet. 70 % of the masses had a diameter smaller than 19 mm (Figure C.6). There were unfortunately also some bigger rocks, with diameters up to about 200 mm.

The masses were transported to Barryneset by truck. Each bag was attached to an elevated funnel (Figure C.7) and filled using a small excavator. It was supported by a box attached to a bigger, 25-ton excavator. Both the funnel and the box were designed in cooperation with Tom Breivik (Store Norske). After the bag was filled, it was moved from below the funnel and an operator closed it with a double seam and an additional short seam across the end of the double seam, in order to reduce the risk of unpicking. The bag was then dumped into an excavator bucket standing on the ground and the operator released the bag box and attached the bucket containing the bag (Figure C.11). This method allowed the operator to see the bag while he was placing it on the ground (Figure C.12). It was a workaround to a *rotortilt*—a mechanism allowing to rotate the bucket—, which we unfortunately did not have.

The bags were placed in four rows parallel to the shoreline on a geosynthetic filter layer and covered the breakwater slope from the east corner to the west side of the breakwater (Figures C.8, C.9 and C.10). We tried to protect the seams by placing the bags close to each other, even with a slight overlap. The bag rows are slightly inclined, the bags at the west corner being about 0.3 m lower than the bags at the east corner.

As mentioned in Section 4.1.2, the bags had to be installed in two phases because the excavator reach was only 10.7 m. The the three lower rows were installed from 25 to 30 August 2006 and the upper row on 30 August 2006.

A drilled crew was able to install one bag every 10 minute.

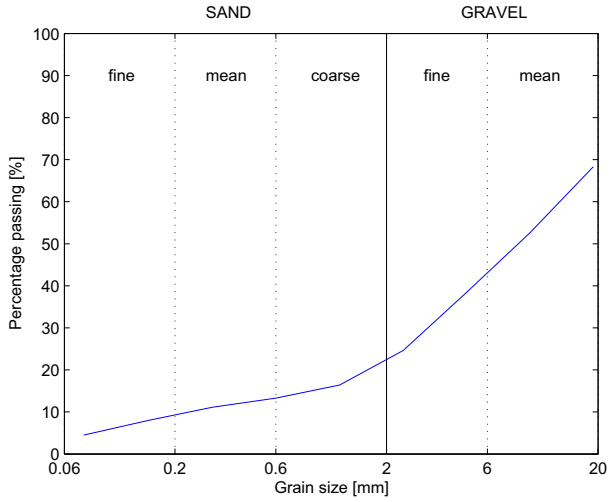

Figure C.6: Grain distribution of the masses used to fill the bags at Barryneset

C.4 Lessons learnt

The construction method used at Barryneset was better than the one used in Longyearbyen but there is still room for improvement.

The masses were dumped from approximately 5 m above the ground. Therefore, the first load probably pinched the bottom of the bags, especially if it contained rocks. I never saw any damage with the naked eye, though.

Pinching also occurred higher up on the bag during filling. The box containing the bag was, in fact, too narrow. When vertical, the side closest to the excavator was below the funnel opening and the fabric was pinched between the top of that side panel and falling masses. In addition, when filled to the top, the bag was overflowing, like the belly of a fat person over his belt, which made it difficult to sew it at the top. The workaround we used was to tilt the box a little so that the masses would hit the opposite side instead. Since that side was longer, and its top above the bottom of the funnel, the masses were hitting

Figure C.7: Elevated funnel used to fill the bags at Barryneset

Figure C.8: View of the breakwater after installation of the geosynthetic bags

with a low angle. Still, it is likely that some invisible damage occured in that area of the bag. The bag area in question is about 1 m below the top and was facing the ground, on installed bags.

Assumedly, the bags are all the more stable as they are full. In addition the fabric tension is higher the more the bag is filled. Higher tension is likely to improve the resistance of the fabric to external loads. It was difficult to optimise the fill ratio because the excavator operator could not see the inside of the bag and, even if he could, it requires good skills to fine-tune the amount of dumped masses. Overfilling should be avoided because the only way to remove the masses is by hand. Besides, after overfilling, the fabric at the of the bag is filled with fine masses, which both makes the sewing more difficult and damages

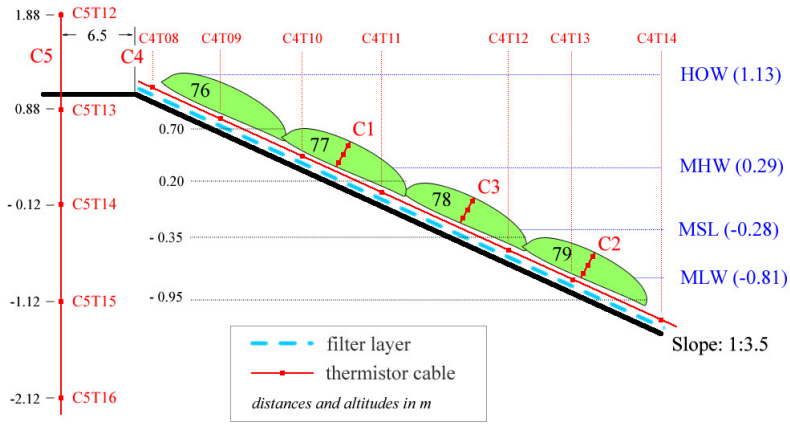

Figure C.9: Profile of the breakwater slope covered with bags along the 19th bag column – bag #80 not drawn

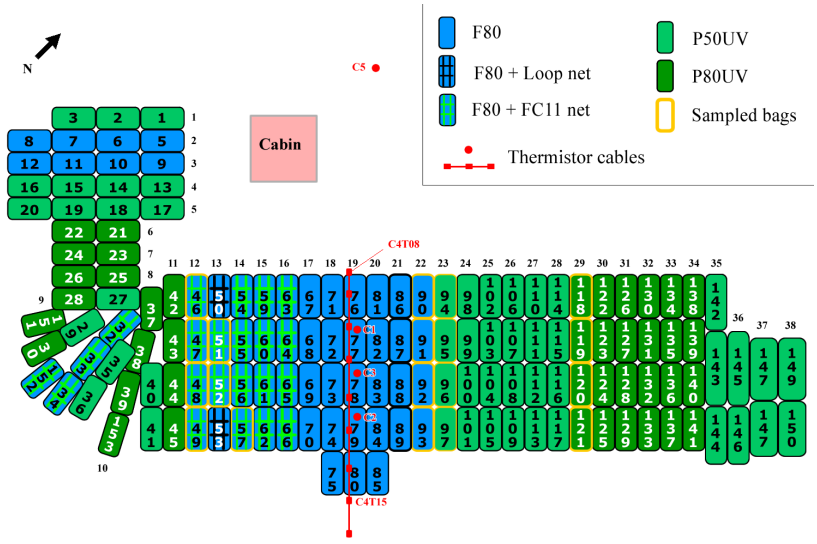

Figure C.10: Map of the bags after construction (September 2006)

the sewing machine.

The method for closing the bag may be improved. The drawbacks with using a sewing machine is that it requires power on-site and makes it difficult to work when it is raining or when there is dust in the air, which happens when it is blowing more than a gentle

Figure C.11: Transferring a bag from the box to the bucket

Figure C.12: Installation of a bag

breeze. I tested out an alternative method based on the roll-down system found on dry, outdoor bags. In place of the buckle I used a rope. Unless a stiff strip is fixed to the top of the bag, it will open too easily. The other problem is that the fabric we used was so thick that it takes almost 1 m of bag length to roll three times. A possible solution would be to sew a thinner fabric with an integrated strip on top, but that may be an expensive solution.

Appendix D

Paper 1: Measurements of stresses in the coastal ice on both sides of a tidal crack

I presented this paper at the 19th IAHR International Symposium on Ice in Vancouver in 2008.

The contents of the paper is presented in Sections 4.2.12, 5.12 and 6.9.

After writing the paper I came to prefer the term *free-floating ice* over *level ice*. *level-ice* is normally used to describe non-ridged ice. Therefore, it does not relate to the location of the ice—as in level ice vs. coastal ice—, rather to its structure.

I also came to prefer the term *hinge zone* over *active zone* (Section 2.2.5).

19th IAHR International Symposium on Ice
"Using New Technology to Understand Water-Ice Interaction"
Vancouver, British Columbia, Canada, July 6 to 11, 2008

Measurements of stresses in the coastal ice on both sides of a tidal crack

Fabrice Caline and Sébastien Barrault
University Centre in Svalbard, Longyearbyen, Norway
Norwegian University of Science and Technology, Trondheim, Norway
fabrice.caline@unis.no, sebastien.barrault@unis.no

Six stress sensors were frozen-in in two rosettes nearby a breakwater at 15 cm depth on each side of a tidal crack from 6 to 11 May 2007 in Van Mijenfjorden, Svalbard, Norway. An additional rosette was installed some distance from the shore in the level ice. The tidal movement of the ice was recorded with differential GPS equipment a week later. The tide is being recorded continuously in the area. Weekly visual observations of the sea ice were done as well.
This paper gives an order of magnitude of the stresses in the active zone and how they are affected by the tide.
The principal stresses next to the tidal crack during one cycle are presented. They are strongly influenced by the tide and are highest, around 150 kPa, at low tide and in the direction parallel to the crack. It is unknown whether these variations are local to the crack or take place in the whole active zone.

1. Introduction

The main coalmine in Svalbard is situated in Svea, by the inner bay of Van Mijenfjorden called Sveabukta. A coal deposit has been found under Mount Ispallen, on the opposite side of the bay. The mining company SNSG is considering building an access road across the fjord. In this context the University Centre in Svalbard (UNIS) has been looking into methods for protecting this causeway against seawater erosion. The study is relevant for a wide range of coastal structures built in shallow Arctic waters like breakwaters and quays. Due to the presence of seasonal sea ice the main challenge is to build an erosion protection system that sustains ice loads.

Few measurements of sea ice stresses close to the shore have been made. Apart from being the first step for evaluating loads on coastal structures, the study of stresses in the coastal ice is necessary for defining the boundary conditions of thermal and/or mechanical stresses in constrained first-year landfast sea ice. Investigations were done in connection with the construction of a coal loading pier in Svea (Instanes, 1979). Moslet (2001) measured in situ stresses in order to estimate sea-ice loads on this structure. Frederking et al. (1986) and Sayed et al. (1988) measured stresses in the area of Adams Island (Canada). Nikitin et al. (1992) studied the behaviour of the ice in the active zone (see definition in part 2) at a location in the Okhotsk Sea. Stander et al. (1988) also studied the coastal ice while Frederking and Nakawo (1984) studied the sea ice close to the piles of the Nanisivik wharf.

Researchers at UNIS have been investigating level ice stresses in Sveabukta for several years and found thermal expansion to have the most significant effect (Teigen et al., 2005, Barrault and Høyland, 2007). In addition, during the winter of 2007 coastal stresses were measured in one location. During the same period weekly observations of the coastal ice were done and its movement was recorded throughout one tidal cycle with differential GPS equipment. Sea level data were obtained from a tide recorder situated 100 m from land.

2. Proposed terminology

The *ice foot* is determined as the ice frozen to the shore when gradual freezing of sea water from tide and wave spray occurs early in the season. It is in effect a block of ice that is fixed to the ground and does not move with the tide (WMO, 1970). At a certain distance from shore the ice, which is unaffected by the shore, is called *level (floating) ice*. In between is a transition zone which Croasdale (1980) calls *active zone*. The active zone is composed of *coastal ice* which forms simultaneously with the sea ice and is subjected to tidal forces significant enough to create tidal cracks.

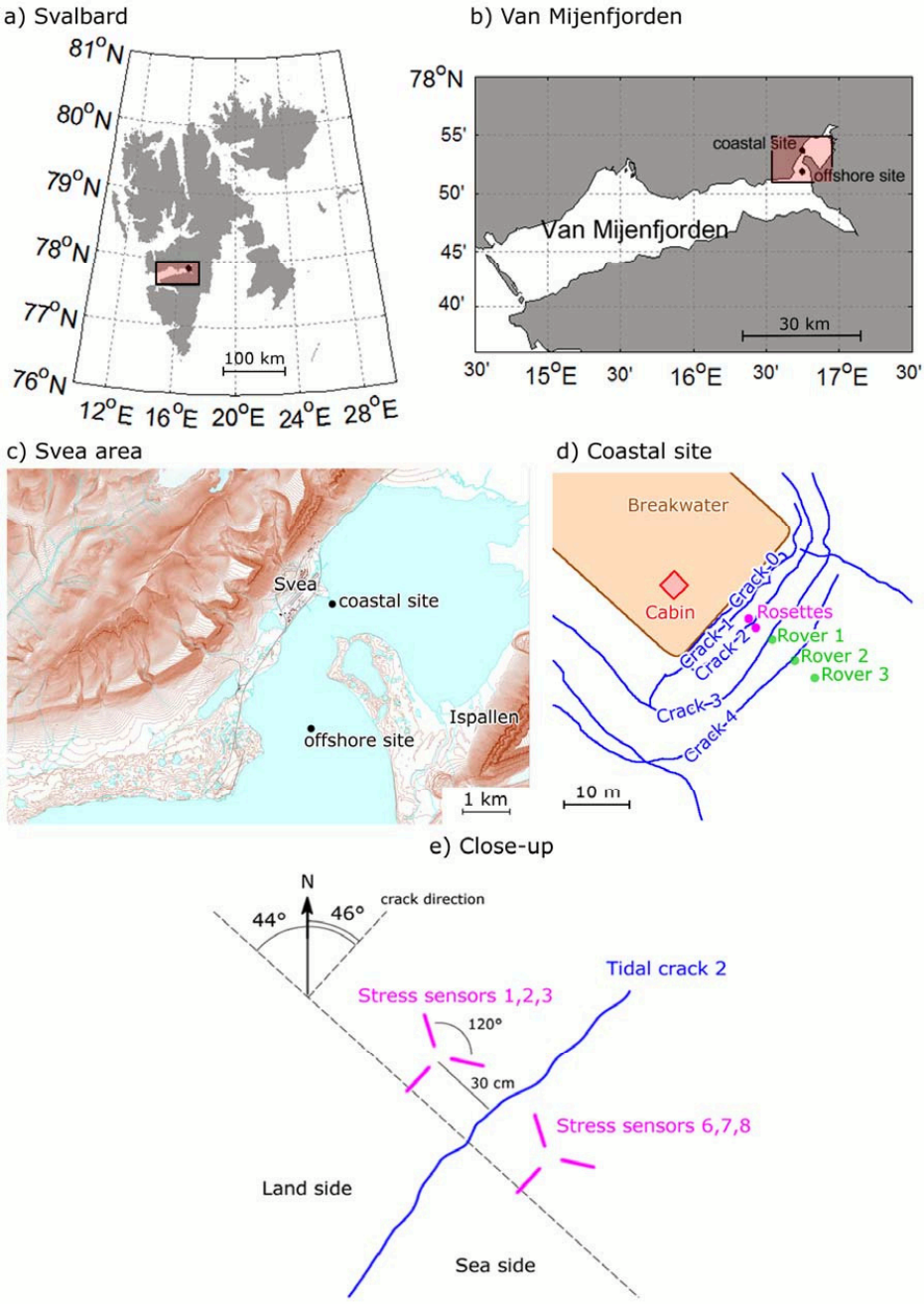

Figure 1. Map of the measurement site and instrument set-up in the innermost basin of Van Mijenfjorden

3. Site and experimental method

A breakwater was built in Sveabukta, the innermost bay of Van Mijenfjorden (Svalbard, Norway) for research purposes. It is 50 m long, 25 m wide and rises 2 m above the mean sea level (MSL), which is taken as the reference level. The depth at the toe is 3.5 m and the slope is 1V:2.5H. During the winter several cracks form in the ice parallel to the breakwater and up to 25 m away. The stress sensors were placed on each side of crack #2 (Figure 1d and 1e) which is oriented 46° to the North and runs through the whole 1.6 m thick ice cover.

The instruments are Amplified Solid State Pressure Sensors 242PC100G and they were deployed from 6 to 12 May 2007. These sensors consist of a disc of 10.5 cm in diameter filled with hydraulic oil and a transducer head measuring the voltage difference. Compressive stresses are obtained with ± 0.1 kPa resolution. Tensile stresses are not measured. They were connected to a CR10X Campbell Scientific datalogger. The sensors were deployed as two rosettes on each side of the crack at a depth of 0.18 m. The centre of the rosettes was at 30 cm from the crack. In both rosettes, one sensor measured stresses perpendicular to the crack (Figure 1e) and the angle between each sensor was 120 degrees. Another rosette of three BP stress sensors was frozen-in in the offshore ice 2.6 km away from the breakwater, in the middle of Sveabukta from 16 February to 17 April (Figure 1). The site, the instrumentation set-up and the logging are described in (Barrault and Høyland 2007).

A Seabird SBE 26Plus tide and wave recorder is permanently placed at 2.5 m depth 100 m from the breakwater. The water level is recorded continuously and averaged every 20 minutes. The ice movement was surveyed with differential GPS equipment on 17 May. A base station was placed on land and three rovers were placed from 8 to 20 m from the shore (Figure 1d). The rover antennas were placed on 1 m-long poles stuck some 20 cm in the snow layer and the position was recorded with 2 cm accuracy every 30 seconds for 20 hours. In additional ice observations and profile measurements were made.

The air temperature of the Svea airport weather station situated at about 1 km west of the site is obtained from the open weather database of the Norwegian Meteorological Institute (http://eklima.met.no).

4. Results

As shown in Figure 2 stresses were identified as periodic events on both sides of the crack with higher pressure on the land side of the crack with a maximal value of 245 kPa compared with 139 kPa on the sea side. The stresses are strongly influenced by the tide and their tidal response is similar during the whole week. There are missing data for the sensor oriented at 46 degrees on the land side. The sensor in fact did not record data when stresses where lower than 24 kPa. During the 6 days of measurements the temperature increased almost linearly from -15 to 0°C. The wind was around 11 $m \cdot s^{-1}$ until 9 May then fell to 5 $m \cdot s^{-1}$. All the time it was blowing from the North-East, i.e. parallel to the tidal crack. The tidal range decreased from 1.26 m on 6 May to 0.56 m on 11 May.

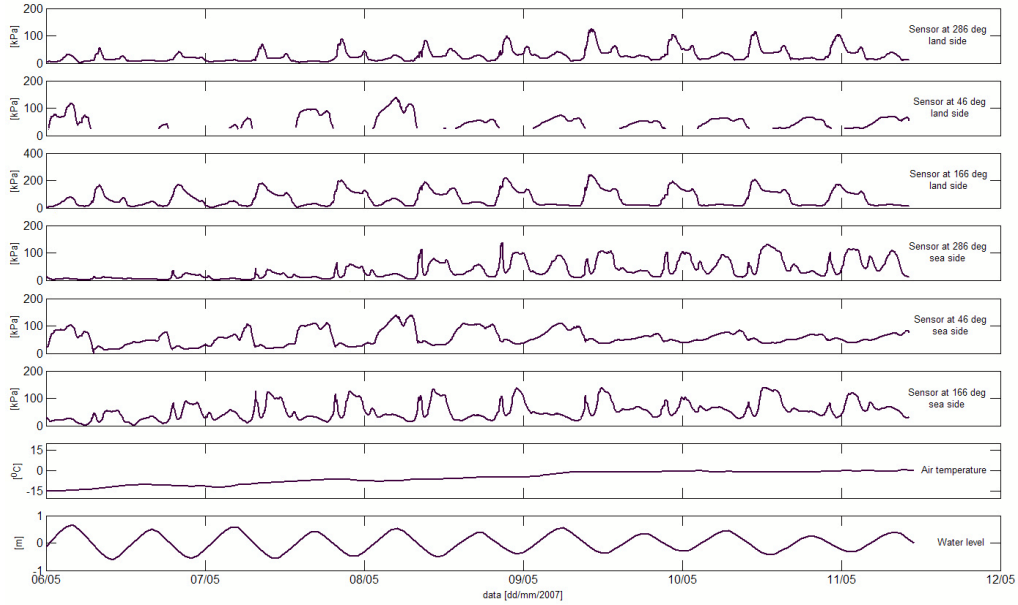

Figure 2. Stresses in the two rosettes on both sides of the crack, air temperature and sea level.

The plot of the calculated principal stresses during one tidal cycle on both sides of the tidal crack (Figure 3) shows they have the same pressure range and their curves have a relatively similar shape. The highest stresses, about 150 kPa, are reached at low tide last for about 3 hours and are oriented parallel with the crack. At high tide the major principal stress is about 70 kPa and oriented perpendicularly to the crack. Finally there is a short 100-150 kPa stress peak oriented parallel the crack when the tide is around mean sea level. This peak is more evident on the sea side.

The results of the DGPS measurements (Figure 4) show that the effect of the tide on the vertical movement of the ice decreases with the proximity to the shore: 20 m from shore, at the location of Rover 3, the ice is completely floating while 8 m from shore, at the location of Rover 1, the ice is moving vertically 60 % less than the sea. The difference in movement is highest at low tide where the sinusoidal curves of the vertical movement of Rover 1 and to a smaller extent Rover 2 are capped. The horizontal movement is perpendicular to the tidal cracks (Figure 4) and is highest at Rover 1 where it attained 22 cm during a tidal cycle.

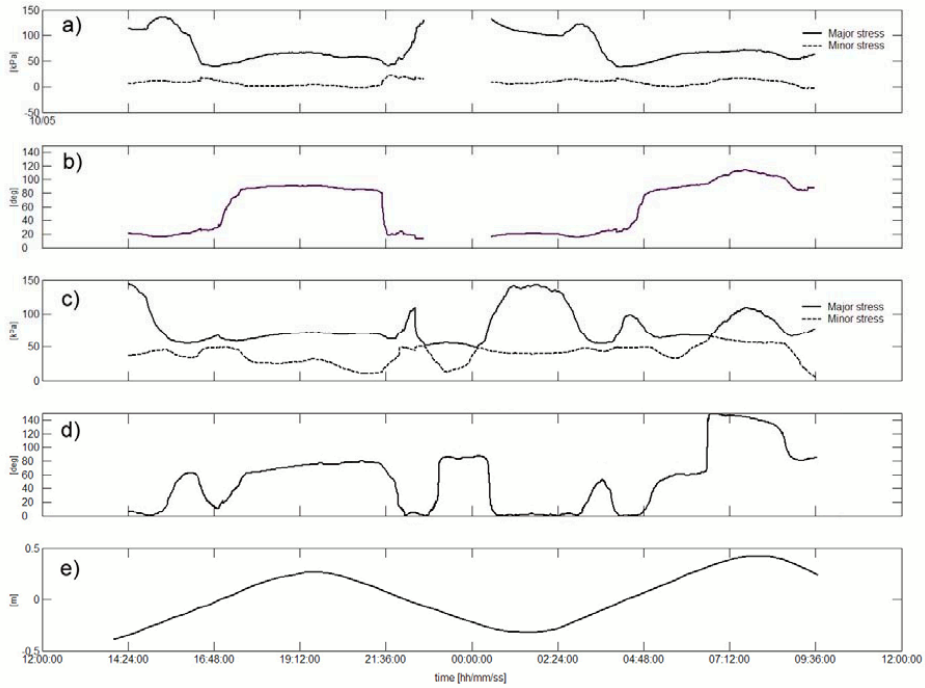

Figure 3. Principal stresses and direction on land side (a and b) and on sea side (c and d) from 10 to 11 May. The sea level is shown on e). The 0 degree reference direction is taken parallel to the tidal crack.

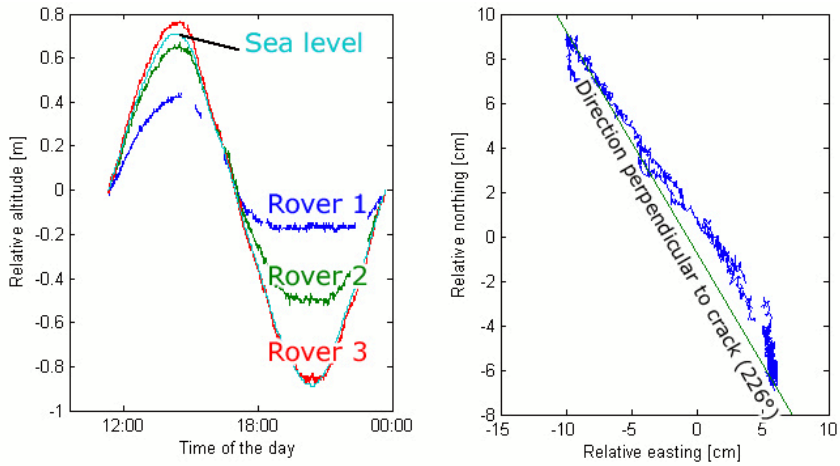

Figure 4. *Left*: DGPS measurement of the vertical movement of the ice top at three locations (Rover 1-3) and sea level during one tidal cycle — *Right*: horizontal movement of Rover 1 during that cycle. Measurements made on 17 May 2007.

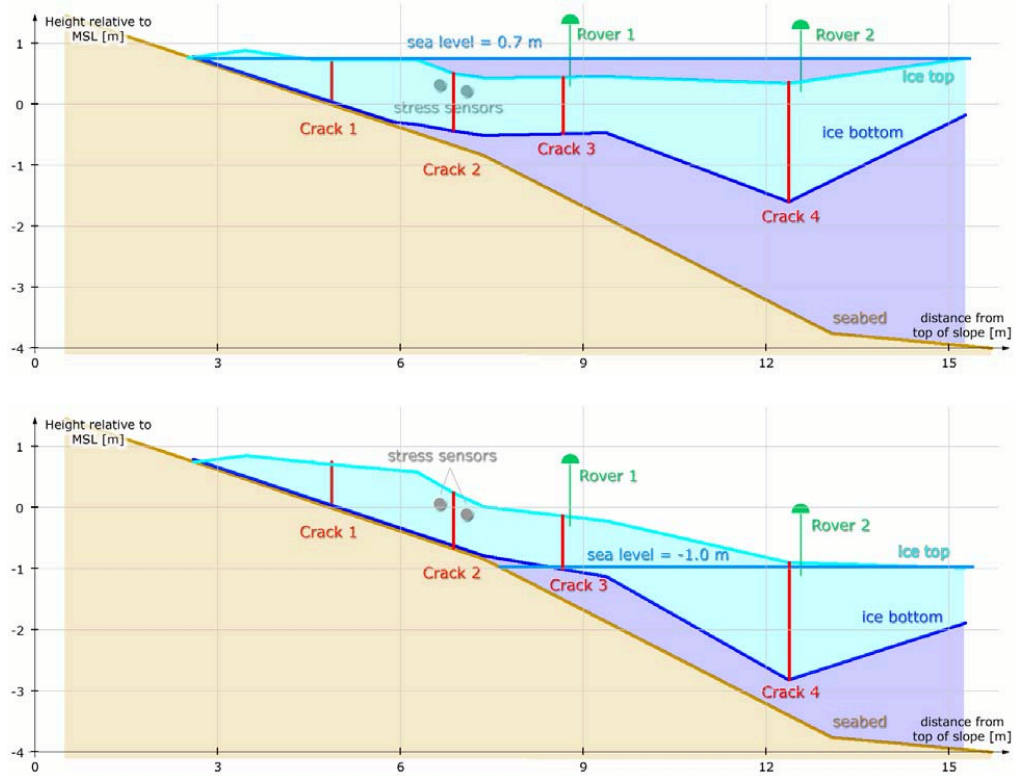

Figure 5. Cross-section of the active zone at high tide (above) and low tide (below)

5. Discussion

Stress data

Stresses in the area close to a coastal crack were measured but it is difficult to say if the stresses in the rest of the active zone vary in the same way. It is possible to give hypotheses of what could have caused the stress variations but testing them would require more measurements. It would be particularly instructive to record stresses at different depths in the 1.6 m-tick ice layer but the current instruments cannot be used because they do not resist to submersion.

Previous studies in Sveabukta (Teigen et al., 2005) showed that the wind does not affect ice stresses below 20 $m \cdot s^{-1}$. Early in the winter 2008, a survey conducted by UNIS researchers measured the tidal current close to the breakwater and found a maximum value of 30 $cm \cdot s^{-1}$. It is unlikely that such a small current would have a major effect on the stresses in the ice cover.

When it comes to thermal effects, the 40 cm-thick snow cover isolated the level ice and no thermal stresses were recorded during the first part of the season. On the coastal ice however the ice was in direct contact with the air through the crack openings. Figure 5 shows that the sea water filled the cracks at every tidal cycle and it is reasonable to suppose that the induced temperature variations would cause thermal stresses. It is expected that the grounding of the ice

(Figure 5) has an effect on the stress distribution in the ice but under a plane strain hypothesis the induced stress variations are expected to be perpendicular rather than parallel to the crack. The plane strain hypothesis might however not be valid since the breakwater is only 25 m wide and there is a rubble accumulation at its western corner which could cause bending in the direction normal to the plane of the cross-section in Figure 5 and hence stress variations in the direction parallel to the crack.

The 20 kPa peak of the stresses perpendicular to the cracks is almost certainly due to the opening and closing of the crack depending on the tide.

The observed stress variations are within the range of values found in the literature. Frederking et al. (1986) measured 70 kPa off the Coast of Adams Island where the tidal range is up to 2 m while Sayed (1988) measured 350 kPa there. Moslet (2001) had 25 kPa in Svea and Nikitin et al. (1992) 500 kPa in the active zone of the Okhotsk Sea with a tidal range of 1.25 m. As in this study they all found that the highest stresses were in antiphase with the tide. However the ice around the breakwater was not translating away from the shore as Frederking and Nakawo (1984) observed around the Nanisivik wharf piles where they measured horizontal displacements of several metres throughout the season. Stander et al. (1988) also recorded horizontal displacements, of several centimetres per day.

DGPS data

The plots of the vertical movement of the ice (Figure 4) show that the coastal ice is not in hydrostatic equilibrium with the sea water. The non-equilibrium is a consequence of friction forces along the cracks. The boundaries are on one side the ice foot which is fixed to the ground and on the other side the level ice which is completely floating. The horizontal movement data are exaggerated because the rover antennas were almost 1 m above the ice top and the vertical movement data reveal that the sections of ice between two cracks has a combined movement of translation and of rotation throughout the tidal cycle. The rotation takes place around a horizontal axis directed like the cracks. A numerical evaluation shows that the correct value of the horizontal movement of the ice at the Rover 1 location is 10 cm rather than 22 cm.

6. Conclusion

Stresses were measured close to a tidal crack in the active zone and showed a strong tidal dependency. The highest stresses were measured in the direction parallel to the tidal crack. The limited amount of stress data makes it difficult to propose more than hypotheses on the mechanical processes taking place in the active zone during a tidal cycle. Close to the tidal cracks the thermal variations caused by the cyclic sea water flooding might create stresses. A simple way to test this hypothesis would be to place a vertical thermistor cable in the ice close to a crack and another one at some distance. The tidal current is expected to have an insignificant effect. In order to measure stresses in more locations and depths in the ices, it is necessary to use a different type of sensors that resist to flooding. A numerical analysis would help optimise the number and location of these sensors.

Acknowledgements
The authors are grateful to Mauri Määttänen from Helsinki Technical University in Finland for the use of his sensors. This survey was supported by the mining company in Svalbard, SNSG and by TOTAL E&P NORGE AS.

References

Barrault, S., Høyland, K.V., 2007. Mechanisms and measurements of generation of stresses in first-year landfast sea ice. 19th International Conference on Port and Ocean Engineering under Arctic Condition (POAC), Dalian, China, 27-30 June, pp 685-694

Croasdale, K.R., 1980. Ice Forces on Fixed, Rigid Structures. Working Group on Ice Forces on Structures, Carstens, T., pp. 34-106.

Frederking, R.M.W., Nakawo, M., 1984. Ice action on Nanisivik wharf, winter 1979-1980. Canadian Journal of Civil Engineering, Vol. 11, No. 4, pp. 996-1003

Frederking, R.M.W., Wessels, E., Maxwell, J.B., Prinsenberg, S., Sayed, M., 1986. Ice pressures and behaviour at Adams Island, winter 1983/1984. Canadian Journal of Civil Engineering, Vol. 13, pp 140-149

Instanes, B., 1979. Coal loading pier in Svea, Svalbard. Proceedings, 5th International Conference on Port and Ocean Engineering under Arctic Conditions (POAC), Trondheim, Norway, Vol. 3, pp. 217-227

Moslet, P.O., 2001. Estimation of loads exerted by sea ice on the quay at Kapp Amsterdam, the Van Mijen fjord. Master thesis, Department of Structural Engineering, NTNU, 93 p.

Nikitin, V.A., Shushlebin, A.I., Sheikin, I.B., 1992. In-Situ Stress Measurements in Fast Ice and Possible Tidal Loads on Structures. Proceedings of the Second International Offshore and Polar Engineering Conference, San Francisco, USA, 14-19 June, Vol. 2, pp. 696-702

Sayed, M., Frederking, R.M.W., Wessels, E., 1988. Field measurements of stresses and deformations in a first-year ice cover adjacent to a wide structure. Canadian Journal of Geotechnics, Vol. 25, No. 4, pp. 726-734

Stander, E., Frederking, R.M.W., Nadreau, J.-P., 1988. The Effects of Tidal Jacking on Ice Displacement and Strain in the Nearshore Environment. Proceedings of the 9th International Symposium on Ice (IAHR), Sapporo, Japan, 23-27 August, Vol. 1, pp. 526-536

Teigen S. H, Høyland K. V., Moslet, P. O, 2005. Thermal stresses in first-year sea ice. Proc. Of Port and Ocean Engineering under Arctic conditions (POAC), Potsdam, USA, pp. 893-906.

WMO, 1970. WMO sea ice nomenclature, (suplement No. 5, 1989). Technical Report MO No. 259.TP.145, World Meteorological Organizartion, Geneva, Switzerland.

Appendix E

Paper 2: Comparison of physical and mechanical properties of coastal ice and level ice

Sébastien Barrault presented this paper at the 19th IAHR International Symposium on Ice in Vancouver in 2008.

The contents of the paper is presented in Sections 4.2.11, 5.11 and 6.8.

The choice of point names was unfortunate since P1, P2, P3 and P4 may be confused with ice types (Michel and Ramseier, 1971). Therefore, I replaced them with Pt1, Pt2, Pt3 and Pt4 in Sections 4.2.11, 5.11 and 6.8.

As in Paper 1, I have come to prefer the term *free-floating ice* over *level ice*. To my mind, *level* only means that there are no ridges. In that sense, the coastal ice at Barryneset was also level. *Free-floating*, on the other hand, means that the shore is not restricting its movement, as opposed to the coastal ice.

19th IAHR International Symposium on Ice
"Using New Technology to Understand Water-Ice Interaction"
Vancouver, British Columbia, Canada, July 6 to 11, 2008

Comparison of physical and mechanical properties of coastal ice and level ice

Magnus Gabrielsen[1,2,3], Sébastien Barrault[1,2], Fabrice Caline[1,2], Knut V. Høyland[2,1]
[1]*University Centre in Svalbard, Longyearbyen, Norway*
[2]*Norwegian University of Science and Technology, Trondheim, Norway*
[3]*now working at Dr.techn.Olav Olsen AS, Lysaker, Norway*
mga@olavolsen.no, sebastien.barrault@unis.no, fabrice.caline@unis.no, knut.hoyland@ntnu.no

Physical and mechanical properties of coastal and level ice were compared. The study is based on the results from horizontal samples taken in March 2007 in Van Mijenfjorden, Svalbard, Norway. The samples were tested in compression and relaxation in a cold laboratory at the University Centre in Svalbard and thin sections were prepared. The results show that the physical properties of the ice are essentially monotone functions of the distance from the shore and that the differences between the ice closest to land and the level ice are important. The porosity varies with a factor 6 while the brine fraction varies with a factor 17. The Young modulus is correlated with the porosity while the residual stress is correlated with the brine content although both correlations are weak. The microscopic analysis shows that the coastal ice is granular while level ice is S2 in the surface and S3 lower down. The size of the grains in the level ice is comparable with the size of the samples, therefore it is important to check their direction when sampling.

1. Introduction

There is a growing interest for constructing coastal structures in ice-infested Arctic waters. Several oil and gas projects are under planning. They will require infrastructure on land. At the same time the reduction of the Arctic ice cover prolongs the shipping season and puts harbour investments on the agenda. Arctic structures must resist ice loads from thermal expansion and tide (Smirnov and Sukhorov, 1994; Nikitin et al., 1992). When the sea ice cover is continuous, the time scale of ice movements is such that the viscosity has an important influence on the maximum loads.

The coastal ice forms in a different way than the level ice and is in addition subjected to important tidal stress variations (Caline and Barrault, 2008). We may therefore expect the physical and mechanical properties of the ice at both locations to differ.

Ice samples were taken at several locations and depths in order to measure physical properties and perform mechanical tests. The main interest was to perform relaxation tests in order to compare the viscous properties of the ice. It was the first time a study based on relaxation tests was made at UNIS, the University Centre in Svalbard.

2. Proposed terminology

The *ice foot* is determined as the ice frozen to the shore when gradual freezing of sea water from tide and wave spray occurs early in the season. It is in effect a block of ice that is fixed to the ground and does not move with the tide (WMO, 1970). At a certain distance from shore the ice, which is unaffected by the shore, is called *level (floating) ice*. In between is a transition zone which Croasdale (1980) calls *active zone*. The active zone is composed of *coastal ice* which forms simultaneously with the sea ice and is subjected to tidal forces significant enough to create tidal cracks (Caline and Barrault, 2008).

3. Site and measurement

The coastal ice and the level ice were surveyed during the winter 2006-07 in the innermost bay of Van Mijenfjorden, Svalbard, Norway (Figure 1). On 14 and 21 March 2007, 6 horizontal ice cores were sampled in level ice at three different depths (H1=10 cm from the ice surface, H2=30 cm, H3=50 cm). On 19 April, 23 horizontal ice cores were sampled in four locations in the coastal ice nearby a breakwater along a profile aligned normal to the shore at 316° from North (Figure 1 d) and e)). All samples had a diameter of 70 mm. They were put in sealed plastic bags and transported to a -20°C storage room at UNIS. The time from sampling to storing was about 3-5 hours and the temperature was kept below the freezing point all the time during transport. The samples were stored from up to three weeks before testing. All samples were tested at -10°C.

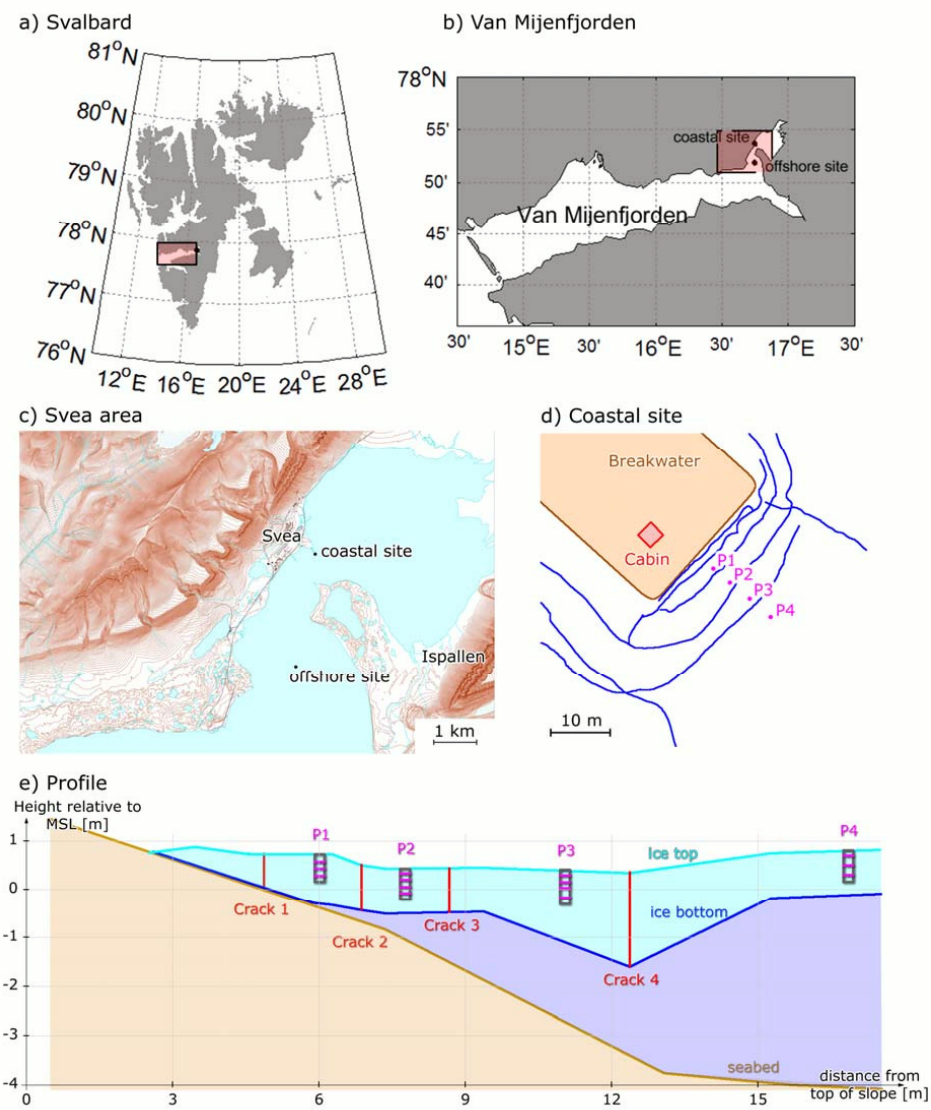

Figure 1. Map of the measurement site and profile in the innermost basin of Van Mijenfjorden

NTNU developed in 1996 a stationary uniaxial compression device, named Knekkis and installed at UNIS. The device can perform maximal strength, creep and relaxation tests. A piston moves upwards and a load cell placed in the upper part of the device records pressure. Data are recorded at a frequency of 0.5 Hz. The relaxation tests were performed by applying a start stress of 500 kPa and keeping the piston immobile for one hour. The compression tests were performed at a constant strain rate of 10^{-3} s^{-1}. For the level ice they were performed on the samples that had

undergone relaxation tests. It was checked that the relaxation tests do not seem to affect the strength or the Young modulus of the samples. For the level ice the data is the average of two samples while for the coastal ice only one test was performed. Young's modulus was taken as the steepest slope of the stress-strain plot. After the tests the samples were melted to measure salinity. Porosity as a function of salinity, density and temperature were calculated from equations developed by Cox and Weeks (1982). Horizontal and vertical thin sections of all level ice samples and four coastal ice samples were made to analyze the ice texture.

4. Results

Formation of the coastal ice

From October to mid-December pancake ice accumulated onshore and consolidated into the ice foot. Below mean sea level the ground remained free of ice. In the end of December the sea was covered with ice which was connected to the shore. In the shore area the ice first moved up and down with the tide but by January it had grown thick enough that it stuck to the ice foot and to the sea bottom so much that it did not move with the same amplitude as the tide. On high tide it resulted in the flooding of the near-shore area and hence the formation of superimposed ice (Figure 2). The structure of the superimposed ice is different from that of the level ice as seen when comparing thin sections in Figures 3-6. The superimposed ice contains much smaller crystals and its porosity is one order of magnitude bigger. It is described as granular and contains more air bubbles. The ice with the lowest density looked more like a mixture of snow and ice. The ice grows faster the closer to the shore. The reasons are a greater heat transfer and the formation of superimposed ice. In the end of January, the ice thickness was 0.80 m at P1 and 0.50 m at P4. In the end of February it was 1.60 m and 0.60 m respectively. In the end of April it was 0.80 m at P4 and it reached 0.95 m in the middle of May.

Figure 2. Pond of surface water close to shore that refreezes on top the coastal ice

Formation of the level ice

Sea ice extended to the offshore site in early January. During a first visit on 14 February the ice was 0.52 m thick. 14 March it reached 0.66 m and a month later ice was 0.58 m thick. The thin sections from level ice H2 and H3 indicate a predominant alignment of the c-axis at an approximate angle of 45˚ (Figure 6). For the H1 cores the orientation of the c-axis is more random. The vertical thin sections from all three levels clearly show an elongation in the vertical

direction. According to these observations the ice from level H1 is characterised as S2-ice, while ice from level H2 and H3 is characterised as S3-ice.

Figure 3. Vertical thin section of P1-H1

Figure 4. Horizontal thin section of P4-H3

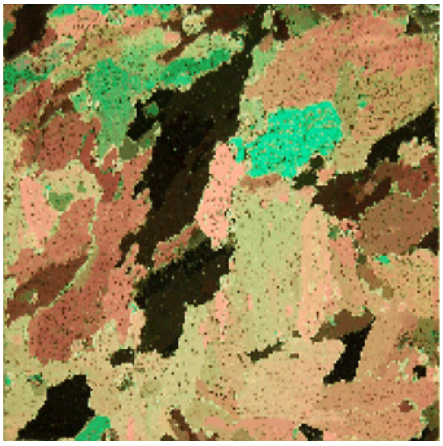

Figure 5. Horizontal thin section of P5-H1

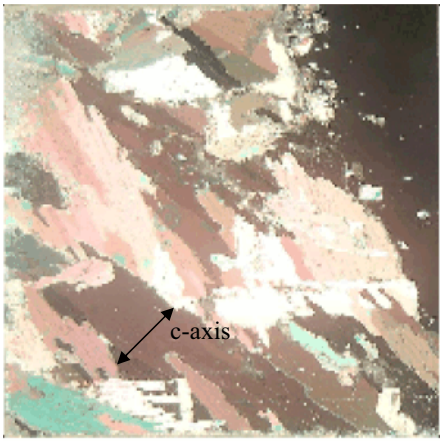

Figure 6. Horizontal thin section of P5-H3

N.B: The diameter of the circular sections and the width of the square sections is 70 mm (Figures 3-6).

Physical and mechanical properties

Table 1 summarises physical and mechanical results obtained in level and coastal ice. All data vary monotonously with the distance from shore. The porosity of coastal ice is decreasing from P1 to P4 and level ice (P5) is 6 times less porous than P1. Air fraction is decreasing as well. In P1 the air fraction is maximal with 99.4 % of the total porosity whereas it is 37 % in the level ice. The brine fraction is highest in the level ice. Ice has the lowest density in P1.

The Young modulus is somewhat higher in the level ice (up to 50% difference) while the residual stress is up to three times higher in the coastal ice than in the level ice.

The residual stress is the only analysed result kept from the relaxation tests. It was chosen not to study the relaxation function partly because it seems that it takes up to 30 minutes for its slope to stabilise after the initial loading and partly because ice is a non-linear visco-elasto-plastic material so no unique relaxation function exists.

Table 1. Comparison of physical and mechanical properties of the floating ice and the coastal ice

		Coastal ice				Level ice
Tested at -10 °C	**Depth**	**P1**	**P2**	**P3**	**P4**	**P5**
Residual stress [kPa]	H1 (10 cm)	170	162	156	156	103
(after one hour relaxation,	H2 (30 cm)	128	150	149	127	76
initial stress 500 kPa)	H3 (50 cm)	132	151	-	104	57
Strength [MPa]	H1	2.7	3.7	2.6	5.1	4.3
(strain rate = 10^{-3} s^{-1})	H2	3.2	3.0	4.2	4.3	4.1
	H3	3.0	4.3	5.2	6.0	3.3
Young's modulus [GPa].	H1	1.1	1.2	1.1	1.2	1.5
	H2	1.1	1.0	1.2	1.2	1.5
	H3	1.0	1.3	1.4	1.6	1.5
Salinity [psu]	H1	0.3	1.0	0.9	2.5	4.6
	H2	0.4	0.9	2.6	6.1	4.6
	H3	0.3	0.7	3.3	4.4	3.7
Density [kg/m^3]	H1	724	789	806	842	916
	H2	720	731	818	861	915
	H3	703	777	-	894	900
Brine fraction [%]	H1	0.13	0.47	0.44	1.26	2.53
	H2	0.17	0.40	1.28	3.15	2.53
	H3	0.13	0.33	-	2.36	2.00
Air fraction [%]	H1	21.2	14.2	12.3	8.6	0.8
	H2	21.6	20.5	11.2	7.0	0.9
	H3	23.5	15.5	-	3.2	2.5
Porosity [%]	H1	21.3	14.7	12.8	9.9	3.4
	H2	21.8	20.9	12.5	10.1	3.5
	H3	23.6	15.8	-	5.5	4.5

As shown in Table 2 ductile failures were observed in all samples except P3-H1 and P5-H3.

Table 2. Failure type of the different samples

	P1	**P2**	**P3**	**P4**	**P5 (level ice)**
H1	Ductile	Ductile	Brittle	Ductile	Ductile
H2	Ductile	Ductile	Ductile	Ductile	Ductile
H3	Ductile	Ductile	Ductile	Ductile	Brittle

5. Discussion

Ice texture analysis

The size and orientation of the crystals have an influence on the results from the mechanical tests. For samples P5-H2 and P5-H3, the crystal size is comparable with the sample size, and the inclination of 45° between loading direction and basal plane direction causes the maximum shear stresses to act along one single basal plane. When the strength of the basal plane is reached through a stress build up, the sample fails in a brittle way.

For samples where crystals have a predominant direction, Peyton (1966) showed that the strength will be lowest when this direction is 45° to the direction of compression while it reaches local maxima at 0° or 90°. It can be seen in Lainey and Tinawi (1984) (after Peyton, 1966 and Wang, 1979) that ice loaded in compression perpendicular or parallel to the c-axis is 2 to 3 times stronger than ice loaded at 45° to it. Since the direction is 45° in the samples analysed in this paper, higher strengths would have been obtained if the samples had been taken in any other directions.

In the coastal ice the size of the crystals compared to the diameter of the samples varies from very small (factor 100) to small (factor 10) as seen in Figures 3 and 4. The unequal grain size originates from the ice formation. Core P1-H1 represents ice formed by snow that gets soaked in sea water at high tide. At low tide the brine is drained, and this causes the ice to be low-saline and very porous. Core P4-H3 represents ice formed directly from sea water.

Residual stresses

In Figure 7 the residual stresses are plotted against the brine content. The two lowest residual stresses (stars) correspond to P5-H2 and P5-H3. As discussed above with strength, the residual stress values would have been expected higher if the samples had been taken with the predominant crystal orientation at 0° or 90° to the direction of compression. It was observed that the residual stress tends to decrease with the brine content, especially when P5-H2 and P5-H3 are not considered. This trend is in accordance with Cole (1997).

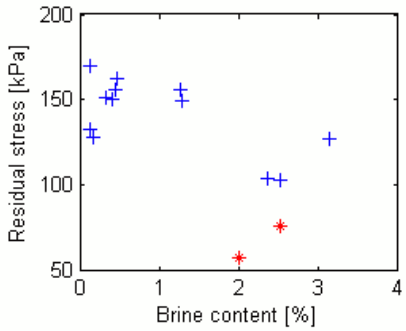

Figure 7. Residual stress vs. brine content

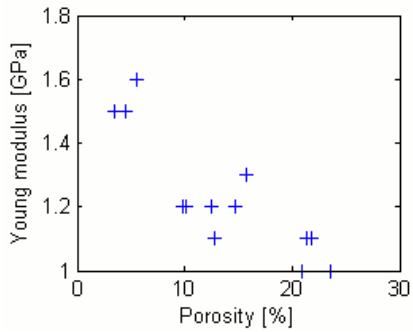

Figure 8. Young modulus vs. porosity

Young modulus

As seen in Figure 8, Young's modulus is decreasing with porosity in accordance with Moslet (2007) and Timco and Frederking (1990). The physical mechanism for elastic deformation is in fact strain of the atomic structure, which is denser the smaller the porosity.

Strength

In Figure 9 the data is split in 3 groups: level ice (star), P3-H1 (circle) and the rest of the coastal ice (cross). The reason why P3-H1 was plotted differently is that it is the only coastal ice sample which failed in a brittle way. It was taken as an indication that its structure is different from that of the other coastal ice samples where, based on the four thin sections, the crystal orientation is random. One good reason why the structure of the ice in P3-H1 would be different is that P3 is located in a place that remained flooded for a couple of weeks in the middle of March and the water froze completely undisturbed. The strengths of the level ice samples are a bit lower than the porosity alone would indicate but the large grains in the level ice reduce its strength (Lee and Schulson, 1986).

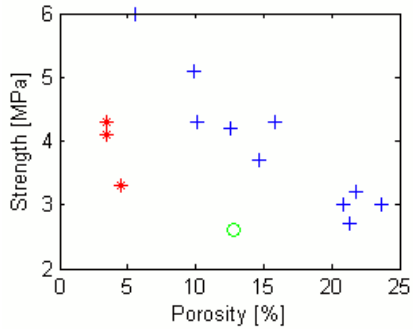

Figure 9. Strength vs. porosity

Mechanical response

Tidal fluctuations have a time constant of 6 hours therefore the ice behaves viscously and the maximum stresses are lower than for a pure elastic material.

Data quality
The margin of error is unknown because of the small number of samples (one per location in the coastal ice). However the strong geographical data dependence is coherent with on-site observations of ice formation and structure. In addition other samples were taken to perform creep and then strength tests and the results show a satisfactory consistency. The storage conditions varied to some extent and the effect of storage time is not well known. Finally note that the coastal ice cores were taken in the top 50 cm while the coastal ice is up to 1.6 m thick (P1). Therefore the results are not fully representative of the coastal ice.

6. Conclusion
Ice was sampled from the level ice and the coastal ice in Van Mijenfjorden on the West Coast of Svalbard, Norway and tests were done to investigate its physical and mechanical properties. The strength, the elastic and the viscous properties were examined by uniaxial compression tests. The strength tests were performed with a nominal strain rate of 10^{-3} s^{-1}. The relaxation tests were done by quickly applying a load of 500 kPa and then allowing the samples to relax. The elastic modulus was taken as the steepest slope of the stress-strain plot.

The level ice has higher density, salinity and brine fraction but lower air fraction and total porosity. It is also stiffer, but significantly more viscous than the coastal ice. The main results are as follows:

- Young's modulus is decreasing with the total porosity as one could expect from the well-known physical mechanism behind elastic deformation
- the strength is also decreasing with porosity but is in addition a function of grain size. The level ice is weaker than the coastal ice even though it is less porous because its grains are up to 100 times bigger.
- the residual stress depended on the brine volume however the orientation of the crystals in the level ice samples may exaggerate this trend in the presented data.

This means that the coastal ice is stronger than level ice when loaded slowly, as with tidal fluctuations, but weaker when loaded faster, as when the wind or a ship pushes the level ice towards the shore.

References

Caline, F. and Barrault, S., 2008. Transmission of level ice stresses to ice foot through a tidal crack. Proceedings of the 19th International Symposium on Ice (IAHR), Vancouver, Canada, 6-11 July.

Cole, D.M., 1997. Modeling the cyclic loading response of sea ice. Int. J. Solids Structures, vol. 35, Nos 31-32, pp. 4067-4075.

Cox, G.F.N. and Weeks, W.F., 1982. Equations for determining the gas and brine volumes in sea ice samples. CRREL Report 82-30.

Croasdale, K.R., 1980. Ice Forces on Fixed, Rigid Structures. Working Group on Ice Forces on Structures, Carstens, T., pp. 34-106.

Lainey, L. and Tinawi, R., 1984. The Mechanical Properties of Sea Ice – a Compilation of Available Data. Canadian Journal of Civil Engineering, 11, pp. 119-127.

Lee, R.W. and Shulson, E.M., 1986. The strength of ductile ice under tension. Journal of Offshore Mechanics and Arctic Engineering, May 1988 vol. 110, pp. 187-191.

Moslet, P.O., 2007. Field Testing of Uniaxial Compression Strength of Columnar Sea Ice. Cold Regions Science and Technology, vol. 48, pp. 1-14.

Nikitin, V.A., Shushlebin, A.I., Sheikin, I.B., 1992. In-Situ Stress Measurements in Fast Ice and Possible Tidal Loads on Structures. Proceedings of the Second International Offshore and Polar Engineering Conference, San Francisco, USA, 14-19 June, vol. 2, pp. 696-702.

Peyton, H.R., 1966. Sea Ice Strength. Technical Report Final Report of Naval Research Arctic Project, 1958-1965, UAG R-182102, University of Alaska, Fairbanks, 285p.

Smirnov, V.N. and Sukhorov, K.K., 1994. Quasi-static thermal stresses in the sea ice. IAHR Ice Symposium, Trondheim, Norway.

Timco, G.W. and Frederking, R.M.W., 1990. Compressive Strength of Sea Ice Sheets. Cold Regions Science and Technology, vol. 17, pp. 227-240.

Wang, Y., 1979. Crystallographic studies and strength tests of field ice in the Alaskan Beaufort Sea. Technical Report, Vol. 1 Exxon, Technical Seminar on Alaskan Beaufort Sea Gravel Island Design.

WMO, 1970. WMO sea ice nomenclature, (suplement No. 5, 1989). Technical Report MO No. 259.TP.145, World Meteorological Organizartion, Geneva, Switzerland.

Appendix F

Paper 3: Temperatures in Coastal Permafrost in the Svea Area, Svalbard

Lene Kristensen presented this paper at the 9th International Conference on Permafrost in 2008. I was in charge of the drilling campaign. Lene and I were also responsible for emptying the dataloggers every second month.

Temperatures in Coastal Permafrost in the Svea Area, Svalbard

Lene Kristensen
The University Centre in Svalbard, UNIS, Longyearbyen, Norway
Hanne H. Christiansen
The University Centre in Svalbard, UNIS, Longyearbyen, Norway
Fabrice Caline
The University Centre in Svalbard, UNIS, Longyearbyen, Norway

Abstract

Temperature data from three boreholes located on an ice-cored moraine near sea level are analyzed. One of these boreholes was drilled 6 m from the shore and shows significantly higher temperatures than the holes about 150 m from the shore. Using meteorological data and measurements of water temperatures, we model the permafrost distribution into the fjord as well as the influence of the sea on permafrost temperatures near the shore. The model results suggest that permafrost, as defined solely on temperature, is present beneath Van Mijenfjorden.

Keywords: borehole temperatures; coastal; geothermal modeling; permafrost; subsea permafrost; Svalbard.

Introduction

Permafrost on Svalbard is classified as continuous. It is more than 500 m thick in the highlands and less than 100 m near the coasts (Humlum et al. 2003). While considerable knowledge of permafrost conditions in the mountains exists from the extensive coal mining, little has been published on the permafrost in the shore areas of Svalbard. Exceptions are Gregersen & Eidsmoen (1988) that compares deep borehole temperatures at the shore with inland boreholes in Longyearbyen and Svea, and Harada & Yoshikawa (1996) that uses DC resistivity soundings to estimate the permafrost thickness of marine terraces at the shore of Adventfjorden near Longyearbyen.

The aim of this paper is to describe the permafrost conditions in the ice-cored moraine, Crednermorenen,a peninsula in Van Mijenfjorden in central Spitsbergen (Fig. 1). Since April 2005 temperatures have been logged every two hrs in three boreholes on the moraine each with 16 thermistors down to eight m. One of the boreholes is located only six m from the shoreline. Permafrost conditions in the shore area are important since the permafrost here is "warm" and thin. When constructing in such areas, particular attention must therefore be given to the permafrost conditions. In most other parts of Svalbard, permafrost is thicker, colder and more stable.

Due to the few previous studies of near-shore permafrost on Svalbard, an attempt was made to model both the effect of the sea on the onshore permafrost as well as the possibility of subsea permafrost. We use a transient 2D finite element geothermal model (TEMP/W from Geoslope International, Calgary, Canada; Krahn 2004) that is forced with meteorological data and measured water temperatures as boundary conditions.

Field Site

Crednermorenen is a lateral moraine deposited by a surge of the tidewater glacier Paulabreen (Fig. 1) around 1300 A.D. (Hald et al. 2001). The moraine forms a peninsula (1x3 km),

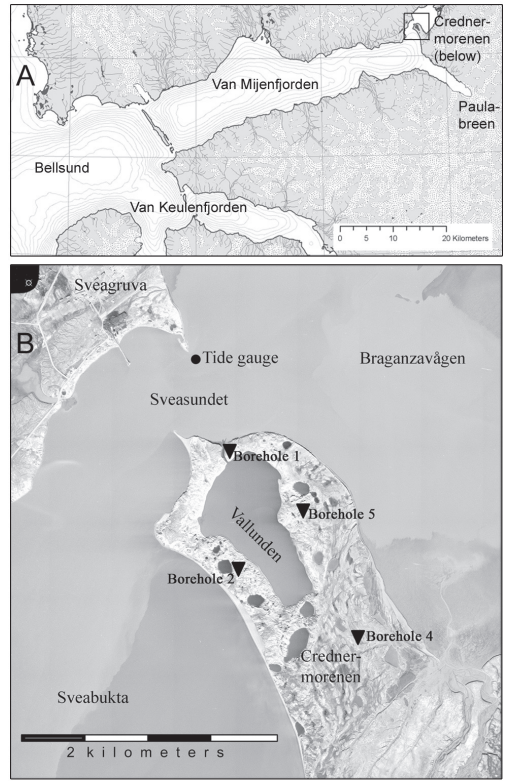

Figure 1. Field site. A) Van Mijenfjorden with Crednermorenen (in upper right corner). Map from: http://www.iopan.gda.pl. B) Crednermorenen with the location of the boreholes and the tide gauge. Air photo: Norsk Polarinstitutt, 1977.

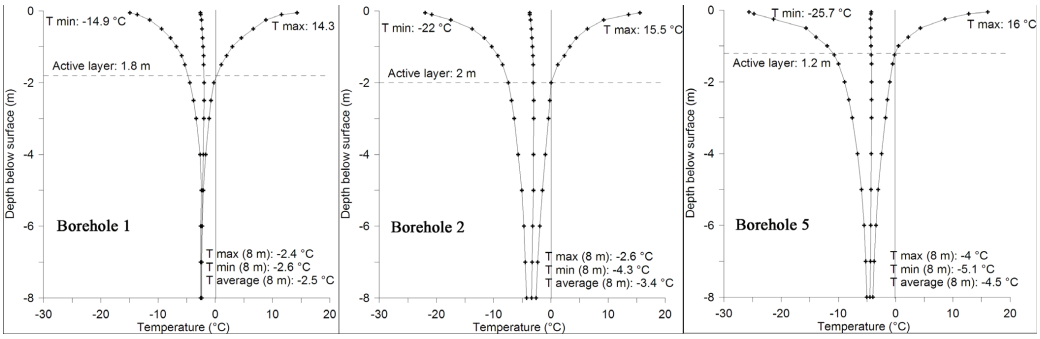

Figure 2. Maximum, minimum, and average temperatures in all depths from 10 September 2006 to 9 September 2007 for Boreholes 1, 2, and 5.

Table 1. Average annual temperature at the ground surface, at the top of the permafrost (TTOP).

	(Air)	Hole 1	Hole2	Hole 5
T surface (°C)	-4.6	-2.6	-3.7	-4.2
TTOP (°C)		-2.0	-3.1	-4.3

partly ice-cored and partly consisting of proglacially pushed marine clays (Kristensen et al., in press). It is surrounded by water on three sides and in its northern part lies a 1 km long lagoon, —Vallunden—that, is connected to the sea by a 15m-wide channel near Borehole 1. The water in Vallunden is salty as the tide flows in and out through the channel.

The oceanography in Van Mijenfjorden is strongly affected by an island at the fjord mouth, Akseløya (Fig. 1A), which nearly blocks the water exchange between the fjord and the warmer Atlantic water outside (Nilsen 2002). The water column is thus dominated by cold local water. Shore-fast ice is usually present from December to June. Bottom water salinity is around 34‰ (Hald et al. 2001), and July temperatures of -1.53°C and and -1.27°C have been measured in two basins in Van Mijenfjorden at 112 m and 74 m depth (Gulliksen et al. 1985). The climate in Sveagruva is slightly colder and more humid than in Longyearbyen 45 km to the NNE, but the meteorological record is shorter and more irregular. Mean annual air temperature close to sea level was -5.4°C in the period 1997–2006, and precipitation in the period 1995–2002 was on average 244 mm/y (www.met.no).

Temperature Measurements in Boreholes

Four 10 m deep boreholes (Fig. 1B) were drilled on Crednermorenen in March 2005 using an air pressure driven drilling rig. Coring was not possible, but the pulverized blown up sediment was collected from three of the holes, described and analyzed for water content and salinity. Borehole 1 was located two m above sea level and six m from the channel that connects Vallunden with Sveasundet. Borehole 2 was drilled into the ice-cored part of the moraine 17 m a.s.l. and 150 m from Sveabukta. Borehole 5 was established on top of the moraine ridge 145 m from Vallunden and 20 m a.s.l. Hole four was located on the marine clay part of Crednermorenen, but was destroyed by a bear in October 2006, and therefore no data are presented from that hole. In each borehole an eight m thermistor string (EBA Engineering, Edmonton, Canada) with 16 thermistors at decreasing spacing towards the surface was inserted. The uppermost sensor in each hole was placed at roughly three cm depth, and was measuring the surface temperature in this paper. Temperatures have been logged every two hour using Lakewood dataloggers; the accuracy of the thermistors is around 0.1°C. The annual temperature envelopes recorded in the three boreholes are shown in Figure 2. The maximum surface temperature for holes one and five occurred on 16 July 2007, and for hole two on 18 June 2007. The maximum temperature was very similar for the three holes, probably indicating that the barren surface provided similar summer conditions. The minimum surface temperature for all three holes occurred on 23 January 2007, which was contemporary with the minimum air temperature (-32.9°C) being recorded. The minimum surface temperature was much lower in hole two and five than in hole one. The latter had usually a snow cover of around 20 cm whereas both holes two and five were usually snow-free in winter due to wind redistribution in these more exposed sites. In Borehole 1 the seasonal temperature fluctuation became insignificant (0.25°C) below six meters depth, whereas the difference between annual maximum and minimum temperature at eight m in Boreholes 2 and 5 were 1.7°C and 1.1°C respectively.

Table 1 shows that all ground surface temperatures in the investigated period were higher than the mean air temperature. Hole one was warmest, reflecting the thickest snow cover during winter. The snow insulated the surface against cold winter temperatures creating a positive surface offset as demonstrated by, for example, Smith & Riseborough (1996). Hole 5 had the smallest surface offset as this site is usually never snow covered.

Smith & Riseborough (1996) also demonstrated that, due to higher thermal conductivity in frozen ground than in unfrozen, temperatures will tend to decrease from the ground surface to the top of the permafrost table (TTOP). Table 1 shows

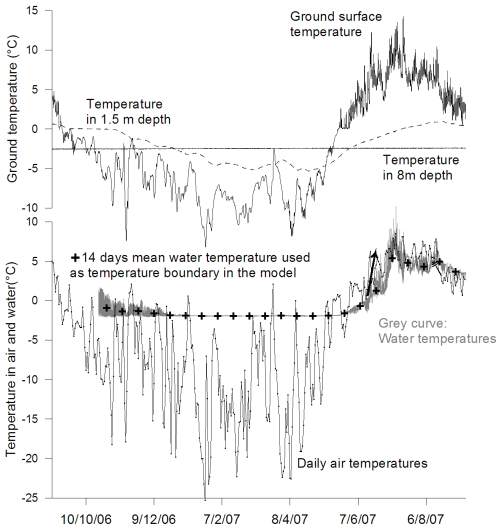

Figure 3. Upper part: Temperatures in Borehole 1 at the surface, in 1.5 m depth (dotted line) and in 8 m depth (no variation). Lower part: Air temperatures and water temperatures.

that in Boreholes 1 and 2 TTOP was higher than the surface temperature whereas in hole five it was practically the same. The active layer offset therefore seemed not to be important for the ground temperatures on the moraine, whereas snow depth in winter certainly was.

Tide and Water Temperature Measurements

Water temperatures in the narrow and shallow strait Sveasundet were measured and recorded every 20 min from 10 October 2006 to 9 September 2007 by a tidal gauge placed at two m water depth. The data can be seen in Figure 3 together with temperature measurements from Borehole 1 from three selected depths and air temperature measurements over the same time interval.

The freshwater from Kjellstrømsdalen passes the Sveasundet strait, and strong tidal currents flowing in and out of Braganzavågen ensure mixing of salt and fresh water here. For this reason the summer water temperatures were high compared to what has been measured in the deep basins in the fjord during summer. Winter temperatures however appeared to be constant around -1.93°C in most of the fjord.

The measured water temperatures can be divided in three distinct periods:

1) An autumn period when the temperature fluctuated in relation to the tide between -1.9 and +1.7°C lasting from 21 October to 26 December. Temperatures rose when the tide was moving through Sveasundet into the tidal flat Braganzavågen and fell when the tide flowed out again. This is consistent with observations that sea ice started forming in Braganzavågen before other places in the fjord. An example

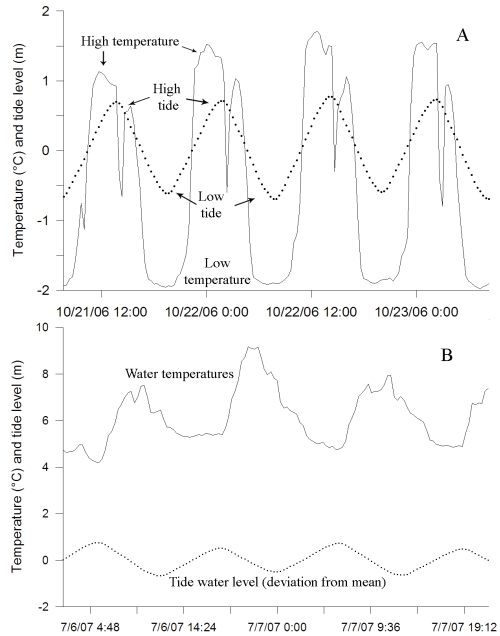

Figure 4. Examples of the relationship between water temperatures and the tide. A: Autumn conditions when the first sea ice forms, B: summer conditions.

of the coupling between tide and temperatures in the autumn can be seen in Figure 4A**.** November 28 was the last time the temperature rose above zero.

2) A winter period from 26 December to 22 May 2007. The temperature was nearly constant around -1.93, and no temperature fluctuations with tide were observed. The temperature corresponded to the freezing point of sea water and the fjord was covered by ice throughout this time. This winter period with constant water temperatures is easily identifiable in Figure 3.

3) A summer period from 22 May 2007 to the end of the measurements. Here the water temperatures increased and gradually approached the air temperature. The water temperature rose above zero for the first time on 13 June 2007. The temperature fluctuations were again controlled by tidal currents and were opposite in phase to those of the autumn. Now rising tide was associated with lower temperatures and falling tide with increasing temperatures (Fig. 4B). The reason is that water was now heated in the tidal flat Braganzavågen, where it was cooled during the autumn.

Modeling the Effect of the Sea on the Permafrost Temperatures

Studying the measured borehole temperatures, one can see that Borehole 1 deviated significantly from Boreholes

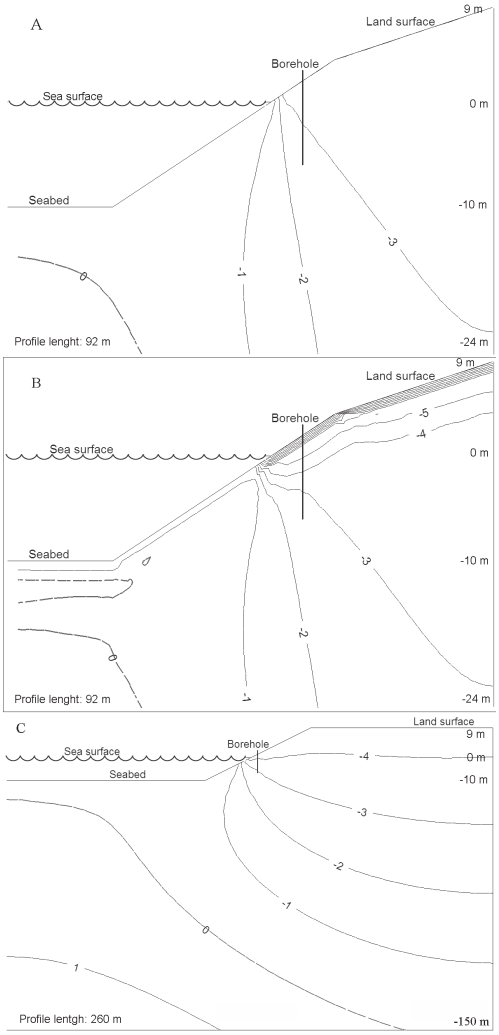

Figure 5. Three model output results. A: Steady state simulation of the ground temperatures in the immediate shore area. B: The same section but run in a transient mode forced with measured climatic data and sea water temperatures. Snapshot from 7 April 2007. C: Steady state simulation of a wider and deeper section with the boundary conditions the same as in A.

2 and 5 in respect both to the thermal regime and the depth of zero annual amplitude. While some of this deviation can be explained by a thicker snow cover during winter, most likely the proximity (6 m) to the sea affected the permafrost temperatures here. Located two m a.s.l. and being eight m deep, most of the borehole also lay below sea level. At eight m depth in Borehole 1, the temperature was -2.5°C. This indicates that permafrost probably extends into the seabed

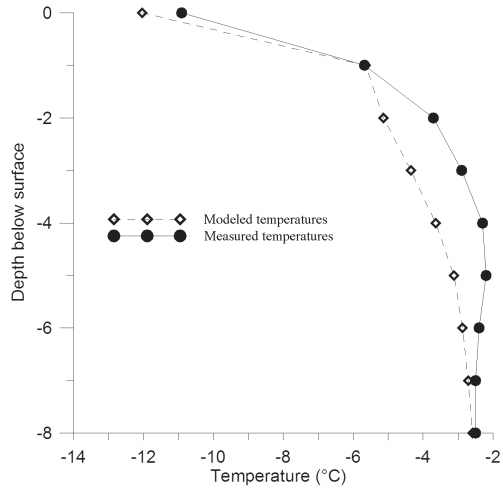

Figure 6. Comparison of the temperatures measured in Borehole 1 on 7 April 2007 and the modeled temperatures on the same day.

from the shore. An attempt was made to model both the effect of the sea on the onshore permafrost temperatures as well as the possibility of subsea permafrost existence. Gregersen & Eidsmoen (1988) previously tried to model the possible subsea permafrost in the area, but they had no information on the water temperatures in the fjord.

Model description and input

A 2D finite element program (TEMP/W) was used to model the permafrost thickness in Crednermorenen and the extent below the fjord bottom. The model is described in detail by Krahn (2004). Two temperature-dependent input functions (unfrozen water content and thermal conductivity) and overall water content are laboratory data from a nearby moraine, Damesmorenen, four km from hole 1, published by Gregersen et al. (1983). Volumetric heat capacity was set to 2000 and 3000 kJ/(m^3 x K) for frozen and unfrozen states respectively. Only one set of thermal properties was supplied to the model. It is obviously incorrect to assume homogeneous subsurface conditions, but we have no other thermal properties data available nor information on the subsea stratigraphy. A geothermal gradient of 35 mW/m^2 was set as a flux boundary condition at the bottom of the profiles. The vertical profile sides were set as zero flux boundaries.

To obtain a first estimate of the subsurface temperatures, the model was initially run in a steady state mode (Figs. 5A, 5C) using an estimated annual surface temperature and the average water temperatures as upper boundary conditions. A ground surface temperature of -4°C was used; this is slightly warmer than the mean annual air temperature due to the surface offset demonstrated in Table 1. A temperature of -0.1°C was used as the seabed boundary condition; this is the mean annual measured water temperature with interpolated

temperatures for the missing 1.5 months of data.

The model was also run in a transient mode (snapshot in Fig. 5B) to compare the model results with the temperatures measured in Borehole 1. In the transient mode, eight simulations were run per day, and each node result was input to the next model run. Here the model was forced with meteorological data from 1 Jan 2006 to 10 September 2007. The meteorological inputs were maximum and minimum daily temperature, maximum and minimum daily humidity, and average wind speed. Latitude and longitude were supplied and the TEMP/W program used an energy balance approach to model the surface energy balance. To simulate the seabed temperature, a time dependent te mperature function was supplied as boundary condition, consisting of the average measured water temperature on 14 day basis. These are seen as crosses in the lower part of Figure 3.

No attempts were made to simulate the tidal fluctuation and its affect on the ground temperatures.

The model was run on two profile sections of different lengths and depths to both obtain detailed information on the near surface conditions, and impressions of the larger-scale ground temperatures in the coastal zone. The profiles were 92 m and 260 m long respectively and simplify a profile across the moraine and into Vallunden crossing Borehole 1.

Model results

Figure 5A shows a steady-state simulation for the immediate shore area. A high horizontal thermal gradient is seen in a narrow zone just below the shoreline. Since the mean annual water temperature is slightly below zero (-0.1°C), permafrost is modeled to be present in a thin layer below the seabed.

Figure 5B shows a snapshot plot from the transient model run from 7 April 2007. The sharp decrease of near surface temperatures reflects the winter freezing on land. A -1 °C isotherm has formed close below the seabed reflecting that the water temperatures approach -2°C during winter.

Figure 5C is a model run of the larger and deeper section but with the boundary conditions as those of Figure 5A. The pattern is similar as the one in Figure 5A but suggests that at depth, the presence of the sea will affect the ground thermal conditions more than 100 m from the shore, and similarly, that the cold temperatures from land will affect the sub-seabed temperatures at a similar distance offshore.

Figure 6 compares the measured and modeled temperatures in Borehole 1 for 7 April 2007. The discrepancy of model temperatures near the surface and towards the bottom is quite small, whereas the modeled temperature is up to 1.4°C wrong in the middle of the borehole. This and other snapshots throughout the year show that, while the general pattern is simulated reasonably well, there are discrepancies. These are often larger than those shown in Figure 6. However, the reasonable agreement of the modeled to the measured temperatures gives us some confidence in the general modeling results.

Discussion

The pronounced sill, Akseløya, restricts warm coastal water from entering Van Mijenfjorden and probably makes this fjord colder than other western Spitsbergen fjords. Sea ice cover is longer-lasting and more stable here. Therefore, this fjord is a primary candidate for possible subsea permafrost in western Spitsbergen fjords.

The modeling results of the subsea permafrost extend presented here should be seen as a minimum scenario. This is because the water temperatures were measured in a shallow, high-current strait, where the fjord water is strongly mixed with warmer fresh water during the summer. July temperature measurements from two deep basins in Van Mijenfjorden (Gulliksen et al. 1985) of -1.53°C and -1.27°C, respectively, indicate that water temperature in the deeper parts of the fjord remains below 0°C all year.

Permafrost, as defined solely on the basis of temperature, may not necessarily indicate cryotic subsea conditions. Sea water freezes at temperatures slightly above -2°C but capillarity and adsorption—in particular in fine-grained sediments—can further reduce the freezing point (Williams & Smith 1989). Thus, depending on the sediment properties, the seabed may well have permafrost by definition but still remain unfrozen. If the seabed consists of saline marine deposits, they will not be cryotic, even if thermally defined permafrost exists.

The 1300 A.D. surge of Paulabreen deposited lateral moraines in a rim around the inner parts of the fjord. A new detailed bathymetric survey indicates that glacial deposits also occupy the seabed here (Ottesen et al., in prep.). A seabed consisting of terrestrial sediments of glacial origin and with fresh rather than saline porewater could actually be frozen, but this hypothesis has not yet been tested.

The Crednermorenen moraine contains large amounts of buried glacier ice. It is possible that the unusual cold water conditions in Van Mijenfjorden are influencing the preservation potential of the ice-core in this moraine.

Conclusions

The permafrost temperatures measured in three boreholes in the ice-cored Crednermorenen moraine were studied for a period of a year. The surface temperatures in all holes were higher than the corresponding air temperature. The highest surface temperature was measured in Borehole 1 that normally has a snow cover of 20 cm while the two other boreholes are nearly snow free during winter. Most likely the warmer surface temperature in Borehole 1 is due to a surface offset (Smith & Riseborough 1996) caused by the insulating effect of snow.

Increasing temperatures were observed from the surface down through the active layer to the top of the permafrost in two of the boreholes. This is opposite to what would be expected if higher thermal conductivity of frozen ground compared to unfrozen ground causes an active layer (or thermal) offset. So this offset appears not to be important here; probably the ground is too dry.

Borehole 1 is located six m from the shore and is significantly warmer than two other boreholes both about 150 m away from the shoreline. To investigate the effect of the proximity to the sea, the finite element program TEMP/W was used to model the ground temperatures at the shore and below the seabed in both a steady-state and transient mode. Meteorological data and water temperature measurements were used to force the model.

The program manages reasonably well to simulate the ground temperatures in the near-shore borehole. The simulations indicate that permafrost, as defined solely on temperature, is present in a thin layer beneath the seabed of Van Mijenfjorden. Whether it is frozen or unfrozen will depend on the material properties.

At depth, the warming effect of the sea on the ground temperatures is modeled to penetrate more than 100 m inland and the cooling effect of land is affecting the seabed at an equal distance. The temperatures closer to the surface, however, are primarily locally controlled.

Acknowledgments

Many thanks to Store Norske Spitsbergen Kulkompani for funding the drilling and instrumentation of the boreholes and for providing logistical support when collecting data. LNSS, local contractor, preformed the drilling. Jomar Finseth, NTNU, supervised the drilling, sediment sampling, and laboratory work. John Inge Karlsen, logistics at UNIS, dived twice in muddy waters to emplace and recover the tide gauge that also recorded the water temperatures. The manuscript was improved by comments of an anonymous reviewer.

References

Gregersen, O. & Eidsmoen, T. 1988. Permafrost conditions in the shore area at Svalbard. *Proceedings of the Fifth International Conference on Permafrost, Trondheim, Norway, August 2-5,1988*: 933-936.

Gregersen, O., Phukan, A. & Johansen, T. 1983. Engineering properties and foundation design alternatives in the marine Svea clay, Svalbard. *Proceedings of the Fourth International Conference on Permafrost, Fairbanks, Alaska, July,17-22, 1983*: 384-388.

Gulliksen, B., Holte, B. & Jakola, K.J. 1985. The soft bottom fauna in Van Mijenfjorden and Raudfjorden, Svalbard. In: J.S. Grey & M.E. Christiansen (eds.), *Marine Biology of Polar Regions and Effects ofStress on Marine Organisms.* Oslo: John Wiley & Sons, 199-215

Hald, M., Dahlgren, T., Olsen, T.E. & Lebesbye, E. 2001. Late Holocene palaeoceanography in Van Mijenfjorden, Svalbard. *Polar Research* 20(1): 23-35

Harada, K. & Yoshikawa, K. 1996. Permafrost age and thickness near Adventfjorden, Spitsbergen. *Polar Geography* 20(4): 267-281

Humlum, O., Instanes, A. & Sollid, J.L. 2003. Permafrost in Svalbard: a review of research history, climatic background and engineering challenges. *Polar Research* 22(2): 191-215. ‘

Krahn, J. 2004. *Thermal modeling with TEMP/W–An engineering methodology*. Calgary, Alberta, Canada: Geo-slope International Ltd., 282 pp.

Kristensen, L., Juliussen, H., Christiansen, H.H. & Humlum, O. 2008. The structure and composition of a tidewater push moraine, Svalbard, revealed by DC resistivity profiling. *Boreas* (in press).

Nilsen, F. 2002. Measured and Modeled Tidal Circulation Under Ice Cover Van Mijenfjorden. Abstract: www.cosis.net/abstracts/EGS02/06395/EGS02-A-06395-2.pdf

Ottesen, D., Dowdeswell, J.A., Benn, D.A., Kristensen, L., Christiansen, H.H., Christensen, O., Hansen, L. & Lebesbye, E. Submarine landforms characteristic of glacier surges in two Spitsbergen fjords (in prep.).

Smith, M.W. & Riseborough, D.W. 1996. Permafrost monitoring and detection of climate change. *Permafrost and Periglacial Processes* 7(4): 301-309.

Williams. P. J. & Smith, M.W. 1989. *The Frozen Earth: Fundamentals of Geocryology.* Cambrigde: Cambridge University Press, 306 pp.